

ALMA MATER STUDIORUM · UNIVERSITÀ DI BOLOGNA

Scuola di Scienze
Corso di Laurea Magistrale in Fisica

**A METHOD FOR AUTOMATED
GENERATION OF RADIOTHERAPY
TREATMENT PLANS FOR LUNG
CANCER**

Relatore:

Dott. Nico Lanconelli

Presentata da:

Giuseppe Della Gala

Correlatore:

Dott. Maarten L.P. Dirkx

Sessione II

Anno Accademico 2014/2015

Abstract

The fight against cancer is one of the main challenges in current medical science and radiotherapy represents one of the most employed techniques, especially for tumors in advanced stage. The radiation deposits energy in the tissues giving rise to reaction processes in the molecules and in the structures they belong to, such as the DNA; damages to the DNA sequence can lead the cell to death, with higher probability in cancer cells.

Along the years, radiotherapy developed always more technically advanced techniques for radiation delivery. Currently, intensity modulated radiotherapy (IMRT), based on the addition of intensity modulated fields to deliver high dose to the target and spare the healthy tissues, is overall the most employed delivery mode, while volumetric modulated arc therapy (VMAT) is a relatively new delivery mode based on IMRT principles, in which radiation is continuously delivered in an uninterrupted arc.

Independently of the delivery mode, radiotherapy treatment plan generation requires a lot of human interaction and experience. A dosimetrist has the task to generate a plan within a list of clinical requirements by selecting cost functions and their goals based on previous experience only, while the treatment planning system looks for the best IMRT segments arrangement. After the evaluation of a physician, the plan generation might start again, in a trial-and-error process that is time consuming, with no guarantee about optimality of the plan with respect to the wishes of the physician, and affected by the dosimetrist's experience and skills.

An alternative way is represented by automated treatment planning. The Erasmus Medical Center Cancer Institute (Rotterdam, The Netherlands) in-house developed Erasmus-iCycle is a multicriterial plan optimization algorithm for beam intensity optimization based on a so called wish list. Outputs of iCycle, used in connection with a treatment planning system, are Pareto-optimal plans with optimized intensity modula-

ted beam profiles. With Pareto-optimal it is meant that none of the objectives in the applied wish list can be improved any further without deteriorating higher prioritized objectives. With automated planning, plan quality is more consistent, overall higher, and plan generation is briefer in terms of hands-on working time by an operator.

In this study, an automated plan generation procedure was developed and evaluated for non-small cell lung cancer at locally advanced stage. The selected delivery mode was VMAT, that was not used in clinic yet at the time of the study for this site. A site-specific iCycle wish list was generated in an iterative procedure on a small set of previously treated patients with the help of two medical physicists and two radiation oncologists. The procedure was then validated on a larger set of patients, previously treated at the Erasmus Cancer Institute between January and August 2015.

In the vast majority of cases the automatically generated plans were judged by the physicians as better than the corresponding clinically delivered, manually generated, IMRT plans. Only in a few cases a brief patient specific manual fine tuning was requested to fulfill all the clinical constraints. For a small set of patient it was shown that plan quality for automated VMAT plans was equal or superior with respect to VMAT plans manually generated by an expert dosimetrist. For some patients the automated procedure was able to generate plans with higher prescription dose with respect to the clinically delivered one without violating any of the clinical constraints.

Overall, this study proved that an automated procedure was able to generate high quality VMAT plans with minimal human interaction. The clinical introduction of the automated VMAT planning procedure for non-small cell lung cancer treatment at Erasmus Medical Center Cancer Institute has been started in October 2015.

La lotta al cancro è una delle sfide più importanti della medicina contemporanea e la radioterapia rappresenta una delle tecniche di cura più utilizzate, in particolare per tumori in stadio avanzato. La radiazione deposita energia nei tessuti, dando origine a processi di reazione nelle molecole e nelle loro strutture di appartenenza, come il DNA; danni alla sequenza genica del DNA possono condurre la cellula alla morte, con una probabilità più elevata nelle cellule tumorali.

Nel corso degli anni, la radioterapia ha sviluppato tecniche sempre più sofisticate di irradiazione. Attualmente, la intensity modulated radiotherapy (IMRT), basata sulla so-

vrapposizione di campi ad intensità modulata per somministrare una dose elevata al target e limitare la dose ai tessuti sani, è complessivamente la tecnica più impiegata, mentre la volumetric modulated arc therapy (VMAT) è una modalità relativamente recente, basata sui principi IMRT, in cui la radiazione è somministrata continuativamente lungo un arco senza interruzioni.

A prescindere dalla tecnica di irradiazione, la generazione di piani di trattamento radioterapici richiede una grande quantità di interazione umana ed esperienza. Un dosimetrista ha il compito di generare un piano entro una lista di requisiti clinici selezionando cost functions e loro obiettivi sulla base dell'esperienza precedente, mentre il treatment planning system si occupa della ricerca della miglior disposizione dei segmenti ad intensità modulata. Dopo il giudizio di un medico, può essere necessario ricominciare la creazione del piano da capo, in un processo di tipo trial-and-error che risulta essere molto dispendioso in termini di tempo, senza garanzie sulla ottimalità del piano rispetto alle richieste mediche, e influenzato dall'esperienza e dalle capacità del dosimetrista.

Una via alternativa è rappresentata dalla generazione automatica di piani di trattamento radioterapici. Erasmus-iCycle, software prodotto presso Erasmus Medical Center Cancer Institute (Rotterdam, The Netherlands), è un algoritmo di ottimizzazione multicriteriale di piani radioterapici per ottimizzazione di intensità basato su una wish list. L'output di iCycle, usato in congiunzione con un treatment planning system, consiste di piani Pareto-ottimali con profili di radiazione ottimizzati ad intensità modulata. Con Pareto-ottimale si intende che nessun obiettivo nella wish list selezionata può essere ulteriormente migliorato senza peggiorare il risultato ottenuto per un obiettivo a priorità più elevata. Con la generazione automatica, la qualità del piano è più coerente e complessivamente più elevata e la generazione del piano è più rapida in termini di tempo di lavoro manuale da parte di un operatore.

Nel seguente studio, una procedura di generazione automatica di piani di trattamento è stata sviluppata e valutata per carcinoma polmonare non a piccole cellule (non-small cell lung cancer) in stadio localmente avanzato. La modalità di irradiazione scelta è stata VMAT, non ancora impiegata nella pratica clinica per questo sito al momento dello studio. Una wish list per iCycle specifica per il sito è stata generata attraverso una procedura iterativa su un ristretto gruppo di pazienti trattati in precedenza con la collaborazione di due fisici medici e due oncologi. La procedura è stata in seguito validata su un gruppo più ampio di pazienti, trattati presso Erasmus Cancer Institute tra gennaio

ed agosto 2015.

Nella grande maggioranza dei casi, i piani generati attraverso la procedura automatizzata sono stati giudicati dagli oncologi migliori rispetto ai rispettivi piani IMRT somministrati in clinica e generati attraverso la procedura manuale standard. Solo in pochi casi una rapida calibrazione manuale specifica per il paziente si è resa necessaria per soddisfare tutti i requisiti clinici. Per un gruppo ristretto di pazienti si è mostrato che la qualità dei piani VMAT automatici era uguale o superiore rispetto ai piani VMAT generati manualmente da un dosimetrista esperto. Per alcuni pazienti la procedura automatica è stata in grado di generare piani con una prescrizione di dose più elevata rispetto a quella somministrata in clinica senza violare alcun vincolo clinico.

Complessivamente, questo studio ha dimostrato che è stato possibile generare piani radioterapici VMAT ad alta qualità attraverso una procedura automatica con interazione umana minima. L'introduzione clinica della procedura automatica per il trattamento del carcinoma polmonare non a piccole cellule presso Erasmus Medical Center Cancer Institute è iniziata nell'ottobre 2015.

Contents

Abstract	iii
Contents	vii
List of Figures	xi
List of Tables	xv
1 Introduction	1
1.1 What is cancer	1
1.1.1 Cancer stages	2
1.2 Interactions between radiations and matter	3
1.2.1 Photons	4
1.2.1.1 Photon beam spectrum	5
1.2.1.2 Photoelectric effect	6
1.2.1.3 Coherent scattering	7
1.2.1.4 Incoherent scattering	7
1.2.1.5 Pair production	8
1.2.1.6 Photon beam intensity attenuation	8
1.2.1.7 Dose delivery	10
1.2.2 Charged particles	11
1.2.2.1 Electrons	11
1.2.2.2 Protons and ions	14
1.3 Biological mechanism of radiotherapy	16
1.3.1 Working principles	16

1.3.2	Stochastic nature of energy deposition	18
1.3.3	Dosimetric units and parameter	19
1.3.4	Cell survival curves	20
1.3.4.1	Oxygenation	21
1.3.4.2	Fractionation	21
1.4	Radiotherapy workflow	22
1.4.1	Aim of radiotherapy	23
1.4.2	Positioning	24
1.4.3	Imaging	25
1.4.4	Volumes definitions	26
1.4.5	Forward and inverse planning	28
1.4.6	Evaluation	29
1.4.7	After radiotherapy treatment: follow up and complications	32
1.5	External beam radiotherapy: radiation delivery	33
1.5.1	Photon beam production	33
1.5.2	Main delivery modalities	33
1.5.2.1	3D Conformal Radiation Therapy (3DCRT)	33
1.5.2.2	Intensity Modulated Radiation Therapy (IMRT) - Step and shoot	33
1.5.2.3	Volumetric Modulated Arc Therapy (VMAT)	37
1.5.2.4	Stereotactic radiotherapy and Cyber Knife	38
1.6	Other cancer treatment modality: brachytherapy and chemotherapy	38
1.6.1	Brachytherapy	38
1.6.2	Chemotherapy	39
2	Lung cancer and treatment planning	41
2.1	Lung anatomy and lung cancer features	41
2.2	Lung cancer treatment options	42
2.2.1	Surgery	42
2.2.2	Chemotherapy	43
2.2.3	Radiotherapy	43
2.2.3.1	4DCT Acquisition	43

2.2.3.2	Structures delineation	43
2.2.3.3	Dose prescriptions and fractionation regimens	44
2.2.3.4	Delivery modalities	44
2.3	Introduction to treatment planning	45
2.3.1	Manual and automated planning	45
2.3.2	Background: research in radiotherapy treatment planning	46
2.3.3	Erasmus-iCycle	47
2.4	Goal of the study	48
3	Methods and materials	49
3.1	Background: system for automated planning	49
3.1.1	Erasmus-iCycle	49
3.1.2	Multi-criterial optimization	49
3.1.3	Wish list	50
3.1.4	Brief introduction to <i>2pec</i> optimization method	51
3.1.5	Wish list generation	52
3.1.6	iCycle VMAT plan generation	54
3.1.7	Treatment planning system: Monaco	54
3.1.8	Export to Monaco	55
3.2	Current study	55
3.2.1	Patients selection and target delineation	55
3.2.2	Clinical requirements for IMRT planning	56
3.2.3	Automated treatment planning with Erasmus-iCycle	57
3.2.4	Construction of the wish list	57
3.2.5	Conversion to Monaco	60
3.2.6	Validation procedure and statistical testing	61
3.2.7	Comparison with manually generated VMAT plans	65
3.2.8	Dose escalation	65
3.2.9	Delivery machines	65
3.3	Considerations about the iCycle wish list	66
3.3.1	Random sampling in iCycle optimization	66
3.3.2	Scattering length	66
3.3.3	Conformality and mean lung dose reduction	67

3.3.4	PTV minus expanded spinal cord (5 mm)	67
3.4	Evaluation tools: DVHs and scatterplots	68
3.5	Uncertainties	71
4	Results	73
4.1	Overview	73
4.2	PTV coverage	76
4.3	Lungs minus GTV	77
4.4	Esophagus and heart	79
4.5	Dose conformality and target dose homogeneity	81
4.6	Unacceptable plans	82
4.7	AutoVMAT vs manual VMAT planning	83
4.8	Dose escalation	86
4.9	Examples	86
4.9.1	Clinical plans, iCycle plans, AutoVMAT plans	86
4.9.2	Fixing unacceptable plans	91
4.9.3	Dose escalation	94
4.10	Further implications	98
4.10.1	Hands-on working time reduction	98
4.10.2	VMAT employment	98
5	Conclusions and perspectives	99
5.1	Conclusions	99
5.2	Perspectives	100
5.2.1	VMAT and IMRT delivery modality	100
5.2.2	Two-step approach and unacceptable autoVMAT plans	101
5.3	Clinical introduction	101
	Bibliography	103

List of Figures

1.1	Diagram of the progression of the cancer disease	2
1.2	Detailed TNM staging of lung cancer (from [2])	3
1.3	Classification of radiation	4
1.4	Spectral distributions of x-rays calculated for a thick tungsten target using Kramer's Equation	6
1.5	Regions of relative predominance of the three main forms of photon inter- action with matter	9
1.6	The total and partial cross-sections for carbon (a) and lead (b) for photon energies from 10 keV to 100 MeV	10
1.7	Relative dose release for different photon energies	12
1.8	Typical central axis percentage depth-dose curves for beam energies from 5 MeV to 20 MeV	13
1.9	Percentage depth doses in water for proton beams at various energies . .	15
1.10	Comparison between the percentage depth doses of a spread out Bragg peak (SOBP) and a single proton beam	15
1.11	Relative dose as a function of the depth for different kinds of radiation .	16
1.12	Energy deposited per unit mass plotted against the mass of the scoring volume	18
1.13	Typical cell survival curves for high LET (densely ionizing) radiation and low LET (sparsely ionizing) radiation	20
1.14	Survival curves for cultured mammalian cells exposed to x-rays under oxic or hypoxic conditions	21
1.15	Surviving fraction of tumoral and normal cells as a function of the number of fractions	22

1.16	Chain of radiotherapy	23
1.17	TCP and NTCP curves	24
1.18	Immobilization for thoracic radiotherapy with a T-bar, lateral elbow supports and a knee rest. Laser lights are used to prevent rotational set-up errors. Picture from [9].	25
1.19	Schematic representation of the volumes defined by ICRU reports	28
1.20	Target volumes delineation in a lung cancer patient	28
1.21	Diagram of the trial-and-error process involved in manual planning . . .	30
1.22	Example of Dose Volume Histogram for a lung cancer patient	32
1.23	Operating scheme of a linac and MLC	34
1.24	Comparison between 3DCRT and IMRT dose distributions for cancer treatment in the pelvic region	35
1.25	Intensity modulation by superposition of MLC shaped fields from the same directions	36
1.26	VMAT treatment	37
1.27	CyberKnife radiosurgery system	38
1.28	Seeds for brachytherapy	39
2.1	Anatomy of the lungs (picture from [11])	42
3.1	Diagram of the automated planning procedure	50
3.2	iCycle wish list for lung cancer treatment	59
3.3	Validation set of patients	64
3.4	Elekta Sinergy system	66
3.5	Comparison between a plan in which the LTCP cost function is applied to the entire PTV (left) and a plan in which LTCP cost function is applied to PTV minus spinal cord expanded by 5 mm (right). Both plans are iCycle dose simulations	68
3.6	Example of DVH	69
3.7	Example of scatterplot for esophagus mean dose	70

4.1	Differences between clinical plans and autoVMAT plans for mean lung dose (MLD), lungs V_{5Gy} , lungs V_{20Gy} , PTV $D_{99\%}$ and PTV $V_{95\%}$. Positive values are in favor for the autoVMAT plans. For visualization purposes the differences of the V_{5Gy} and V_{20Gy} of the lungs and PTV D_{99} were multiplied by 0.1, 0.1 and 0.5 respectively.	74
4.2	Differences between clinical plans and autoVMAT plans for esophagus mean dose, heart mean dose, conformity index R_{50} and homogeneity index (HI). Positive values are in favor for the autoVMAT plans. For visualization purposes the differences of the R_{50} and HI were multiplied by 10 and 100 respectively.	75
4.3	Scatterplots of PTV D_{99} (a) and PTV V_{95} (b). Red circles indicate the plans that were not clinically acceptable. Points lying above the equality line show improvement for autoVMAT plans.	77
4.4	Scatterplots of lungs minus GTV mean dose (a), V_{20Gy} (b) and V_{5Gy} (c). Red circles indicate the plans that were not clinically acceptable. Points lying below the equality line show improvement for autoVMAT plans. . .	78
4.5	Scatterplots of esophagus mean dose (a), esophagus V_{45Gy} (b) and heart mean dose (c). Red circles indicate the plans that were not clinically acceptable. Points lying below the equality line show improvement for autoVMAT plans.	80
4.6	Scatterplots of R_{50} (a) and homogeneity index (b). Red circles indicate the plans that were not clinically acceptable. Points lying above the equality line show improvement for autoVMAT plans.	81
4.7	Scatterplots of PTV D_{99} (a), PTV V_{95} (b), lungs minus GTV mean dose (c), V_{20Gy} (d) and V_{5Gy} (e).	84
4.8	Scatterplots of esophagus mean dose (a)	85
4.9	Image set and volumes delineation for patient GDGCPerspIM7 in axial (a), sagittal (b) and coronal view (c)	87
4.10	Comparison between dose volume histograms of clinical plan (solid line), autoVMAT plan (dashed line) and iCycle plan (dotted line) for patient GDGCPerspIM7	90
4.11	DVHs of the main organs at risk for the clinical plan (solid line) and the iCycle dose distribution (dotted line) for patient GDGCPerspIM42 . . .	92

4.12	DVHs of the main organs at risk for the clinical plan (solid line), the iCycle dose distribution (dotted line) and the autoVMAT plan (dashed line) for patient GDGCPerspIM42	92
4.13	DVHs of the main organs at risk for the clinical plan (solid line), the iCycle dose distribution (dotted line) and the autoVMAT plan after the relaxation in the translation of the MLD (dashed line) for patient GDGCPerspIM42	93
4.14	DVHs for the clinical plan (solid line), the iCycle VMAT plan (dotted line) and the autoVMAT plan (dashed line) for patient GDGCPerspIM44 with a prescribed dose of 60 Gy	96
4.15	DVHs of the clinical plan with a prescription dose of 60 Gy (solid line) and autoVMAT plan with prescription dose increased to 66 Gy (dashed line) for patient GDGCPerspIM44	97

List of Tables

3.1	Clinical requirements for NSCLC	56
3.2	Details for automated generation of Monaco templates	60
3.3	Prescribed doses and fractionation regimens	62
4.1	Dose statistics that violated the clinical constraints for the six unacceptable plans	82
4.2	Dose statistics comparisons between autoVMAT and manually generated VMAT plans	83
4.3	Comparison between dose distributions of clinical plan, iCycle plan and autoVMAT plan for patient GDGCPerspIM7	87
4.4	Main dose statistics of the three plans for patient GDGCPerspIM7 . . .	91
4.5	Main dose statistics for the clinical plan, the iCycle plan, the autoVMAT with the standard translation and the autoVMAT plan with the modified translation	93
4.6	Dose distributions for the clinical IMRT plan and the autoVMAT plan for patient GDGCPerspIM44	94
4.7	Main dose statistics for clinical and autoVMAT plan with prescribed dose of 60 Gy and for autoVMAT plan with prescribed dose of 66 Gy.	97

Chapter 1

Introduction

1.1 What is cancer

Cancer is the name given to a collection of related diseases (more than 100, generically classified by the type of cell that is initially affected) which involves abnormal cell growth with the potential to spread into surrounding tissues. The peculiarity of spreading distinguishes malignant tumors (the real cancer) and benign tumors. Cancer may be caused by genetic and environmental factors.

The human body is made up of trillions of cells which normally grow and divide to form new cells as the body needs them. When cells grow old or become damaged, they die and new cells take their place. This process takes the name of apoptosis. In contrast to necrosis, which is a form of traumatic cell death due to an acute cell injury, apoptosis is a highly regulated and controlled process. It can be considered as a deliberate suicide of the cell that takes place when it is needed by the whole system: self-sacrifice—as opposed to survival of the fittest—is then the rule. Thus, to survive and divide without limit, a prospective cancer cell must accumulate mutations that disable the normal safety mechanisms that would otherwise induce a cell that is stressed, in this or in other ways, to commit suicide. In fact, one of the most important properties of many types of cancer cells is that they fail to undergo apoptosis when a normal cell would do so. Nevertheless, this does not mean that cancer cells rarely die: on the contrary, in the interior of a large solid tumor, cell death often occurs on a massive scale, because of the severe competition among the cancer cells for oxygen and nutrients, but typically this happens much more by

necrosis than by apoptosis. The whole tumor grows because the cell birth rate outpaces the cell death rate, but often by only a small margin. For this reason, the time that a tumor takes to double in size can be far longer than the cell-cycle time of the tumor cells [1].

As previously outlined, cancer cells are also characterized by the ability of invading and colonizing territories normally reserved for other cells. Invasiveness makes the difference between benign and malignant tumors. In particular, the formation of secondary tumors, called metastases, is often the actual cause of the death of the patient.

1.1.1 Cancer stages

Staging is a classification of the tumors which describes the extent or spread of cancer at the time of diagnosis (Fig. 1.1). Proper staging is essential in determining the choice of therapy and in assessing prognosis. A cancer's stage is essentially based on the size or extent of the primary tumor and whether it has spread to nearby lymph nodes or other areas of the body. Different staging systems are used to classify cancer. For instance, a system is used for descriptive and statistical analysis of tumor registry data and is particularly useful for looking at trends over time. According to this system, if cancer cells are present only in the layer of cells where they developed and were not yet spread, the disease is in situ. If cancer cells have penetrated beyond the original layer of tissue, the cancer has become invasive and is categorized as local, regional, or distant, based on the extent of spread.

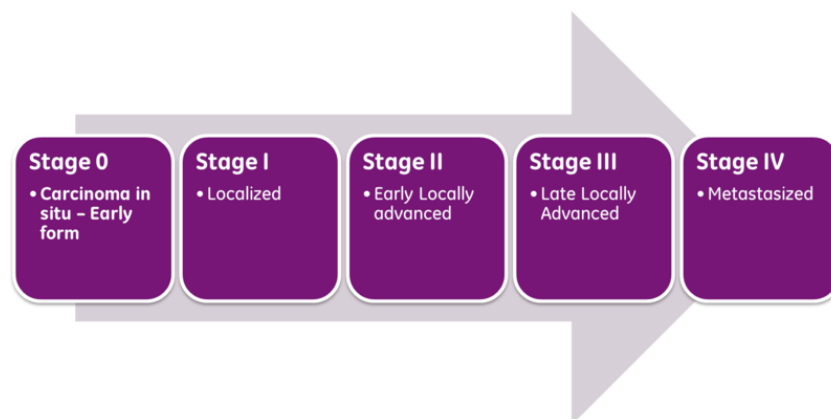


Figure 1.1: Diagram of the progression of the cancer disease

The ionizing process can also follow different ways. In particular, a remarkable distinction between directly and indirectly ionizing particles can be made. In contrast to directly ionizing particles (electrons, protons, ions), indirectly ionizing particles (photons and neutrons) have no charge. As the name states, in this case ionization is a secondary process of the interaction between the radiation and matter, generating fast charged particles.

Radiotherapy takes advantage of ionizing radiation to kill cancer cells and treat the tumor, by application of photons, electrons, protons, neutrons or ions. The interaction between radiation and matter depends strongly on mass and charge of the radiation.

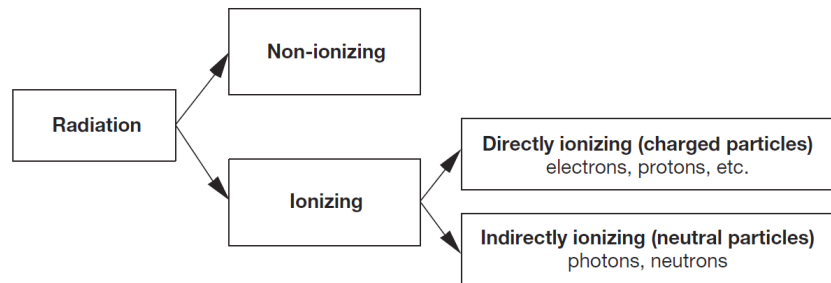


Figure 1.3: Classification of radiation

1.2.1 Photons

Depending on their origin, photon radiation generation falls into one of the following categories[4]:

- Bremsstrahlung (continuous X-rays), generated through electron-nucleus interactions
- Characteristic, discrete X-rays, emitted during transitions of orbital electrons from one orbit to a vacancy in another inner orbit
- Gamma-rays (discrete), emitted through nuclear transition in gamma decay
- Annihilation radiation (discrete, 0.511 MeV), emitted through positron-electron annihilation

Photons may undergo various possible interactions with the atoms of a material. The probability to manifest each interaction depends mainly on the energy of the photon and on the atomic number Z of the attenuator. The energy of the interacting photon can generate free fast charged particles (such as electrons) being entirely absorbed or may undergo a process in which the outcome consists in a fast charged particle plus a scattered photon. The generated charged particles gradually lose energy by transferring it to the atoms of the material and by causing ionizations.

1.2.1.1 Photon beam spectrum

External beam radiation therapy is commonly based on X-ray photon beams as bremsstrahlung radiation (electron - nucleus interaction) or characteristic X-rays (electron - electron interaction). This radiation is obtained by interaction of a high-energy electron beam (typically 4-23 MeV) with a high- Z target (often tungsten, $Z = 74$) in the head of the treatment machine. The resulting photon beam spectrum consists of contributions of both processes: a continuum energy spectrum generated by bremsstrahlung and discrete energy peaks caused by characteristic radiation of the target material.

If no filtration of the beam is applied, the energy spectrum will be a straight line and mathematically given by Kramer's equation:

$$I_E = KZ(E_{MAX} - E) \quad (1.1)$$

where I_E is the intensity of photons with energy E , Z is the atomic number of the target, E_{MAX} is the maximum photon energy, and K is a constant. The maximum possible energy that a bremsstrahlung photon can have is equal to the energy of the incident electron, which is generally between 4 and 25 MeV in radiation therapy. The addition of a filter modifies the spectrum. The filtration primarily affects the low-energy part of the spectrum and hardly affects the high-energy photon distribution. This process is known as beam hardening and has the effect to increase the average energy of the beam by absorbing lower-energy components of the spectrum, thereby improving the penetrating power of the beam. In figure 1.4 the spectrum is shown for a X-ray tube.

Since X-rays have a spectral distribution in energies, it is difficult to characterize the beam quality. In radiotherapy, beam quality is globally indicated by the maximum photon energy in the spectrum, as determined by the energy of the electrons used to

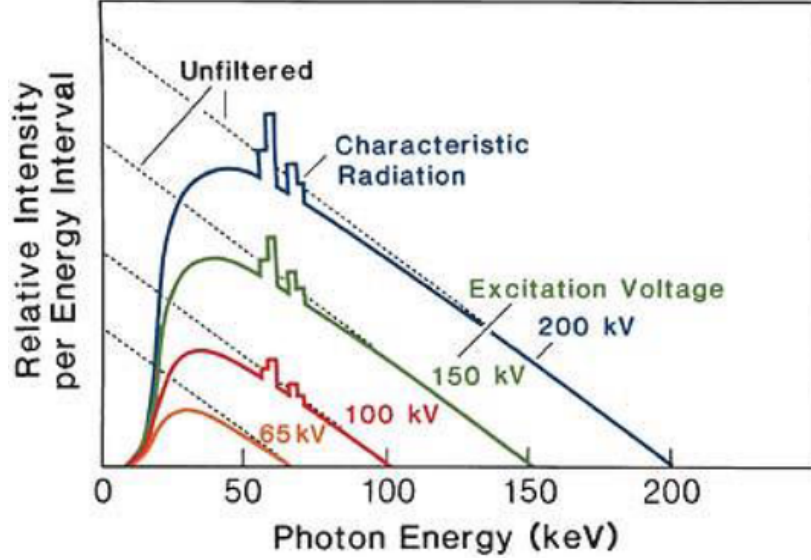


Figure 1.4: Spectral distributions of x-rays calculated for a thick tungsten target using Kramer's Equation (1.1). Dotted curves are for no filtration and solid curves are for a filtration of 1 mm aluminum.

generate the X-rays. For instance, a beam with a maximum photon energy of 6 MeV is called a 6MeV photons beam. A rule of thumb which is often used states that the mean photon beam energy is approximately one third of the maximum energy, but this one-third rule is a rough approximation since filtration may significantly alter the mean energy[5].

1.2.1.2 Photoelectric effect

In the photoelectric effect, a photon interacts with a tightly bound orbital electron of a material and disappears, while ejecting the orbital electron from the atom as a photoelectron with a kinetic energy E_K given as:

$$E_K = h\nu - E_B \quad (1.2)$$

where $h\nu$ is the incident photon energy and E_B is the binding energy of the electron. This process cannot occur with a free electron: the atom is needed in order to conserve momentum[6].

In general, the cross section σ_{pe} for photoelectric absorption increases strongly with

decreasing photon energy. The cross section displays a series of discontinuities at energies corresponding to the binding energies of the electrons in the atomic shells, known as absorption edges. Below the absorption edge, the photon does not have sufficient energy to liberate an electron from the shell; at energies just above the edge, the photon has sufficient energy to liberate the electron. Therefore, the cross section abruptly increases because the number of electrons that can take part in the absorption process increases.

The cross section for photoelectric effect depends strongly on atomic number. Above the K-shell absorption edge, the cross section per atom as a function of photon energy and atomic number is approximately given by

$$\sigma_{pe} \propto Z^4 / (h\nu)^3. \quad (1.3)$$

This points to the strong impact of this process at low photon energies and, particularly, at high atomic numbers.

1.2.1.3 Coherent scattering

In coherent (or Rayleigh) scattering, a photon interacts with a bound orbital electron. The event is elastic in the sense that the photon loses essentially none of its energy and is scattered through a small angle only. Since no energy transfer occurs from the photon to charged particles, Rayleigh scattering plays no role in the energy transfer coefficient, but it contributes to the attenuation coefficient.

In tissue and tissue equivalent materials, the relative importance of Rayleigh scattering in comparison with other photon interaction processes is small, as it contributes a few percent or less to the total attenuation coefficient only[4].

1.2.1.4 Incoherent scattering

The Compton effect (incoherent scattering) consists of a photon interaction with an essentially ‘free and stationary’ orbital electron. The incident photon energy $h\nu$ is much larger than the binding energy of the orbital electron ($h\nu \gg E_B$). The photon transfers part of its energy to the recoil (Compton) electron and is scattered as photon $h\nu'$ through a scattering angle θ .

To satisfy the conservation of momentum and energy, the scattered photon is char-

acterized by an energy

$$h\nu' = \frac{h\nu}{1 + \frac{h\nu}{m_e c^2}(1 - \cos \theta)} \quad (1.4)$$

where $h\nu$ is the energy of the incident photon, m_e is the rest mass of the electron, and θ represents the angle between the incident photon direction and the direction of the scattered photon.

Compton scattering cross section is given by the Klein-Nishina equation, which shows a linear dependence on the atomic number Z of the attenuator. In the usually applied MeV energy photon beams, the Compton effect is the dominant interaction type.

1.2.1.5 Pair production

In pair production, a photon is absorbed in the electric field of the nucleus and an electron-positron pair is created and emitted with a total kinetic energy equal to $h\nu - 2m_e c^2$, due to the conservation of energy. The process requires a minimum photon energy (energy threshold) of $2m_e c^2 = 1.022 \text{ MeV}$, necessary to create the two particles. On average, the electron-positron pair about equally shares the kinetic energy available. This energy is then lost into the attenuator material.

The cross section for pair production in the nuclear field is zero below threshold and rapidly increases with increasing energy for higher energies. Above threshold, it varies approximately as the square of the nuclear charge Z , i.e.

$$\sigma_{pp} \propto Z^2. \quad (1.5)$$

Regions of relative predominance of photoelectric, Compton and pair production effects are shown in Figure 1.5.

1.2.1.6 Photon beam intensity attenuation

The intensity of a photon beam is defined as the flow rate of photon energy through a unit area lying perpendicular to the beam direction. When a X-ray beam passes through matter, the beam intensity is reduced due to attenuation by the medium. This process involves absorption, scattering and transmission.

It is straightforward to demonstrate that the intensity $I(x)$ of a narrow beam of monoenergetic photons, attenuated by an absorber of variable thickness x , is given by

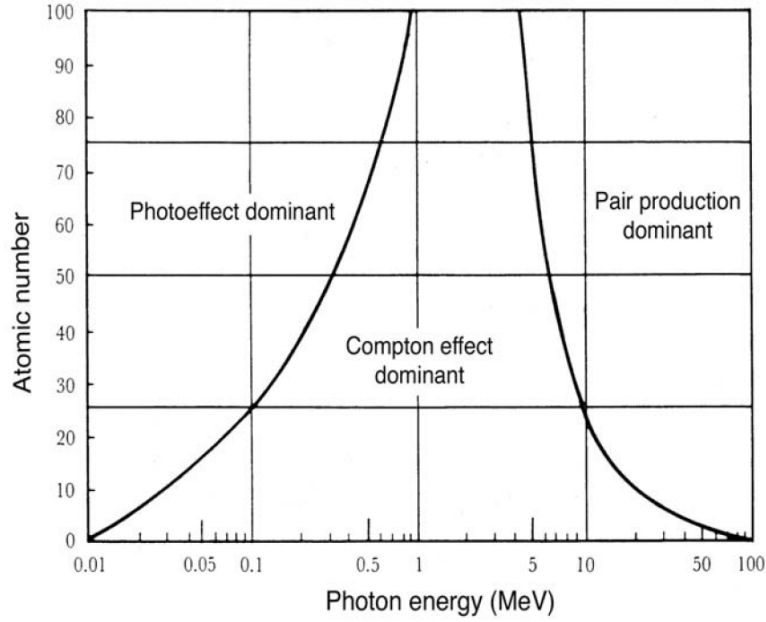


Figure 1.5: Regions of relative predominance of the three main forms of photon interaction with matter. The left curve represents the region where the atomic coefficients for the photoelectric effect and the Compton effect are equal, the right curve is for the region where the atomic Compton coefficient equals the atomic pair production coefficient.

the following equation:

$$I(x) = I_0 e^{-\mu x} \quad (1.6)$$

where I_0 is the intensity incident on the absorber and $\mu = \mu(h\nu, Z)$ is the total linear attenuation coefficient, which depends on the beam energy $h\nu$ and the atomic number Z of the attenuator.

The linear attenuation coefficient is the probability per unit length for interaction and is related to the total atomic cross section σ_{tot} through the relation

$$\mu = N\sigma_{tot} \quad (1.7)$$

where N is the number of target entities per unit volume, i.e.,

$$N = \frac{N_A}{A} \rho \quad (1.8)$$

N_A is the Avogadro's number ($N_A = 6.022 \times 10^{23} \text{ atoms/mol}$), A is the relative atomic

mass of the target element and ρ is its density. It is also useful to define the mass attenuation coefficient $\mu_m = \mu/\rho$, which can be considered as a more fundamental coefficient than the linear coefficient, since its dependence on the nature of the material does not involve density but rather the atomic composition. The total attenuation coefficient is the sum of the coefficients for individual photon interactions.

In radiotherapy, beams energies typically vary between 4 and 23 MeV, so the predominant effect is the Compton scattering (Fig. 1.6).

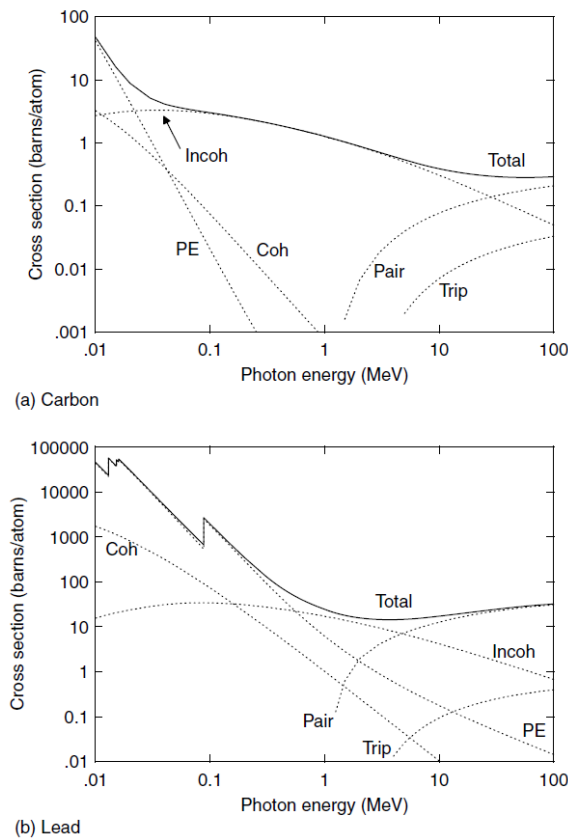


Figure 1.6: The total and partial cross-sections for carbon (a) and lead (b) for photon energies from 10 keV to 100 MeV

1.2.1.7 Dose delivery

When a photon beam enters the patient body, it interacts with its tissues by depositing energy following the previously described processes. The absorbed energy is

therefore not only deposited locally at the site where the photon has interacted, but also at a further distance. This happens due to the creation of fast electrons or positrons that will gradually lose energy while moving away from the photon interaction site.

These charged particles often have a large velocity component in the forward direction and for this reason dose is mainly released forward, resulting in a low dose near the surface, the so-called dose buildup region. High energy photons produce high-speed electrons and the dose buildup region is then more significant. With depth, the photon beam intensity reduces, resulting in less dose at larger depth.

The delivered dose as a function of depth in a medium varies depending on many parameters, like beam energy, field size, and the distance from the source (Fig. 1.7). One way of characterizing the central axis dose distribution is to normalize dose at a certain depth with respect to dose at a specific reference depth. The percentage depth dose may be defined as the quotient, expressed as a percentage, of the absorbed dose (indicated here by the symbol D) at any depth d to the absorbed dose at a fixed reference depth d_0 , along the central axis of the beam. Percentage depth dose (PDD) is thus:

$$PDD = \frac{D_d}{D_{d_0}} \times 100 \quad (1.9)$$

For orthovoltage X-rays (up to 400 keV), the reference depth is usually the surface ($d_0 = 0$); for higher energies, the reference depth is taken at the position of the peak absorbed dose (typically 1.5 cm for a 6 MV beam and 3 cm for a 23 MV beam).

1.2.2 Charged particles

Charged particles are fundamental to the medical use of radiation. They may be delivered as primary radiation beam, using electrons, protons or so called heavy ions like carbon. Alternatively, if the primary radiation is a photon beam, charged particles, known as secondary radiation, are causing the biological effect. Therefore, it is important to obtain a model for the transport of energy by the charged particles.

1.2.2.1 Electrons

Electron beams of MeV energy are used for treatment of superficial tumors (i.e., less than 5 cm in depth), e.g. in the skin, breast and head and neck area (Fig. 1.8). The

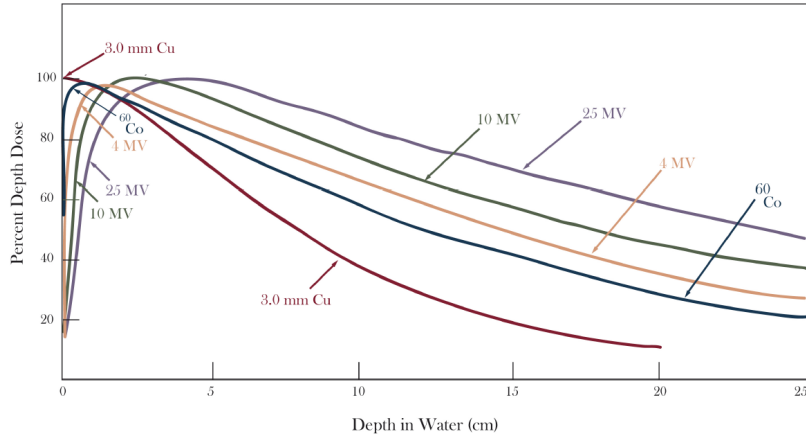


Figure 1.7: Relative dose release for different photon energies. Field size $10 \times 10 \text{ cm}^2$; source to surface distance (SSD) = 100 cm for all beams except for 3.0 mm Cu half-value layer (250 kV) ($SSD = 50 \text{ cm}$). It is possible to observe the dose build-up region, clinically known as the skin sparing effect.

principal way that charged particles lose energy in the materials is by Coulomb interaction in inelastic processes with the bound atomic electrons (ionizations and excitations) and atomic nuclei (bremsstrahlung). The particle creates a trail of ionizations and excitations along its path and through these processes the electron may lose its kinetic energy or change its direction of travel (scattering).

- The rate of energy loss by collisional losses (ionization or excitation) depends on the electron density of the medium and is greater for low atomic number Z . This happens both because high Z materials have a low electron density and because high Z materials have more tightly bound electrons, which are not available for this type of interaction. The energy loss rate first decreases and then increases with an increasing electron energy.
- The rate of energy loss by radiation losses (bremsstrahlung) is approximately proportional to the electron energy and to the square of the atomic number Z . This means that X-ray production is more efficient for higher energy electrons and absorbers with a higher atomic number.

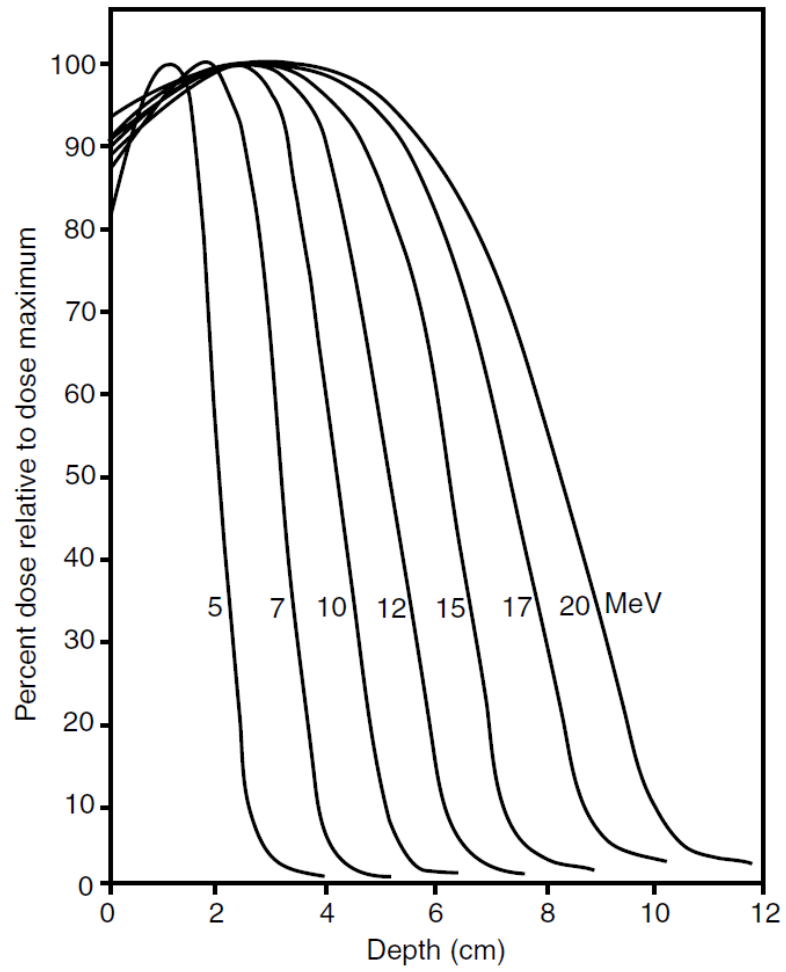


Figure 1.8: Typical central axis percentage depth-dose curves for beam energies from 5 MeV to 20 MeV

1.2.2.2 Protons and ions

Protons are charged particles and are relatively heavy compared to electrons. The rest mass of a proton is 1836 times the rest mass of an electron. Depending on their energy (i.e., their velocity), they interact with the medium through mechanisms as inelastic or elastic collision with the nucleus or with the bound atomic electrons.

Because of the strong electric force between protons and the atoms of a medium, these particles can be stopped by matter with relative ease. Especially compared to photons, protons release a great amount of energy in a shorter distance and they are stopped more rapidly. As the beam traverses the tissue, the dose deposited is approximately constant with depth until near the end of the range, where the dose peaks out to a high value followed by a rapid fall off to zero. The region of high dose at the end of the particle range is called the Bragg peak. Immediately after the Bragg peak, the proton beam stops completely and does not deposit any dose (Fig. 1.9).

The characteristic dose distribution makes protons very suitable for tumor treatment. If the selected proton energy has the Bragg peak corresponding to the tumor site, much of the energy is deposited in the tumor itself and the adjacent organs at risk are relatively spared. On the other hand, a very good dose calculation is needed to assure the tumor being irradiated properly.

In clinical practice, the raw peak is too narrow for clinical applications. One solution is to superimpose, during the irradiation, a certain number of peaks placed at various depths with a modulator to ensure a homogeneous coverage of the target volume. The resulting dose distribution takes the name of Spread Out Bragg Peak (SOBP, Fig. 1.10). With this approach, the dose at the surface will be increased relative to the peak of the SOBP and the skin dose could be higher than that caused by a high-energy photon beam, representing one of the principal limitations of the use of proton beams for therapy.

Recently not only proton therapy has rapidly developed, but also therapy with heavy ions (e.g., carbon ions) has gained attention. Compared to protons, carbon ions have the advantage of a higher biological efficiency due to a higher density of ionization at the end of their range. In other words, the Bragg peak in the dose distribution is even higher and the dose fall off is even steeper compared to protons. On the other hand, heavy ions have the disadvantage that beyond the Bragg peak the dose does not decrease to zero, showing a tail in the depth dose distribution.

A comparison between photons, electrons and protons percentage depth doses is shown in Figure 1.11.

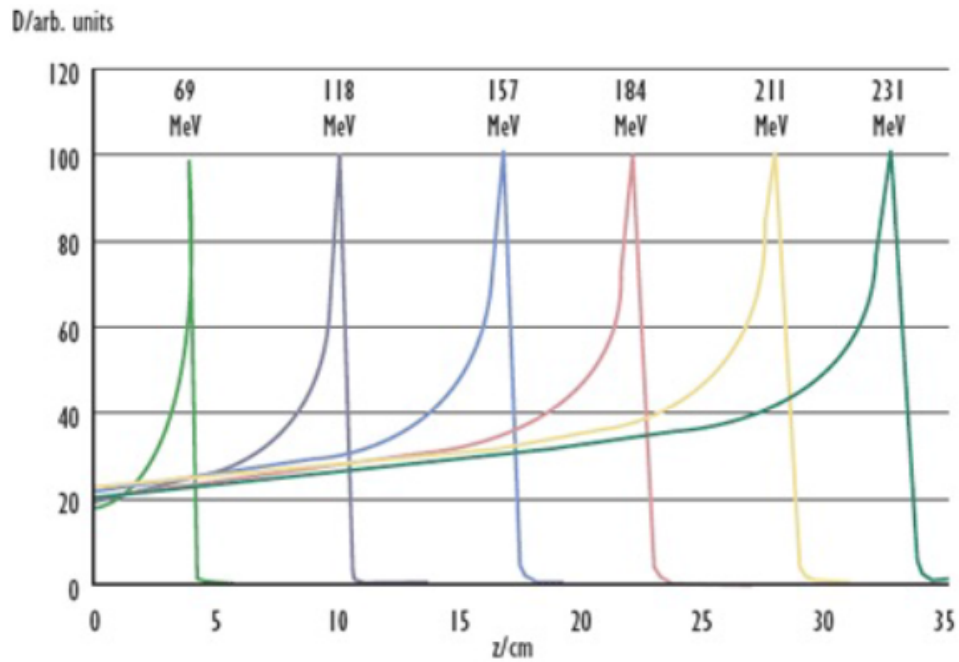


Figure 1.9: Percentage depth doses in water for proton beams at various energies

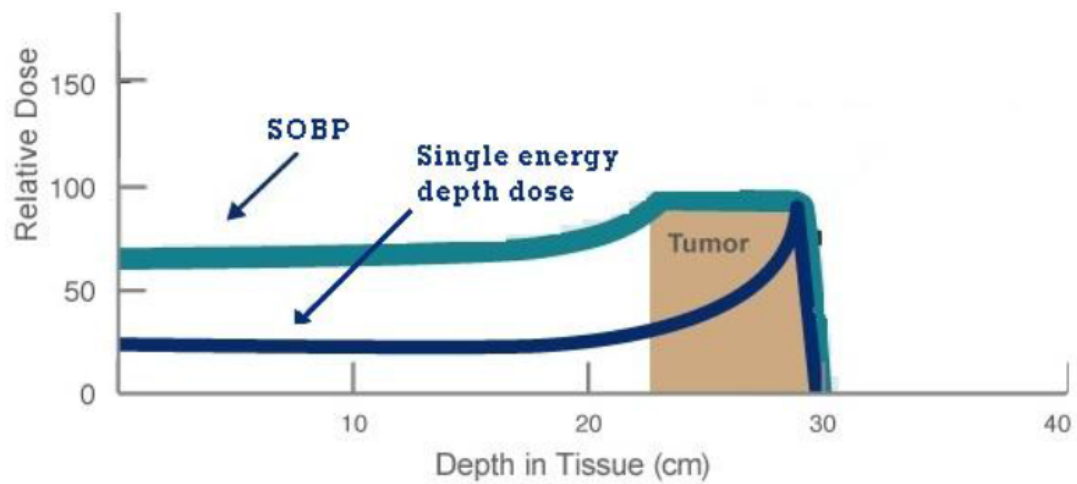


Figure 1.10: Comparison between the percentage depth doses of a spread out Bragg peak (SOBP) and a single proton beam

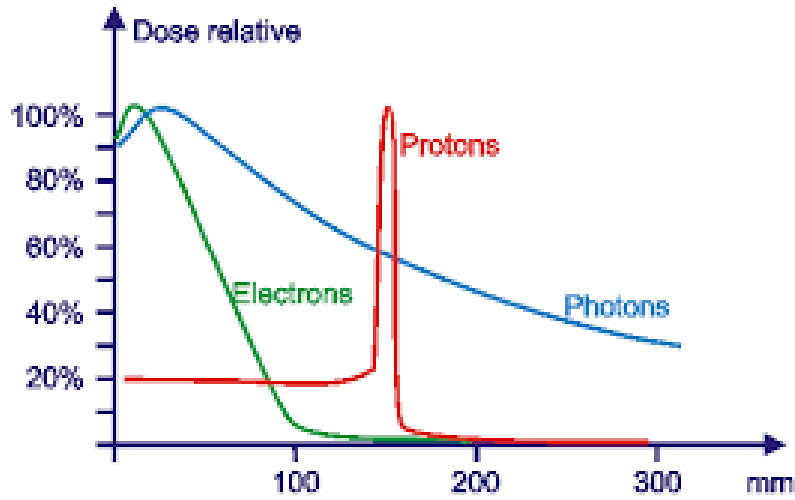


Figure 1.11: Relative dose as a function of the depth for different kinds of radiation

1.3 Biological mechanism of radiotherapy

1.3.1 Working principles

A beam of ionizing radiation that passes through biological matter gives rise to phenomena of interactions with the atoms, as previously described. During these processes, the radiation transfers a certain quantity of energy, typically higher than the binding energies of atoms and molecules, to the atoms. The energy transfer causes ionization and excitation of the atoms, enhancing their chemical receptivity and giving rise to reaction processes with consequent modifications of the structure of the molecules they belong to. In particular, when water (which is the most prevalent molecule within the cell) is irradiated, so called free radicals are created by radiolysis. Free radicals are highly unstable and react with other nearby molecules, therefore transferring chemical damage to them. All components of the cell may be damaged in this way, such as proteins, enzymes and so on, but a damage to most of them probably has little impact on the viability of the cell. But one cellular component is almost unique: DNA. Radiation damage may lead to modification of some of the genes that form the DNA and thus to loss of specific functions (some of which may be essential for survival). For this reason DNA is the most vulnerable part of a cell to radiation damage: even small changes in its composition may cause the loss of the colony-forming ability of the cell. In order to prevent this, cells have

very efficient repair processes, based on enzymes which are able to continually monitor the integrity of the DNA, recognize damage and repair it[6]. The radiosensitivity of cells varies considerably as they pass through the cell cycle. Cells are most sensitive during the mitosis phase, part of the cell reproduction cycle. This is probably due to the fact that at that moment cells have little time to repair radiation damage before being called upon to divide. The main features of tumor cells that make radiotherapy a successful cancer treatment are their faster speed to reproduce and their reduced ability to repair DNA damage compared to most healthy tissue cells. Unrepaired DNA damages accumulate in cells that reproduce, finally leading to cell death. The action of ionizing radiation on biological structure can be divided in four stages: physical, physical-chemical, chemical and biological stages, characterized by very different times.

- Physical stage: this is the first stage of the energy transfer to the biological system. The interactions of the radiation with the atoms cause the ejection of one or more atomic electrons, producing secondary ionizations due to subsequent chemical transformations. The ionization density that is generated along the path of the charged particles is described by the Linear Energy Transfer (LET), defined as the mean energy delivered by the primary and the secondary charged particles over a distance of $1\mu\text{m}$.
- Physical-chemical stage: the absorption of energy from ionizing radiation produces damage to molecules by direct and indirect actions. Direct action involves the ionization of atoms on key molecules that causes inactivation or functional alteration of the molecule. Indirect action involves the production of reactive free radicals, neutral atoms or molecules characterized by the presence of an unpaired electron in the external orbit that causes a very high chemical receptivity. Direct effect is the predominant cause of damage in reactions involving high LET radiation (i.e., alpha particles, neutrons, protons and heavy ions) whereas indirect action is predominant for low LET radiation, like photons.
- Chemical stage: during this stage reactions involving free radicals occur, provoking the formation of molecules with abnormal structures.
- Biological stage: during the last stage, formation of injuries on all levels occurs. This involves transformations in cell structures and functions and mutations of the

chromosomal content of the cells that may prevent further cell reproduction and lead to cell death.

1.3.2 Stochastic nature of energy deposition

The absorbed dose arises from the deposition of energy in matter by radiation tracks. This is an inherently random process. Figure 1.12 shows the amount of energy E , being deposited in ever decreasing volumes of mass m centred on the same point in a uniform medium, for series of irradiations of identical duration[6]. For large volumes, E/m has the same value each time; below a certain value of m , fluctuations start to appear which increase as m decreases. Energy is deposited through interactions with particles along the tracks. When the volume gets small enough, it may contain only few or even no particles along the tracks, while others still contain many. Therefore, in the same fluence condition, at some size of the elementary volume the randomness of energy deposition will become apparent.

At large values of m E/m is not constant either. At that point, the path length becomes comparable with the mean free path for radiation interactions. For this dissertation, this is not relevant.

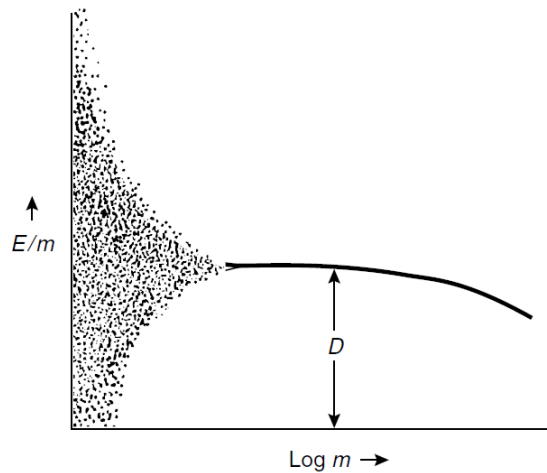


Figure 1.12: Energy deposited per unit mass, plotted against the mass, m , of the scoring volume, as this volume is gradually changed in size for a given incident radiation fluence. The shaded portion represents the range where statistical fluctuations become important as the volume (i.e., the mass) is getting smaller

1.3.3 Dosimetric units and parameter

The most important unit in radiation dosimetry is the absorbed dose D , defined as

$$D = \frac{d\bar{\epsilon}}{dm} \quad (1.10)$$

where $d\bar{\epsilon}$ is the mean energy imparted by ionizing radiation to matter of mass dm . The unit of absorbed dose is the Gray [Gy], or Joule per kilogram [$J \cdot kg^{-1}$].

The *kerma* (kinetic energy released to the matter), labelled with K , is the quotient dE_{tr} by dm , where dE_{tr} is the sum of the initial kinetic energies of all the charged ionizing particles liberated by uncharged ionizing particles in a material of mass dm :

$$K = \frac{dE_{tr}}{dm} \quad (1.11)$$

The unit of kerma is identical to the one for absorbed dose (Gy or $J \cdot kg^{-1}$). In contrast to absorbed dose, kerma applies to indirectly ionizing radiation, like photons, only.

The equivalent dose H is a dose quantity to represent the probability of cancer induction and genetic damage. It is based on the absorbed dose, but takes into account the biological effectiveness of the radiation, which is dependent on the radiation type and energy:

$$H_T = \sum_R W_R \cdot D_{T,R} \quad (1.12)$$

T denotes a specific tissue, $D_{T,R}$ is the absorbed dose deposited in tissue T by radiation type R and W_R is the radiation weighting factor.

The effective dose E is the tissue-weighted sum of the equivalent doses in all specified tissues and organs of the body and represents the stochastic health risk, which is the probability of cancer induction and genetic effects of ionizing radiation delivered to the body:

$$E = \sum_T W_T \cdot H_T \quad (1.13)$$

W_T is the tissue weighting factor and H_T is the equivalent dose delivered to tissue T . To obtain the total effective dose, it is necessary to sum over all irradiated tissues. The unit of effective dose is Sievert [Sv], which corresponds to 1 Joule per kilogram [$J \cdot kg^{-1}$]. Although this unit is identical to the one of absorbed dose, its meaning is different.

1.3.4 Cell survival curves

The aim of radiotherapy is to kill tumor cells by irradiation, while healthy tissue cells should be able to withstand, at least at a percentage, in order to avoid compromise in organ functionality. In order to quantify this, cell survival curves are introduced. A cell survival curve shows the relation between the deposited dose (or a generic cell-killing agent) and the fraction of surviving cells. When plotted on a linear scale, the survival curve for cells irradiated in tissue culture is often sigmoid. In practice, cell survival curves are generally plotted on a logarithmic scale, because this allows effects at a very low survival levels to be shown and compared more easily, which is very important because the cure of a tumor requires many orders of magnitude of cell kill.

The type of radiation (high or low Linear Energy Transfer, LET) plays a role in defining the shape of the survival curve: for high LET radiation, the curve turns out to be much steeper (Fig. 1.13). Other important factors which influence the cell's radiosensitivity are the phase of the cell cycle (as reported in section 1.3.1), its oxygenation level and the fractionation of the delivered dose.

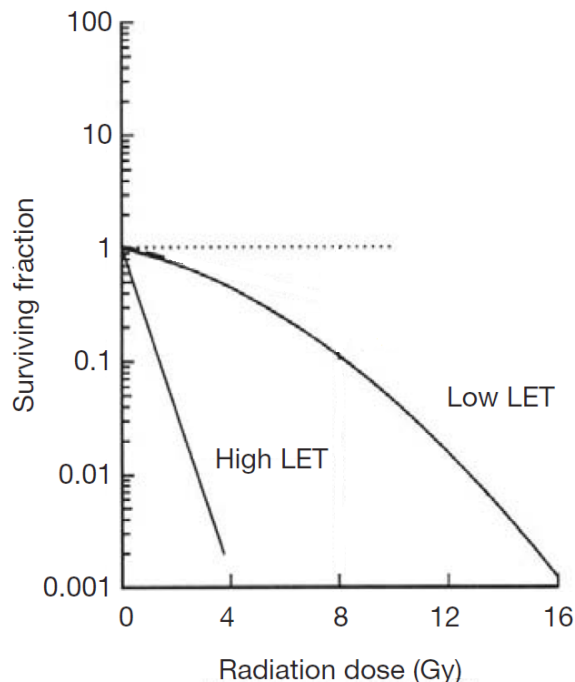


Figure 1.13: Typical cell survival curves for high LET (densely ionizing) radiation and low LET (sparsely ionizing) radiation

1.3.4.1 Oxygenation

The response of cells to ionizing radiation is strongly dependent upon oxygen. With a higher level of oxygen, more free radical reactions will occur, leading to more DNA damage. The impact is similar at all levels of the survival curve (Fig. 1.14).

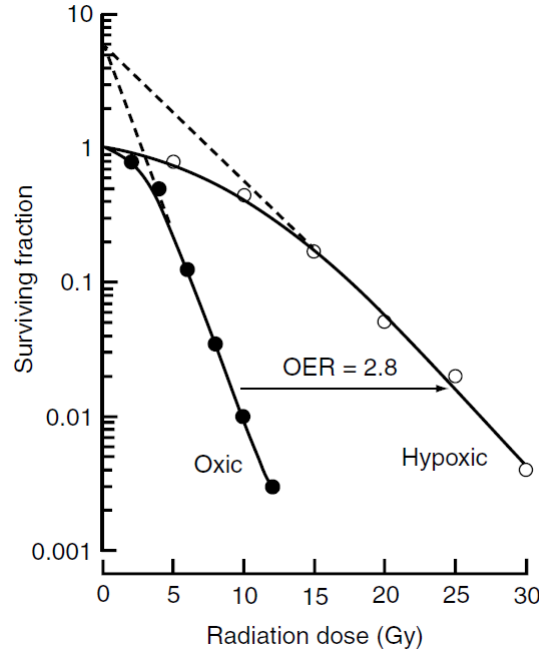


Figure 1.14: Survival curves for cultured mammalian cells exposed to x-rays under oxic or hypoxic conditions. The shown oxygen enhancement ratio (OER) represents the ratio of the doses in hypoxia and in air needed to achieve the same biological effect

1.3.4.2 Fractionation

A basic schedule of a radiotherapy treatment consists of irradiating the tumor with a given total dose D , divided in n fractions of a certain amount of dose d , that are administered with a certain frequency in a specific period of time t . The response of the treatment is strongly dependent on this schedule.

Fractionation guarantees a discrimination between tumor and normal tissue cells. By delivering the total dose in n fractions, normal tissues may generally be spared to a larger extent, because during the time between subsequent fractions repair of sublethal damage is enabled. As previously described, normal tissue cells have a faster repair

mechanism than tumor cells. Furthermore, fractionation increases the amount of damage to the tumor because it allows re-oxygenation between fractions, due to revascularization processes. The cell survival curve for tumoral and normal cells is shown in Figure 1.15 as a function of the number of fractions.

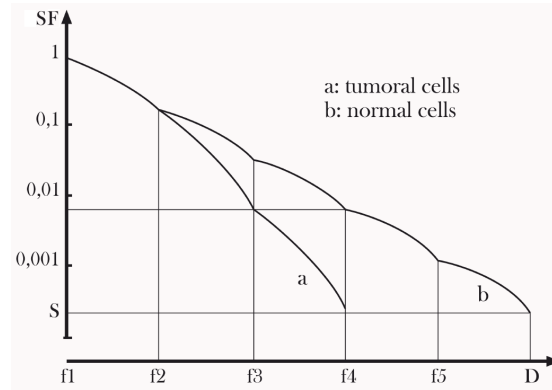


Figure 1.15: Surviving fraction of tumoral and normal cells as a function of the number of fractions

Many schedule for fractionation have been proposed. Most frequently, radiotherapy treatment schedules are based on a dose of 2 Gy per fraction, delivered once a day, except during weekends. But also hyperfractionation (i.e., with a reduced dose per fraction and increased numbers of fractions, generally delivered twice a day), hypofractionation (i.e., with a larger dose per fraction and a smaller number of fractions, delivered in a shorter overall time) and accelerated fractionation (i.e., with a conventional dose per fraction, but a reduced overall treatment time, e.g., by irradiation during weekends as well) have been clinically applied, with different benefits and drawbacks. The choice of fractionation schedule is often highly dependent on whether radiotherapy is used with curative intent or to reduce complaints of the patients (i.e., palliative intent) and whether other modalities (i.e., surgery or chemotherapy) are included in the radiotherapy treatment as well.

1.4 Radiotherapy workflow

In the generation of a radiotherapy treatment plan, many steps are involved. All stages have to be properly analyzed and performed, in order to achieve the best feasible solution. Any fault in one of the steps could compromise the success of the whole process.

In Figure 1.16 the so called chain of radiotherapy is shown[6].

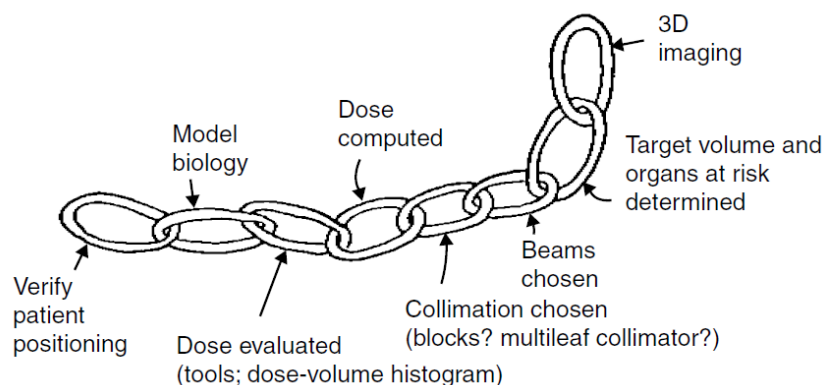


Figure 1.16: The chain of processes leading to conformal radiotherapy and illustrating that the physical basis of radiotherapy depends on good performance at each state

1.4.1 Aim of radiotherapy

As mentioned before, the purpose of radiotherapy is to deliver sufficiently high dose to the tumor while minimizing damage to surrounding healthy tissues. It is usual to talk about optimizing the so-called therapeutic ratio, i.e., finding the best balance between trying to ensure that all tumor cells receive a lethal dose of radiation and that acute and late effects in normal tissues are tolerable. To evaluate the therapeutic ratio, generally the tumor control probability (TCP) and normal tissue complication probability (NTCP) are used. TCP and NTCP are mathematical models, describing the probability of complete tumor eradication and any complication resulting from the radiotherapy treatment, respectively. Both concepts are referring to probability, because the sensitivity to ionizing radiation is different from one person to another. TCP and NTCP are sigmoid curves (Fig. 1.17) and the aim is to deliver a dose distribution that results in a TCP close to 1, while NTCP remains at a low value. It is important to keep in mind that any changes to the treatment regimen (e.g., fractionation, concurrent chemotherapy, and so on) affect the therapeutic ratio and have to be properly evaluated.

In general, the radiotherapy intent can be curative or palliative. In the first case, the objective is the destruction of all clonogenic tumor cells (i.e., cells characterized by the ability of colony forming). For this aim, radiotherapy is often combined with other

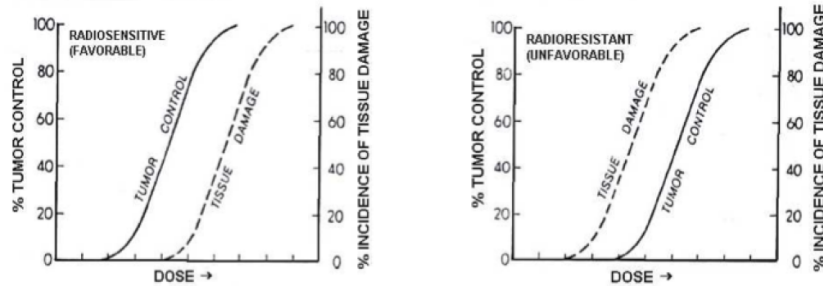


Figure 1.17: TCP and NTCP curves

treatments such as chemotherapy and surgery. In palliative treatment the aim is to reduce or eliminate eventual symptoms of the disease such as pain, bleeding and compression given by the tumor mass expansion. This kind of treatment is applicable when a definitive treatment is not possible (e.g., because tumor cells were spread throughout the body), mainly aiming at an improvement of the patient's quality of life.

1.4.2 Positioning

An important issue in the radiotherapy process is the ability to reproduce accurately the same patient position throughout the treatment and to keep the patient still during each fraction. This fixed position must be decided upon before acquisition of the 3D image set of the patient (cf. 1.4.3). The option to use optimal beam directions for treatment without risk of collision with the treatment machine or accessories should carefully be considered. Positioning accessories or immobilization devices (for instance thermoplastic casts) are often used to achieve a high accuracy and reproducibility in patient position during each treatment session. Before acquisition of the imaging data, tattoos or other skin marks are often placed as a reference for patient positioning, to be used in combination with the projection of lasers in the treatment room, coinciding at the treatment isocenter.

In lung cancer treatment, patients are generally positioned supine with their arms immobilized above their head in a comfortable arm support. The patient holds on to a T-bar device with their elbows supported laterally. A knee support enables a more comfortable, and therefore reproducible, set-up (Fig. 1.18).



Figure 1.18: Immobilization for thoracic radiotherapy with a T-bar, lateral elbow supports and a knee rest. Laser lights are used to prevent rotational set-up errors. Picture from [9].

1.4.3 Imaging

Once the patient positioning is defined, it is important to get 3D image information of the patient, which is required to define the exact shape, position and electron density of the tumor and the organs at risk. The ideal imaging modality should be well-tolerated and atraumatic for the patient, quick (in order to minimize adverse effects of movements), and should have a high resolution and a good contrast between different soft tissues, lungs and bones.

For radiotherapy, the default image acquisition technique is Computed Tomography (CT). CT is able to give anatomical information about the patient by measuring the absorption of X-rays photon beams from a continuous rotation. For CT generally photons of about 100 keV are used. As previously discussed (cf. 1.2.1), for this energy the Compton effect is the dominant interaction process, showing an attenuation that varies propor-

tionally to the electron densities of the tissues and obtaining a spatial distribution of the tissues absorption coefficients. As described in section 1.2.1.6, thickness is the feature that mainly influences absorption, but, for equivalent thicknesses, the more the attenuation, the higher the electron density. Besides CT scans, other imaging techniques such as the Magnetic Resonance Imaging (MRI) or Positron Emission Tomography (PET) are used as aid for volume definition. Some of these scans may give additional information about the metabolic processes in the cells, enabling the identification of tumor masses that are characterized by high reproducibility rate or which are well oxygenated. Especially a MRI scan often has a better contrast than a CT scan. Nevertheless, a CT scan is still routinely used for treatment planning because, in contrast to MRI and PET images, the pixel values (expressed in Hounsfield units) are proportional to electron densities, which are required for an accurate dose calculation.

1.4.4 Volumes definitions

Once that the image acquisition is completed, the next step consists of delineation of the tumor and normal tissues volumes. This task is mainly performed by a physician or a trained dosimetrist following specific protocols (International Commission on Radiation Units (ICRU) published recommendations Report 50 [1993], 62 [1999] and 83 [2010]). After completion, a structure set containing at least the following volumes is defined:

- **Organs at Risk (OARs):** these structures are critical normal tissues whose radiation sensitivity may significantly influence treatment planning and/or prescribed dose. In some cases, it is necessary to add a margin which is able to take into account uncertainties in daily patient positioning and/or changes in position and shape of those organs during treatment delivery, yielding a Planning Organ at Risk Volume (PRV). In lung cancer treatment, the main OARs to be considered are the healthy lung tissues, spinal cord, esophagus, heart and plexus.
- **Gross Tumor Volume (GTV):** this volume corresponds to the primary tumor volume. In some cases, it can be useful or necessary to support the anatomical imaging technique (i.e., CT) with a functional one (like PET). GTV always contains the highest tumor cell density and is absent after complete surgical resection.
- **Clinical Target Volume (CTV):** CTV contains the GTV and subclinical microscopic

disease that has to be eradicated to cure the tumor. Generally, subclinical disease is too small to be identified as tumor cells in 3D imaging, but from literature it is known to what regions cells from the GTV may expand. The margin between GTV and CTV is derived by many aspects, such as histological examination, biological characteristics of the tumor, local recurrence patterns and the experience of the radiation oncologist. Variation in CTV delineation by the clinician is the greatest geometrical uncertainty in the whole treatment process.

- **Planning Target Volume (PTV):** due to changes in patient positioning and/or in position and size of specific organs, both during a treatment fraction and in between fractions, the position of the CTV may also change. Therefore, in order to ensure a homogeneous dose delivery to the whole CTV throughout a fractionated treatment, an additional margin is generally added around the CTV itself. This margin has to take into account physiological organ motions (internal margin, which identifies the Internal Target Volume, or ITV) and possible variations in patient positioning and beam alignments (set-up margin). Internal margin has to contemplate organ and tumor motion. Variations in organ motion may be small (e.g., in the brain), larger and predictable (e.g. respiration or cardiac pulsation), or unpredictable (e.g., due to rectal and bladder filling). In lung cancer treatment, CTV-PTV margin has to take into account all possible positions of the CTV during a respiratory cycle. To reduce this safety margin, it can be useful to suspend patient respiration with a technique such as the active breathing control (ABC) device. During a fractionated course of radiotherapy, variations in patient position and in alignment of beams will occur both during and in between treatment fractions. To take this into account, a margin for set-up errors is incorporated in the CTV-PTV margin as well. Errors may be systematic or random.

A schematic representation of the volumes defined by ICRU reports is shown in Figure 1.19. The target volumes delineation for a lung cancer patient is shown in Figure 1.20.

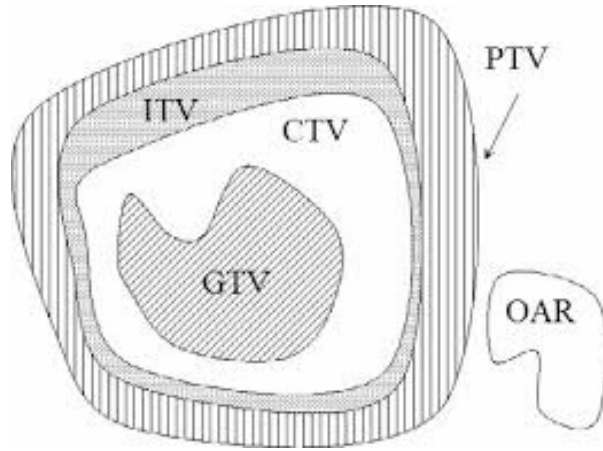


Figure 1.19: Schematic representation of the volumes defined by ICRU reports

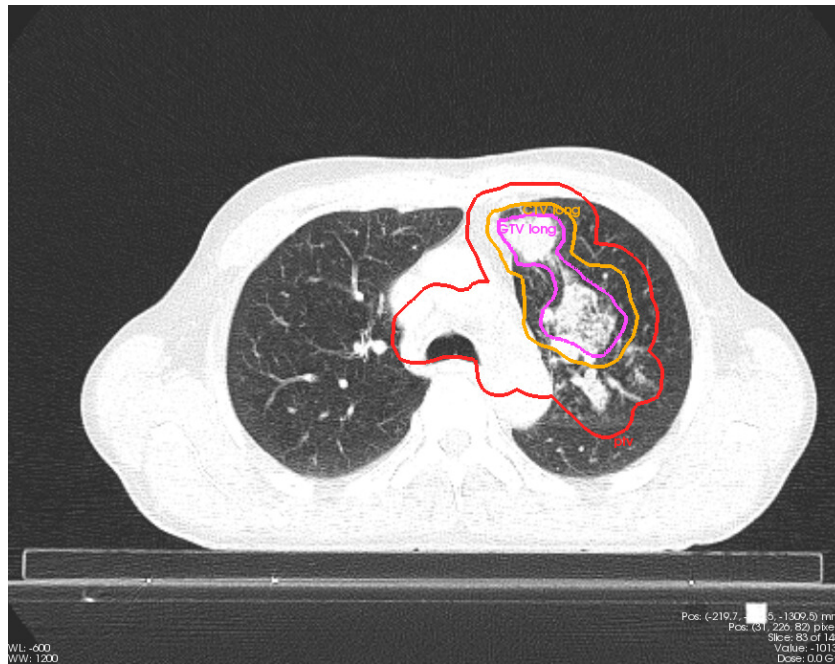


Figure 1.20: Target volumes delineation in a lung cancer patient

1.4.5 Forward and inverse planning

Plan generation can be performed following two different strategies. In forward planning, the dosimetrist places beams in a treatment planning system by choosing the number of beams, beam orientations and weights. Generally each beam is shaped according to the projection of the PTV. This technique has been used for years, but has

little possibilities to tightly shape the high dose volume around the PTV and minimize the dose in organs at risk. To improve plan quality, more sophisticated delivery techniques, like Intensity Modulated Radiation Therapy (IMRT) and Volumetric Modulated Arc Therapy (VMAT) have recently become available (cf. 1.5.2.2 and 1.5.2.3). It is hardly possible to plan those techniques with a forward, manual technique, so in the majority of cases an inverse planning technique is applied, in which the computer tries to get a treatment plan that best satisfies the prescription of the user. So, this planning strategy requires specification of the dose to be delivered in the GTV, CTV, PTV and OARs, in terms of various constraints.

But also inverse planning generally involves a trial-and-error process. It is not straightforward to define planning constraints that are realistic (but sufficient challenging) for a specific patient, so often several attempts will be required to get an acceptable plan (Fig. 1.21). This means that for treatment planning still quite some time is required. Furthermore in the end it is still very difficult to assess whether the quality of the obtained plans can still be improved. This makes that the final plan quality is partly determined by the dosimetrist's experience and by the available time to generate the plan.

1.4.6 Evaluation

Before the delivery, the treatment plan requires a careful evaluation by a radiation oncologist who has the task to assess whether the derived plan is adequate for treatment. The plan has to fulfill a list of clinical requests relating to a proper coverage of the tumor by the high dose region and a satisfactory sparing of OARs. This clinical list is strongly related to the treatment modality (such as prescribed dose, fractionation and so on); an example for lung cancer treatment can be found in section 3.2.2.

Many factors contribute to a proper evaluation of a radiotherapy treatment plan. Some of them are strictly quantitative, while others can be more patient-specific: for instance, for patients with a very low pulmonary function, more strict criteria on healthy lung sparing may be required, even at the cost of worse target coverage.

- Dose Volume Histograms (DVH) are used to condense and display the 3D dose delivery to an organ in a graph. A differential DVH shows *the summed volume of elements receiving dose in a specified dose interval, against dose*. Generally, it is

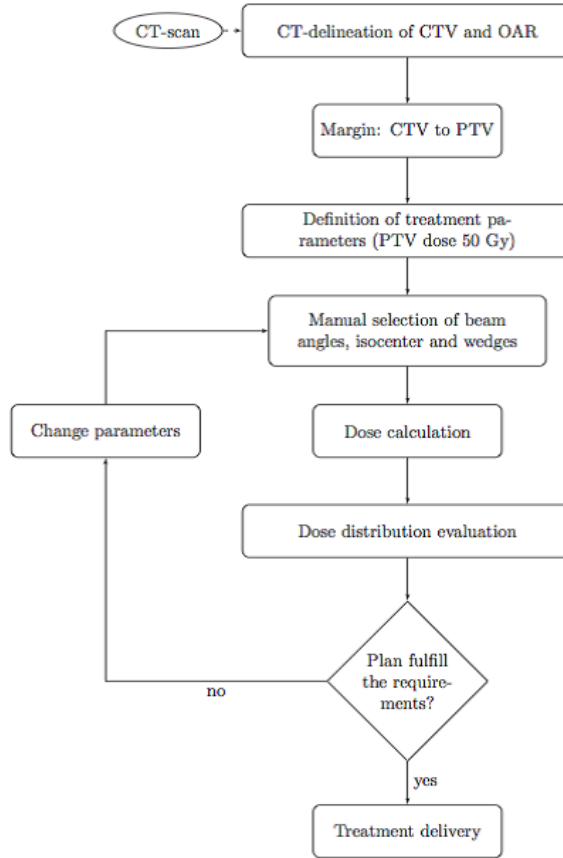


Figure 1.21: Diagram of the trial-and-error process involved in manual planning

more common to use cumulative dose volume histograms in which *the total volume receiving a dose greater than, or equal to, a given dose is plotted against dose*. Usually volumes are expressed as a percentage of the total volume. It is important to realize that in a DVH positional information is lost (e.g., it is unknown in which part of the volume the highest dose is delivered). Therefore, the display of DVHs and the delivered dose in each of the CT slices are usually used in conjunction with each other during treatment plan evaluation. For the PTV, the DVH should show a uniform high dose delivery in the volume; i.e., preferably, the shape should be a step function around the prescribed dose. DVHs for organs at risk should preferably have a concave appearance: it may be generically acceptable either to deliver a relatively high dose to a small volume or a low dose to a large volume.

Through the use of DVHs it is straightforward to define dose volume reference points: these parameters are points on the DVH curve and are usually expressed as $V_{D_{ref}}$, where D_{ref} represents a dose expressed in Gy or a percentage of the prescribed dose. For instance, V_{5Gy} indicates *the percentage of the total volume which receives a dose greater than, or equal to, 5 Gy*, while V_{95} is *the percentage of the total volume receiving a dose greater than, or equal to, 95% of the prescribed dose*. It is sometimes useful also to define reference points as $D_{V_{ref}}$ which indicates the dose delivered to a volume equal to or greater than V_{ref} (expressed as percentage of the total volume of the structure). In addition, it is straightforward to evaluate whether the dose in an OAR does not exceed a specified maximum tolerable dose level (e.g., 50 Gy for the spinal cord). A typical example of cumulative DVH for lung cancer is shown in Fig. 1.22.

- Conformity Index (CI): conformity is an important feature of a treatment plan which can be used to evaluate to which extent the high dose volume is limited (i.e., conformed) to the tumor shape. A conformal plan does not present hot spots, i.e. points with a high dose, far from the border of the target. Many conformity indexes have been introduced; the most common is defined as the ratio between the absolute V_{95} in the whole patient and the volume of the PTV. If $CI = 1$ and the high dose is only in the PTV the conformity is optimum; $CI < 1$ indicates an underdosage in parts of the PTV; $CI > 1$ shows that the high dose volume is extending outside the PTV, causing potential damage to healthy tissues. More refined conformity indexes able to consider the location of the high dose were introduced.
- Homogeneity Index (HI): the homogeneity index is intended to represent the level of homogeneity of the dose delivered to the target. It is defined as

$$HI = (D_{2\%} - D_{98\%})/D_{50\%} \quad (1.14)$$

In the ideal situation, $HI = 0$.

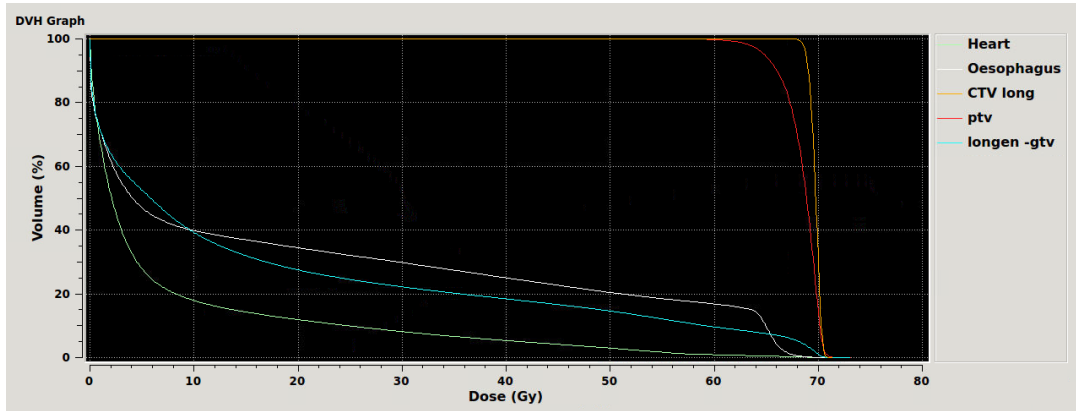


Figure 1.22: Example of Dose Volume Histogram for a lung cancer patient

1.4.7 After radiotherapy treatment: follow up and complications

During the months after the radiotherapy treatment, patients are regularly checked by the physician to evaluate the tumor response to the treatment and to take care of possible side effects. Complications are strongly connected to treatment modality and involved sites; most common mid-term side effects are related to skin (such as, very dry skin, darker appearance or different feeling to touch), hair (different hair color or texture in the treated area, hair loss), development of red spidery marks on your skin (telangiectasia) caused by small broken blood vessels, and loss of tissues elasticity. For lung cancer treatment the most relevant side effect is pneumonitis, which appears three to six months after irradiation.

Follow-up cancer care involves regular medical checkups that include a review of a patient's medical history and a physical exam. Follow-up care may include imaging procedures, endoscopy, blood work, and other lab tests. Follow-up care is important because it helps to identify changes in health. The purpose of follow-up care is to check for recurrence (the return of cancer in the primary site) or metastasis. Follow-up care visits are also important to help in the prevention or early detection of other types of cancer, to address ongoing problems due to cancer or its treatment, and check for physical and psychosocial effects that may develop months to years after treatment ends[8].

1.5 External beam radiotherapy: radiation delivery

In external beam radiotherapy (EBRT) beams of ionizing radiation are produced outside the patient and directed towards the tumor.

1.5.1 Photon beam production

Photon beams are generated by a linear accelerator (linac, Fig. 1.23(a) and 1.23(b)). An electron gun is the source of electrons that are to be accelerated. The electrons are obtained from a heated cathode by the process of thermoionic emission and are accelerated by interaction with an electromagnetic field. The electrons are then focused onto a high-atomic-number target (often tungsten), where they lose their energy by bremsstrahlung radiation. At megavoltage energies, the principal directions of bremsstrahlung emission is the forward direction, so it is often necessary to bend the electron beam before the target is reached. The obtained X-ray beam, which is generically characterized by a maximum extension of about $40 \times 40 \text{ cm}^2$, is then collimated by a multi-leaf collimator (MLC) which enables modelling the beam with various shapes (Fig. 1.23(c)). The MLC has up to 80 pairs of leaves that can move independently, allowing any beam shape to be produced subject to the width of the leaves (generally $0.5 - 1 \text{ cm}$).

The challenge for accelerator design is to produce a stable (nearly) monoenergetic high current electron beam concentrated onto a small focal spot, ensuring the production of a sharply focused X-ray beam.

1.5.2 Main delivery modalities

1.5.2.1 3D Conformal Radiation Therapy (3DCRT)

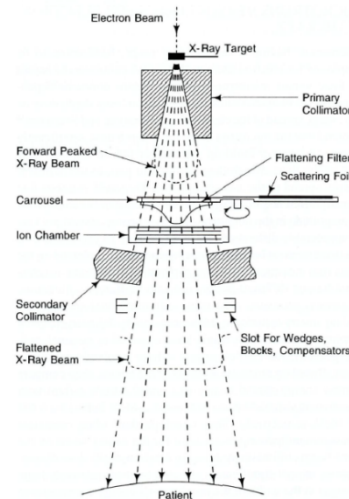
Treatments are based on a 3D CT scan and a 3D delineation of the tumor and OARs. Beam profiles are flat (i.e., uniform intensity over the field) or rather simply shaped by a standard wedge.

1.5.2.2 Intensity Modulated Radiation Therapy (IMRT) - Step and shoot

IMRT is frequently used in EBRT. IMRT allows a better control of the delivered dose, by varying the intensity within the treatment beam (fig. 1.25). Thanks to the use of



(a)



(b)



(c)

Figure 1.23: Operating scheme of a linac and MLC

the MLC, each treatment field can easily be divided in different subfields, characterized by a different shape, position and intensity. Compared to 3DCRT, this allows to better shape the dose delivery and to obtain a dose distribution which turns out to be more conformal to the target volume and with a steeper dose fall-off towards organs at risk. This is very important when treating tumors very close to sensitive organs at risk.

IMRT is usually delivered in step-and-shoot modality. A certain number of beam orientations, typically between five and nine for lung cancer patients, are selected by the dosimetrist. The treatment beam is switched off while changing from one subfield to the other and while changing to the next treatment beam (i.e., no dose is delivered while the MLC or gantry is moving). Due to the very large number of optimization parameters in IMRT, inverse planning is generally used for treatment planning (cf. 1.4.5).

A comparison between 3DCRT and IMRT dose distributions for cancer treatment in the pelvic region is shown in Figure 1.24.

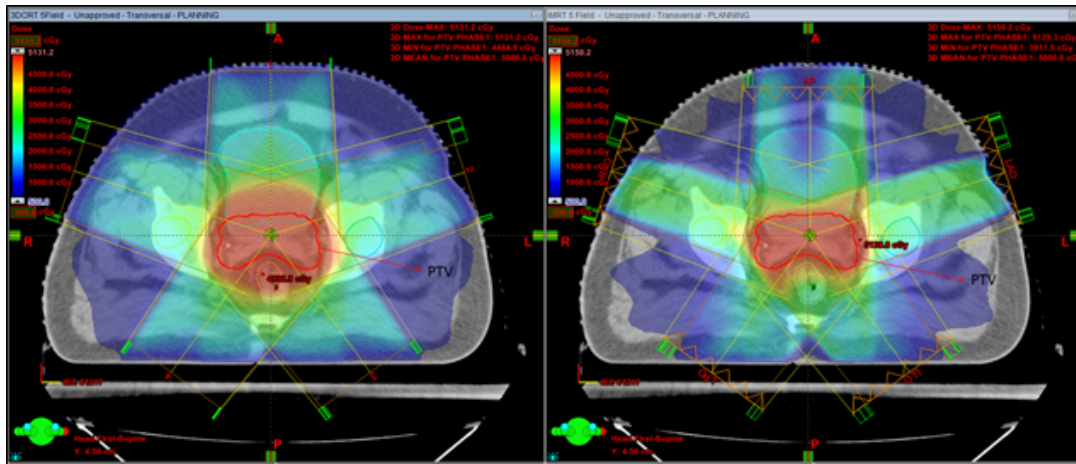


Figure 1.24: Comparison between 3DCRT (left) and IMRT (right) dose distributions for cancer treatment in the pelvic region. The figure shows how intensity modulation of the beams affects the shaping of the high dose regions. Reported by Ekambaran et al., 2014[10].

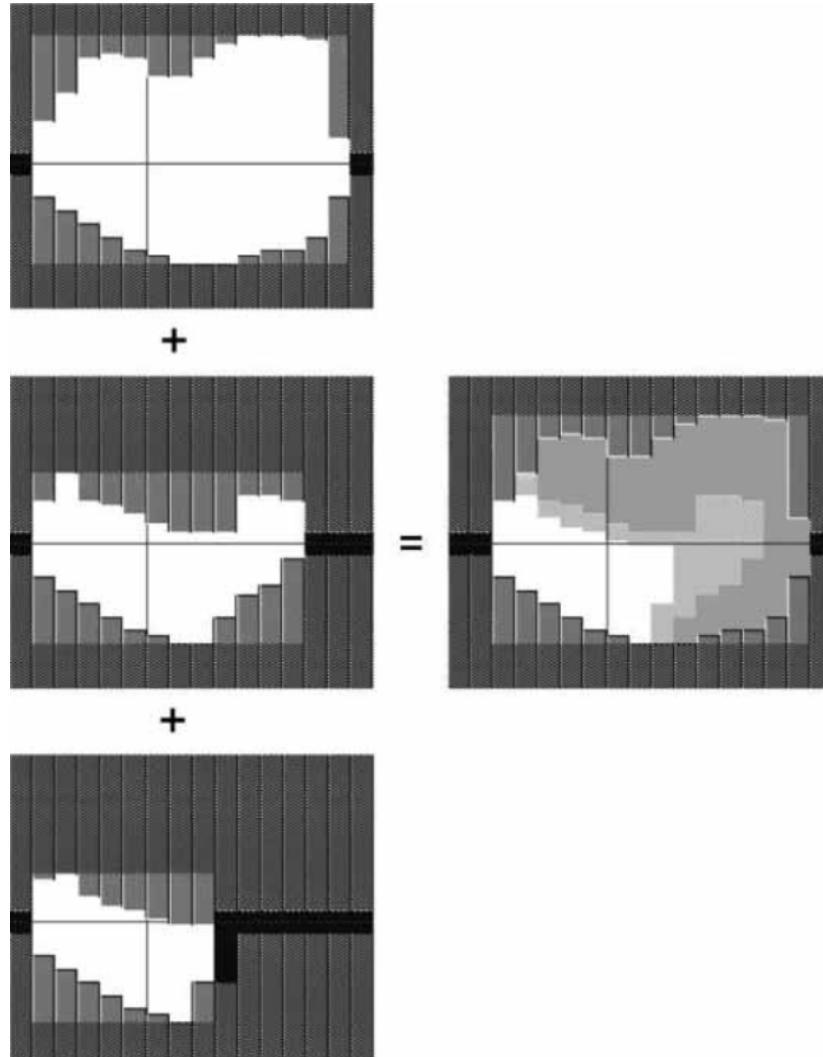


Figure 1.25: Intensity modulation by superposition of MLC shaped fields from the same directions. Vertical gray bars symbolize the tungsten leaves, white area in the centers symbolizes the exposed area of the field. On the right, total intensity levels are symbolized by gray values. White = high total intensity, dark = low intensity

1.5.2.3 Volumetric Modulated Arc Therapy (VMAT)

As an alternative for IMRT, VMAT is often used. With VMAT radiation beams sweep in uninterrupted arc(s) around the patient (Fig. 1.26), thereby allowing the delivery of a very conformal treatment plan in a shorter delivery time than with IMRT (about 8 minutes instead of 20 minutes for lung cancer treatments). VMAT employs a dynamic generation of intensity modulated fields: this means that the leaves of the MLC move continuously during the dose delivery, allowing an infinite number of subfields. A disadvantage of VMAT might be that in general a larger volume is treated to a low dose. But for most tumor sites, this seems to be irrelevant. Due to the higher complexity level, the optimization and calculation of the final dose distribution often takes longer than for the other techniques, making a trial-and-error procedure even more time-consuming.



Figure 1.26: VMAT treatment

1.5.2.4 Stereotactic radiotherapy and Cyber Knife

Stereotactic radiotherapy is a specialized high precision type of external beam radiation therapy. Many non-coplanar photon beams are used to deliver a prescribed dose in a very localized lesion with a very steep dose fall-off. The Elekta CyberKnife is a machine developed for stereotactic treatment with a linac mounted on an industrial robotic arm (Fig. 1.27). The CyberKnife is able to deliver photon beams from a lot of different and even non-coplanar directions, yielding an increased degree of freedom for generating optimal dose distributions.



Figure 1.27: CyberKnife radiosurgery system

1.6 Other cancer treatment modality: brachytherapy and chemotherapy

1.6.1 Brachytherapy

The word *brachy* originates from the Greek word for *short*. So, brachytherapy can roughly be translated as *short-distance therapy*. A radioactive material is inserted directly into or next to a tumor and concentrates the dose there, with a rapid fall-off. This delivery mode has many physical and biological advantages because it makes possible to deliver a high dose to the tumor and a substantially lower dose to the surrounding tissue, due to the inverse square law that regulates the dose fall-off. The disadvantages

of brachytherapy are that an operative procedure is often needed to access the tumor, skilled personnel is required, and specific radiation protection measures has to be taken to protect patient, staff and general public. Moreover, brachytherapy can only be used for relatively small tumors. Brachytherapy is considered whenever possible for accessible localized, small tumors. It is contraindicated when the tumor infiltrates bone, when the margins of the tumor or target volume cannot be clearly identified and when there is an active infection in the tissues.

The application of so-called “seeds” (Fig. 1.28) can be temporary or permanent and the decision is taken by evaluating many aspects, such as the type of source, the shape of the tumor and the possibility to reach an optimal source localization. Alternatively, a source of low-energy gamma photons (e.g., iridium) can be inserted in or near the target through a set of inserted needles.

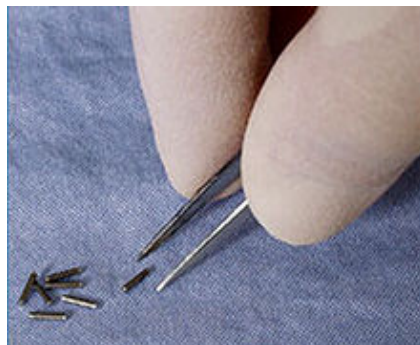


Figure 1.28: Seeds for brachytherapy

1.6.2 Chemotherapy

Chemotherapy is a cancer treatment based on chemical drugs. It is often applied when there is a high risk that tumor cells may be spread to other parts of the body. The intent can be curative or palliative. Chemotherapy is often adopted as part of a wider therapy which can also involve radiotherapy. In this case it is used to talk about concurrent chemotherapy, when the therapy is administered contemporarily to the radiation delivery, and sequential chemotherapy, when one therapy follows the conclusion of the other. Chemotherapy plays an important role in the selection of the treatment regimen.

Chapter 2

Lung cancer and treatment planning

2.1 Lung anatomy and lung cancer features

The lungs are a pair of spongy, air-filled organs located on either side of the chest (thorax). The trachea (windpipe) conducts inhaled air into the lungs through the bronchi, which then divide into smaller and smaller branches (bronchioles), finally becoming microscopic. The bronchioles eventually end in clusters of microscopic air sacs called alveoli. In the alveoli, oxygen from the air is absorbed into the blood. Carbon dioxide, a waste product of metabolism, travels from the blood to the alveoli, where it can be exhaled. Between the alveoli there is a thin layer of cells called the interstitium, which contains blood vessels and cells that help support the alveoli. The lungs are covered by a thin tissue layer called the pleura. The same kind of thin tissue, lining the inside of the chest cavity, is also called pleura. A thin layer of fluid acts as a lubricant allowing the lungs to slip smoothly as they expand and contract with each breath[11] (Fig. 2.1).

There are two major types of lung cancer:

- Small cell lung cancer (SCLC)
- Non-small cells lung cancer (NSCLC)

The name small cell lung cancer originates from the fact that under the microscope the cancer cells look small and are mostly filled with the nucleus. SCLC occurs in about 15% of the total lung cancer patients. It often starts in the bronchi near the center of the chest and tends to grow and spread quickly. In most cases it has already spread to

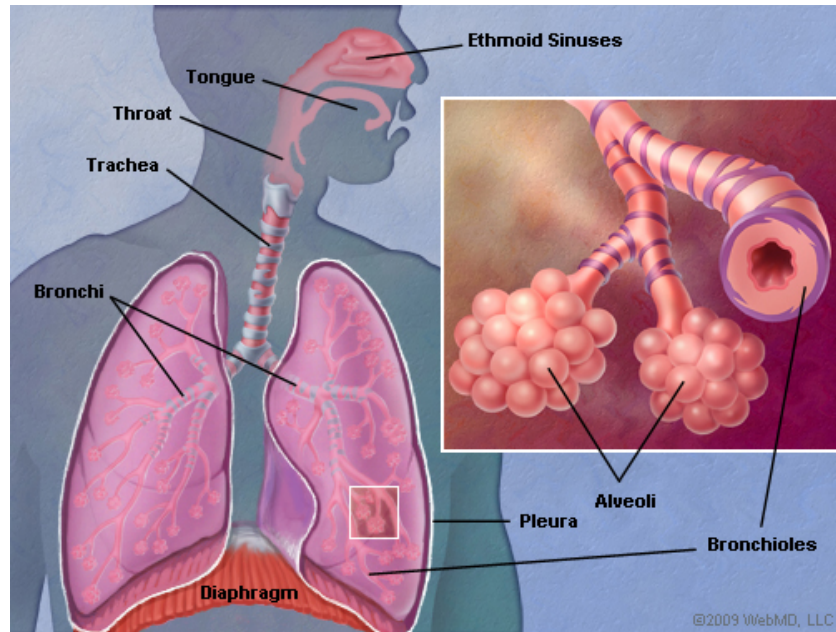


Figure 2.1: Anatomy of the lungs (picture from [11])

distant parts of the body before the patient experiences complaints and the tumor is detected. About 85% of lung cancer cases are classified as NSCLC. A combination of small and non-small cell lung cancer is very uncommon. For NSCLC three main subtypes can be distinguished: squamous cell carcinoma (25-30% of the total), adeno carcinoma (40%) and large cell undifferentiated carcinoma (10-15%). These subtypes are identified by different sites of origin, cells appearance, and behavior [12].

2.2 Lung cancer treatment options

2.2.1 Surgery

Surgical removal of the gross tumor, often in combination with other treatments, is in general an option for early stage NSCLC and it often provides the best chance to healing. In advanced stage (i.e., III and IV) NSCLC, surgery is frequently not feasible due to the size of the tumor or to its spread to close lymph nodes. Different operations can be used requiring general anesthesia [13]:

- Pneumonectomy: the entire lung that contains the tumor is removed

- Lobectomy: an entire lobe (i.e., anatomically and functionally independent structures in which the lungs are divided) is removed
- Segmentectomy: part of a lobe is removed

2.2.2 Chemotherapy

Chemotherapy drugs can be injected into veins or taken by mouth and similar treatments can be useful for cancer in any part of the body. The therapy can be applied at different stages of the whole treatment: before surgery, to shrink the tumor (neoadjuvant therapy); after surgery, to try to kill the cancer cells that may have been left behind (adjuvant therapy); as main treatment, in combination with radiation therapy, especially for advanced stage NSCLC. This can happen either concurrently to the radiotherapy or sequentially (cf. 1.6.2). Chemotherapy is given in cycles (usually 1 to 3 days) followed by a rest period to allow the body time to recover. An entire chemotherapy cycle generally lasts about 3 to 4 weeks (4 to 6 for advanced stage)[14].

2.2.3 Radiotherapy

Radiotherapy is the main treatment option for advanced stage NSCLC. At Erasmus Medical Center Cancer Institute, the clinical procedure involves IMRT (cf. 1.5.2.2) with the number of beams varying from 5 and 9. The dose delivery usually takes up to 20 minutes.

2.2.3.1 4DCT Acquisition

The image acquisition is made with a 4DCT, i.e. many 3DCT scans (cf. 1.4.3) at multiple phases of the breathing cycle where each image is tagged with breathing signals, so that images can be sorted to the corresponding breathing phase. At Erasmus MC the 4DCT is acquired in free breathing condition [15].

2.2.3.2 Structures delineation

The GTV, CTV and organs at risks are delineated manually slice by slice on the 50% exhale phase of the 4DCT scan (cf. 1.4.4) by expert dosimetrists under supervision of

an oncologist physician. The PTV is generated by expanding the CTV automatically with a 3D margin. The margin depends among other on the breathing amplitude of the tumor, as determined on the 4DCT scan. The operators can be helped by the use of software that can reconstruct intermediate slices by connecting manual delineations few slices distant when the organs shape is smooth enough.

2.2.3.3 Dose prescriptions and fractionation regimens

The full prescribed dose for NSCLC treatment is 66 Gy. The dose can be mainly delivered in two fractionation regimens: 33 fractions (i.e., 2 Gy per fraction) and 24 fractions (i.e., 2.75 Gy per fraction). The first regimen is prescribed for patients subject to concurrent chemotherapy, the second for patients who will receive sequential chemotherapy (cf. 1.6.2). This prescription dose cannot always be achieved during the planning phase without violating one or more clinical constraints (cf. 3.2.2). In these cases, the number of fractions is reduced to 30 (i.e., 60 Gy) or 22 (i.e., 60.5 Gy) or less, without considering the intermediate dose reduction due to limitation in the available time for planning.

When the prescribed dose is not achievable even after the first dose reduction or in presence of specific reasons (such as strict limitations in the overall therapy cycle interval), a lower dose can be prescribed, typically 45 Gy. For this prescription dose, the 3 Gy per fraction regimen is adopted (cf. 3.2.6). As shown in the clinical requirements table (Table 3.1), minor adjustments to the requirements are applied for different fractionation regimens.

2.2.3.4 Delivery modalities

For many years lung cancer patients have been treated with 2D or 3D conformal radiotherapy treatment techniques (cf. 1.5.2.1). With those techniques, the possibility to escalate the target dose while not exceeding the dose tolerances for organs at risk (such as healthy lung tissue) was limited. With the introduction of intensity-modulated radiotherapy (IMRT, cf. 1.5.2.2) the dose to organs at risk could be reduced due to a better shaping of the high dose region around the target volume and steeper dose gradients outside ([16], [17]).

In recent years volumetric modulated arc therapy (VMAT, cf. 1.5.2.3) is increas-

ingly used because of its improved delivery efficiency over fixed-field IMRT. The shorter treatment time of VMAT may increase patient throughput, reduce the risk of intrafraction motion, and improve patient comfort during treatment [18]. For lung cancer stage III/IV treatment, this is mirrored by a treatment time reduction from at about 20 minutes (IMRT) to at around 8 minutes (VMAT).

2.3 Introduction to treatment planning

2.3.1 Manual and automated planning

In the vast majority of radiotherapy departments generation of a treatment plan requires a lot of human interaction and experience. After the delineation of the target volume and organs at risk, a dosimetrist has the task to generate the best plan he/she is able to achieve within the clinical constraints and requirements. This also applies for generation of an IMRT or VMAT plan (cf. 1.5.2.2 and 1.5.2.3) using inverse planning (cf. 1.4.5). The operator still has to select the beam orientations and has to define specific constraints or objectives and weights for the target volume and organs at risk. Also their goals have to be selected blindly, i.e., based on the dosimetrist's experience only. Then the treatment planning system looks for the IMRT segments arrangement that minimizes an objective that is the weighted sum of different cost functions. The different objectives are balanced without any information about relative importance or priority. After optimization, the user evaluates the derived dose distribution. If the plan is unsatisfactory, the process starts again with the definition of different constraints, objectives and/or goals. This indicates that generation of an IMRT or VMAT plan is a trial-and-error process. Due to this nature, the process is characterized by at least three remarkable drawbacks:

- The process is time-consuming: the generation of a single final treatment plan may take up to an entire day of work and, sometimes, the improvement is stopped because no more time is available for the planner.
- The process is heuristic: it usually ends with a treatment plan for which, even if it achieves all the clinical requirements, there is no guarantee that it best reflects the wishes of the radiation oncologist.

- The treatment plan quality is affected by the dosimetrist’s experience and ability and by the complexity of the case.

Since these features are inherently tied to a manual planning procedure, an alternative and extremely promising way is represented by automated planning. The Erasmus MC in-house developed Erasmus-iCycle is a multicriterial plan optimization algorithm for integrated beam angle and beam intensity optimization. Outputs of iCycle are Pareto-optimal plans with optimized beam setup or optimized beam profiles. With Pareto-optimal it is meant that none of the objectives in the applied “wish list” can be improved any further without deteriorating higher prioritized objectives[19]. For more details on iCycle working principles see 3.1.1. The main point here is that the use of iCycle allows to obtain treatment plans with the following features:

- Plan quality is more consistent and not operator-dependent.
- The time necessary for plan generation is predictable and briefer than manual planning.
- The overall quality increases and it is made sure to achieve an actual optimal solution.
- Since the plan generation time is strongly reduced and the whole process does not need any operator interaction, it is easier to investigate dose escalation (i.e., to test whether it is possible to deliver a higher dose to the target without exceeding the clinical constraints to the organs at risk) or intermediate dose reduction (cf. 2.2.3.3).

2.3.2 Background: research in radiotherapy treatment planning

Radiotherapy plan generation is a very lively field of study and research. During the last years intense research all over the world was able to change the face of this discipline and to achieve great improvements. In the next lines, a brief introduction to contemporary issues about radiotherapy treatment planning is proposed to the reader.

For IMRT and VMAT it is still common practice that dosimetrists have to select the optimization parameters manually in the previously described trial-and-error process. To

tackle the drawbacks of this planning strategy, currently different automated planning optimization procedures are being developed ([20], [21], [22]), aiming to achieve a high quality treatment plan for any patient, independently of the dosimetrist’s skills. In addition, the required hands-on working time for plan generation may significantly be reduced.

Tol et al [22] designed an automatic interactive optimization procedure for VMAT plan optimization based on dose-volume constraints and dose-volume histograms analyses (DVHs, cf. 1.4.6). This method requires that the user knows the input priorities that generally result in acceptable treatment plans for the majority of patients. But, with this method, optimal plan quality for individual patients may not be guaranteed. In addition, DVHs do not provide spatial information, such as the locations of the high- and low-dose regions (“hot” and “cold” spots) inside the volume of interest[23]: small high-dose regions may be unavoidable very close to the target volume but unacceptable far from the tumor. Zhang et al [20] showed a completely automated process based on an in-house developed optimization algorithm which employed a beam angle optimization process by using a library of treatment plans delivered to previously treated patients. They compared VMAT and IMRT planning techniques, and showed that the automatically generated plans were generally preferred by oncologists when compared to manually generated plans [18]. Their method did not apply a multi criteria optimization technique, but they stated that it would be interesting to assess its additional value.

2.3.3 Erasmus-iCycle

At the Erasmus Medical Center Cancer Institute (Rotterdam, The Netherlands), a fully automated and multi-criterial planning procedure was developed. In combination with a treatment planning system, iCycle is able to generate Pareto-optimal radiotherapy treatment plans by the use of a user-defined, cancer site specific wish list without any human interaction (cf. 3.1.1).

Currently, this method is used in automated plan generation for patients with prostate cancer [21] and head-and-neck and cervical cancer[24]. The conclusion of the mentioned studies was that even an expert dosimetrist, in the absence of time pressure, could not beat the procedure for fully automated plan generation. In this study its use has been extended to lung cancer treatment and the clinical introduction has been started.

2.4 Goal of the study

The aim of this study was to employ Erasmus-iCycle to develop a fully automated treatment planning procedure to generate VMAT plans for stage III/IV non-small cell lung cancer patients, treated with curative intent, and to compare them with manually generated, clinically delivered IMRT plans for a large set of patients. Since VMAT was not used in clinic yet, it was requested to an expert dosimetrist to generate a limited number of VMAT plans without the use of iCycle and any prior knowledge about the delivered plan to assess a comparison in plan quality between automatically and manually generated VMAT plans. The whole study was performed in cooperation with two medical physicists and two oncologist physicians, who supplied for the indispensable clinical feedback to the work.

Chapter 3

Methods and materials

3.1 Background: system for automated planning

3.1.1 Erasmus-iCycle

Erasmus-iCycle is an in-house developed algorithm for multi-criteria optimization of beam intensity profile (IMRT, cf. 1.5.2.2) and beam angles. iCycle has been developed at Erasmus Medical Center Cancer Institute since 2012[25] and represents a powerful tool in an automated planning strategy. Since iCycle is not a treatment planning system (TPS), i.e., it is not able to directly give input to the delivery machines, this software is used in combination with the Elekta TPS Monaco (cf. 3.1.7) to generate actually deliverable radiotherapy treatment plans. A diagram of the entire procedure is shown in Fig. 3.1.

3.1.2 Multi-criterial optimization

Radiotherapy treatment planning is a problem with a high level of complexity. The optimization problem consists of different, conflicting goals. On the one hand the tumor should receive a certain minimal dose level, while the surrounding healthy tissues, that all have specific different tolerances of radiation, should receive as little dose as possible. Therefore, in multi-criterial optimization, multiple objectives are in competition with each other, so that reaching one objective can lead to not fully fulfilling the others. Typically, no single optimal solution exists that simultaneously optimizes each objective.

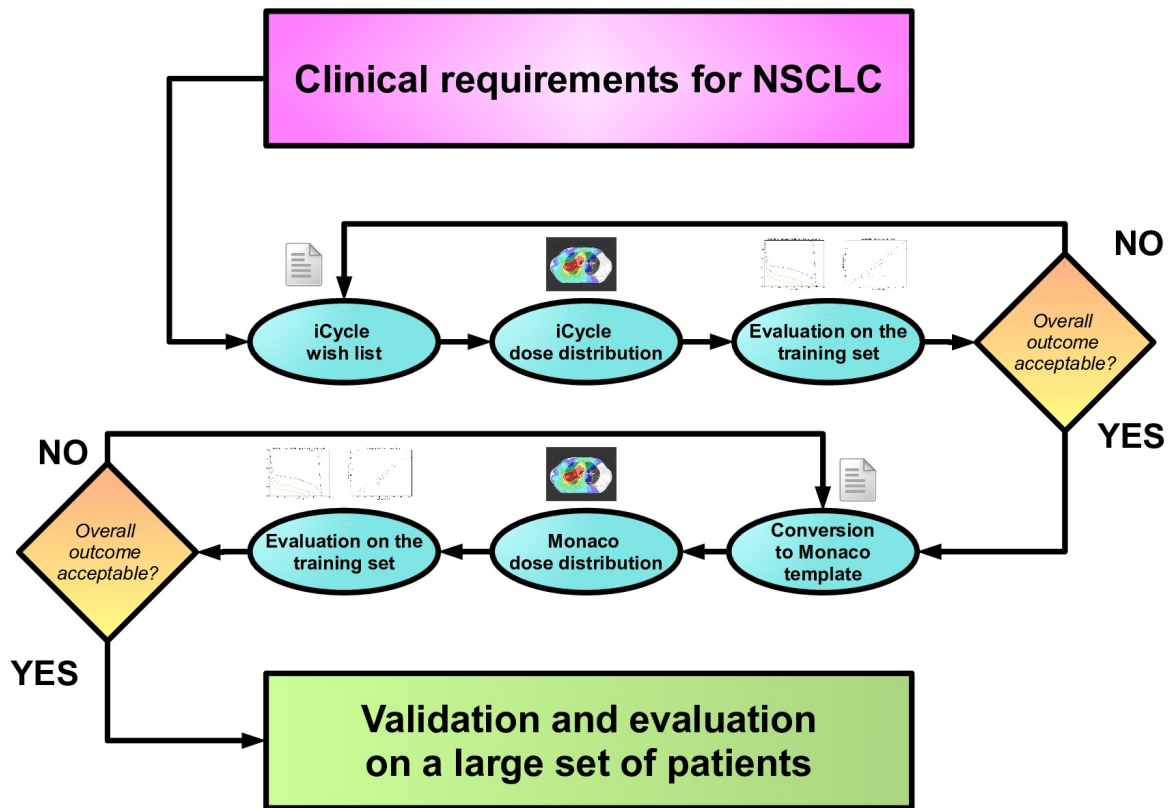


Figure 3.1: Diagram of the automated planning procedure

A solution is called Pareto-optimal if none of the objective functions can be improved without deteriorating other objective values. Without additional preference information, all Pareto optimal solutions can be considered mathematically equally good: then, it is necessary to introduce user-defined preferences in order to differentiate and choose between various solutions.

3.1.3 Wish list

In iCycle the optimization operation is based on a user defined wish list which contains hard constraints and objectives with given priorities. Every element of the wish list consists of a specific cost function, a priority and a goal.

- Constraints must be strictly met, otherwise the plan is considered invalid. It is proper to consider that too strict constraints may limit possibilities to generate attractive plans.
- Objectives are cost functions whose goals have to be met as much as possible (without violating the imposed constraints).

In iCycle the objectives are optimized one by one in order of priority. Priorities play a crucial role in determining the outcomes. In iCycle, a later objective is optimized as far as it does not affect the result of the previous ones: even inverting priorities of two objectives, especially for complex anatomies, may strongly affect the entire outcome.

3.1.4 Brief introduction to $2p\epsilon c$ optimization method

iCycle uses the $2p\epsilon c$ algorithm for prioritized optimization. The $2p\epsilon c$ algorithm, proposed by Breedveld et al.[26], is an extension of the $\epsilon - constraint$ method[27], in which one objective at a time is optimized while keeping the others (higher prioritized) constrained. The method is extended to a 2 phase constraint optimization ($2p\epsilon c$), where a goal can be assigned to each objective in the first phase of the optimization, while in the second phase a full optimization of the objectives is applied.

Hard constraints and prioritized objectives are given in a wish list which completely regulates the whole optimization process. The idea at the base of the approach is that when it is possible to minimize the dose below a certain threshold (i.e., its goal) for one objective, it is often more desirable to minimize the dose for the other (lower prioritized) objectives first than to directly minimize the dose for the higher objectives to its fullest extent.

The wish list defines hard constraints and a list of n objectives $f_i(x)$ characterized by a priority i and a goal b_i . During the first iteration of the first phase, the objective having highest priority is optimized:

$$\text{minimize } f_1(x)$$

$$\text{subject to } \mathbf{g}(x) \leq 0$$

$f_1(x)$ is the objective with priority 1 and $\mathbf{g}(x)$ is a vector which represents the list

of the constraints which are to be met at all times. Based on the solution x^* of this optimization, a new bound for the optimized objective is defined and it is set as constraint during the optimization of the following objective. The new bound is chosen according to the following rule:

$$\epsilon_1 = \begin{cases} b_1 & \text{if } f_1(x^*)\delta < b_1 \\ f_1(x^*)\delta & \text{if } f_1(x^*)\delta \geq b_1 \end{cases}$$

where b_1 and ϵ_1 are respectively the goal and the new bound of the objective with priority 1, $f_1(x^*)$ is the obtained value for the objective $f_1(x)$ and δ is a slight relaxation to create some space for the subsequent optimizations (usually set to 1.03, i.e. 3%). In practice this relaxation is mandatory to avoid the optimization algorithm from stalling due to numerical problems. The next step is the optimization of the second objective, $f_2(x)$, while the obtained result for f_1 is added to the constraints list:

$$\begin{aligned} & \text{minimize } f_2(x) \\ & \text{subject to } \mathbf{g}(x) \leq 0, f_1(x) \leq \epsilon_1 \end{aligned}$$

This is repeated for all n objectives.

In the second phase of the multi-criterial optimization, all the objectives which met their goals are minimized to their fullest, while keeping all others constrained: so, for each f_i which met its goal b_i , the following problem is solved:

$$\begin{aligned} & \text{minimize } f_i(x) \\ & \text{subject to } \mathbf{g}(x) \leq 0, f_k(x) \leq \epsilon_k, k \in \{1, \dots, n\} \end{aligned}$$

3.1.5 Wish list generation

Many cost functions are available, allowing a large degree of freedom in the generation of the wish list. Any of them can be used in “minimize maximum” or “maximize minimum” mode.

- Linear: when used in conjunction to minimize maximum, this cost function regulates the maximum allowed dose. It is mainly employed to settle undesired over-

doses and to strictly govern the maximum allowed dose to organs at risk characterized by serial complication mechanism (i.e., organs in which the cost of increasing the dose to an already hot sub-volume rises tremendously, following a strongly non-linear behavior, such as the spinal cord[28])

- Mean dose cost function
- Logarithmic tumor control probability (LTCP): LTCP is defined as

$$LTCP = \frac{1}{m} \sum_{j=1}^m e^{-\alpha(d_j - D^P)}$$

where m is the number of voxels in the target structure, D^P is the prescribed dose, d_j is the dose in voxel j and α is the cell sensitivity parameter, in this study set to 0.8[19]. LTCP is able to guarantee a proper target coverage.

- Equivalent uniform dose (EUD): this function is regulated by the parameter k in the formula

$$EUD = \sqrt[k]{\frac{1}{m} \sum_{j=1}^m d_j^k}$$

where m is the number of voxels in the target structure and d_j is the dose in voxel j . For $k = 1$ the meaning of EUD is the same as the arithmetic mean; for $k > 1$ the high dose regions gain more importance in the weighted sum and, ideally, for $k = \infty$, EUD is equal to the maximum dose in the structure.

- Dose-volume reference points: these cost functions try to force the DVH (cf. 1.4.6) related to a certain structure to achieve the requested value. Due to non-convexity, the use is discouraged because it may lead to sub-optimal solutions of the problem.

Wish lists are stored in *.xml* format by the in-house developed software Lucy. Within the same wish list it is possible to define specific features of the optimization process, such as conditions on beam angles selection, prescribed dose to the target, number of fractions, and detailed resolution for selected structures.

3.1.6 iCycle VMAT plan generation

iCycle is specifically suitable to IMRT plans because it does not need to define a priori the number of orientations in a plan; beams are added sequentially, so if adding beams does not longer result in clinically significant improvements, the process can be stopped. The user can also select the Pareto optimal plan with the best trade-off between number of beams used and plan quality. Nevertheless, it is possible to simulate VMAT delivery mode with adequate accuracy: in this study, the preselected configuration consisted of 23 equi-angular beams. It was previously proven that further increasing the number of beams increased calculation time but did not lead to an improve in plan quality[21].

3.1.7 Treatment planning system: Monaco

iCycle is a very efficient tool that can be employed to investigate and find the optimal dose distributions, as defined by a wish list. Nevertheless, to obtain deliverable treatment plan it is needed to work in combination with a treatment planning system (TPS).

Monaco is a TPS developed by Elekta. The treatment planning system is used to create treatment plans for any cancer patient for whom external beam IMRT or VMAT is prescribed. Monaco offers many features, such as tools for structure contouring, enhanced voxel property definitions, collection of biological and dose-based cost functions, Monte Carlo simulation for dose calculation, and more.

The planning activity is based on inverse planning strategy, which requires a user defined identification of the clinical goals in order to find the best configuration of beam intensities, and the optimization process is organized in two phases. The first produces the preliminary result, while the second stage converts ideal fluence to deliverable segments, using the same prescription defined in stage one. For this stage of optimization, the Monte Carlo dose calculation algorithm is used to calculate the dose distribution. For the description of the requirements and of the clinical goals, Monaco offers a set of dose-based and biological cost functions. The set is composed of cost functions such as target penalty, target EUD, serial model, parallel model, quadratic under/over dose, under/over dose DVH, maximum dose and conformality. For details, cf. [29]. It is important to consider that during the optimization every cost functions receives a weight. If the assigned weight exceeds a certain threshold, the objective turns to infeasible and is not considered in the calculation anymore. Thresholds are cost function-specific and

depend on the selected calculation modality: the Pareto mode allows higher weights to cost functions referring to the target, the Constrained mode assigns higher thresholds to organs at risk objectives.

Monaco is an efficient TPS but does not provide plan optimization functionalities. Plan quality exclusively depends on the quality of the selection of the cost functions and their goals that is made by the dosimetrist. Monaco does not consider different levels of importance (i.e., priorities) between the objectives of the optimization list, so the cost function goals should already be achievable values to obtain good RT plans. This is exactly the task of iCycle as preoptimization of Monaco: to generate a list of feasible, optimized dosimetric parameters, leaving Monaco with the assignment to elaborate the best IMRT segments arrangement to reproduce the optimized dose distribution.

3.1.8 Export to Monaco

The reproduction of the iCycle optimized dose distribution is made by an automated translation of the iCycle output into a Monaco template, i.e., a list of cost functions and respective goals and parameters that leads the optimization process to the desired dose distribution. The translation is realized by an in-house developed tool which is able to make the whole process fully automated. The conversion, including possible multiplying factors, is site specific and needs to be fine-tuned in a trial and error process (cf. 3.2.5).

3.2 Current study

3.2.1 Patients selection and target delineation

A set of consecutive locally advanced stage III-IV NSCLC patients treated between January and August 2015 at Erasmus MC Cancer Institute were included in this study. All patients were treated with curative intent. Patients who received prior radiotherapy or surgery were excluded, leaving a total of 48 patients (Table 3.3).

A 4D CT scan was acquired and the 50% exhale phase was used for delineation of the targets and OARs. The CTV of the primary tumor was generated by expanding the GTV with a margin of 5 mm and was allowed to be edited manually. Affected lymph nodes as determined on diagnostic CT scan and PET scan were encompassed by

the CTV. The PTV was defined as the CTV of the primary tumor and lymph nodes expanded by a margin of 1 cm. For patients with wide tumor motion the margin was increased in the superior-inferior direction with individual margins.

Patients were treated with IMRT with 5 to 9 beams and according to one of three different fractionation schedules with prescription doses varying between 30 Gy and 66 Gy depending on the capability to deliver the prescribed dose without violating the clinical constraints. Treatment planning goals are shown in Table 3.1.

3.2.2 Clinical requirements for IMRT planning

The clinical requirements are given by the radiation oncologists; Erasmus MC guidelines are shown in Table 3.1. The clinical requirements can vary for different fractionation regimens and, in particular, for the dose delivered per fraction; this is due to the tissue ability of recovering the radiation damage during the inter-fraction time and to the regimen that patients are subject to in terms of chemo-radiotherapy. The 2 Gy per fraction regimen is typical for concurrent chemotherapy, the 2.75 Gy is mostly used in cases of sequential radiotherapy (cf.1.6.2).

During weekly meeting with physicians, it was experienced that not all the requirements were actually characterized by the same importance. Esophagus and heart could be sacrificed to achieve a satisfactory PTV coverage; lungs-GTV V_{5Gy} had lower priority compared to obtaining a high level of plan conformality. These OARs requirements were therefore to be intended as objectives, following the iCycle terminology (cf. 3.1.3).

Table 3.1: Clinical requirements for NSCLC

Organ	66 Gy	66 Gy	60 Gy	50 Gy	Volume/ Dose
	$33 \times 2 Gy$	$24 \times 2.75 Gy$	$20 \times 3 Gy$	$20 \times 2.5 Gy$	
Spinal Cord	50.0 Gy	49.3 Gy	46.3 Gy	46.3	0 cc
Esophagus	$\leq 25\%$	$\leq 25\%$	$\leq 25\%$	$\leq 25\%$	V_{45Gy}
Heart	40 Gy	40 Gy	40 Gy	40 Gy	$< 100\%$
	50 Gy	50 Gy	50 Gy	50 Gy	$< 66\%$
	66 Gy	66 Gy	66 Gy	66 Gy	$< 33\%$
Plexus	66.0 Gy	60.0 Gy	56.6 Gy	56.6 Gy	$< 1\%$

Continued on next page

Table 3.1 – *Continued from previous page*

Organ	66 Gy $33 \times 2 \text{ Gy}$	66 Gy $24 \times 2.75 \text{ Gy}$	60 Gy $20 \times 3 \text{ Gy}$	50 Gy $20 \times 2.5 \text{ Gy}$	Volume Dose
Lungs - GTV	20 Gy	20 Gy	20 Gy	20 Gy	< 35%
	5 Gy	5 Gy	5 Gy	5 Gy	< 60%
	$\leq 20 \text{ Gy}$	$\leq 20 \text{ Gy}$	$\leq 20 \text{ Gy}$	$\leq 20 \text{ Gy}$	Mean Dose
GTV	95 – 107%	95 – 107%	95 – 107%	95 – 107%	Target Dose
	62.7 Gy	62.7 Gy	57 Gy	57 Gy	D2cc
	(95% P.D.)	(95% P.D.)	(95% P.D.)	(95% P.D.)	
	< 1%	< 1%	< 1%	< 1%	$V_{110\%}$
CTV	95 – 107%	95 – 107%	95 – 107%	95 – 107%	Target Dose
	62.7 Gy	62.7 Gy	57 Gy	57 Gy	D2cc
	(95% P.D.)	(95% P.D.)	(95% P.D.)	(95% P.D.)	
	< 1%	< 1%	< 1%	< 1%	$V_{110\%}$
PTV	95 – 107%	95 – 107%	95 – 107%	95 – 107%	Target Dose
	59.4 Gy	59.4 Gy	54 Gy	54 Gy	D2cc
	(90% P.D.)	(90% P.D.)	(90% P.D.)	(90% P.D.)	
	> 95%	> 95%	> 95%	> 95%	$V_{95\%}$
	< 1%	< 1%	< 1%	< 1%	$V_{110\%}$

Table 3.1 - End

3.2.3 Automated treatment planning with Erasmus-iCycle

Automated treatment planning was implemented as a two-step approach. First, 23 equiangular beams IMRT treatment plans were generated with Erasmus iCycle, our in-house developed multicriterial dose distribution optimizer. Next the plans were automatically converted into patient specific Monaco templates and the resulting deliverable Monaco plans were saved for review.

3.2.4 Construction of the wish list

All the iCycle plans were obtained by employing one fixed wish list. Only minor changes for different prescription doses and/or fractionation regimens were applied. This

wish list was developed through the teamwork with oncologist physicians and medical physicists during weekly meetings throughout the whole stay at Erasmus MC Cancer Institute. The wish list was established and fine-tuned by applying an iterative procedure of automated planning, plan evaluation by the physicians and wish list adjustments on a training set of 7 patients (Table 3.3). The development proceeded until no further improvements in plan quality could be observed.

The final wish list is shown in Fig. 3.2. The 8 constraints were employed to keep general overdose below the threshold of 107% of the prescribed dose (A) and to set specific fractionation dependent maximum dose constraints for spinal cord and plexus. A mean dose constraint was applied to the lungs at 19 Gy, slightly below the clinical requirements, to leave the process with some room for the translation to Monaco (cf. 3.2.5).

First priority was CTV and PTV coverage. It was previously proved that the use of the LTCP cost function (cf. 3.1.5) is able to ensure a proper target coverage. The sensitivity value α was set to 0.8, as suggested by previous studies[19]. When the spinal cord was close to the target or overlapped it, the objective was applied to the target to which the spinal cord expanded by 5 mm was subtracted. This happened to steer the acceptable underdosage to the part of the PTV/CTV closest to the spinal cord.

An objective with priority 3 aimed to reduce the maximum dose 4 cm far from the PTV at 60% of the prescribed dose. This was followed by an objective for further reduction in mean lungs dose and two more objectives (*Shell PTV +1cm* and *Shell PTV +3cm*) with priorities 5 and 6 to realize a steep dose fall-off outside the PTV. To minimize the esophagus volume treated to a high dose, an equivalent uniform dose (EUD, cf. 3.1.5) objective with parameter $k = 8$ and an esophagus mean dose objective were used (priority 7 and 8). Further reduction in MLD, mean heart dose and other OARs dosimetric parameters were applied from objectives 9 to 13. In the first phase of the 2pec optimization (cf. 3.1.4) objective functions were minimized, when possible, to the corresponding goal in the wish list; in the second phase, all objectives were consecutively minimized to their fullest extent.

Prescribed A: <input type="text" value="66.000"/> B: <input type="text" value="0.0000"/> C: <input type="text" value="0.0000"/> D: <input type="text" value="0.0000"/> E: <input type="text" value="0.0000"/> F: <input type="text" value="0.0000"/> G: <input type="text" value="0.0000"/> In no. Frac <input type="text" value="33"/>										
	Structure	Min/Max	Type	Goal	Limit	Sufficient	Priority	Weight	Parameters	Active
1	Spinal Cord +3mm	Minimize (maximum) ↓	linear	47			Constraint	1		Yes
2	patient	Minimize (maximum) ↓	linear	A*1.07			Constraint	1		Yes
3	CTV Left Lung	Minimize (maximum) ↓	linear	A*1.07			Constraint	1		Yes
4	CTV Right Lung	Minimize (maximum) ↓	linear	A*1.07			Constraint	1		Yes
5	PTV-CORD+5	Minimize (maximum) ↓	linear	A*1.07			Constraint	1		Yes
6	Plexus Left	Minimize (maximum) ↓	linear	63			Constraint	1		Yes
7	Plexus Right	Minimize (maximum) ↓	linear	63			Constraint	1		Yes
8	Lungs minus GTV	Minimize (maximum) ↓	mean	19			Constraint	1		Yes
9	CTV Right Lung	Minimize (maximum) ↓	LTCP	1			1	1	A 0.8	Yes
10	CTV Left Lung	Minimize (maximum) ↓	LTCP	1			1	1	A 0.8	Yes
11	PTV-CORD+5	Minimize (maximum) ↓	LTCP	0.5			2	1	A 0.8	Yes
12	Patient - (PTV+4cm)	Minimize (maximum) ↓	linear	A*0.6			3	1		Yes
13	Lungs minus GTV	Minimize (maximum) ↓	mean	15			4	1		Yes
14	Shell PTV+1cm	Minimize (maximum) ↓	linear	A*0.9			5	1		Yes
15	Shell PTV+3cm	Minimize (maximum) ↓	linear	A*0.8			6	1		Yes
16	Esophagus	Minimize (maximum) ↓	EUD	44			7	1	8	Yes
17	Esophagus	Minimize (maximum) ↓	mean	15			8	1		Yes
18	Lungs minus GTV	Minimize (maximum) ↓	mean	5			9	1		Yes
19	Heart	Minimize (maximum) ↓	mean	15			10	1		Yes
20	Spinal Cord +3mm	Minimize (maximum) ↓	linear	42			11	1		Yes
21	Unspecified Tissue	Minimize (maximum) ↓	linear	40			12	1		Yes
22	Plexus Left	Minimize (maximum) ↓	mean	20			13	1		Yes
23	Plexus Right	Minimize (maximum) ↓	mean	20			13	1		Yes

Figure 3.2: iCycle wish list for lung cancer treatment

3.2.5 Conversion to Monaco

The multicriterially optimized dose distribution obtained with iCycle was used to feed a template for the TPS Monaco, i.e., a list of cost functions whose goals (isoconstraint) were determined by the iCycle output, to reproduce the same dose distribution in a deliverable treatment plan. The iCycle plan could not be directly used as treatment plan because of the absence of a leaf sequencing algorithm (i.e., an algorithm that simulates a real multi leaves collimator) and the employment of a pencil beam dose simulation algorithm that was mirrored in small inaccuracies in the final patient dose distribution when compared to a Monte Carlo simulation. Small discrepancies could be observed especially in tissue inhomogeneities. The translation followed a standard procedure at Erasmus MC Cancer Institute previously successfully tested on other cancer sites[21]. The only significant difference lied in the need of a 5% relaxation of the iCycle achieved mean lungs dose and V_{20Gy} (cf. 3.1). Since a site-specific translation was not investigated, secondary improvements in this stage of the work cannot be firmly excluded.

Table 3.2: Details for automated generation of Monaco templates

Structure	Cost function	Parameter	Goal
PTV-CORD+5	Quadratic Overdose	109% P.D.	0.500
	Underdose DVH	95% P.D.	98.5% iCycle achieved V_{95}
	Target Penalty		P.D.
Lungs - GTV	Serial	1	105% iCycle achieved mean dose
	Parallel	105% iCycle achieved mean dose	45%
	Overdose DVH	20 Gy	105% iCycle achieved V_{20Gy}
	Overdose DVH	5 Gy	105% iCycle achieved V_{5Gy}

Continued on next page

Table 3.2 – *Continued from previous page*

Structure	Cost function	Parameter	Goal
Heart	Serial	1	iCycle achieved mean dose
	Parallel	iCycle achieved mean dose	45%
Esophagus	Serial	1	iCycle achieved mean dose
	Parallel	iCycle achieved mean dose	45%
Plexus Left	Maximum Dose		65.0 Gy
Plexus Right	Maximum Dose		65.0 Gy
Spinal Cord	Maximum Dose		iCycle achieved maximum dose
Patient	Maximum Dose		109% P.D.
	Shell 1 cm		80% iCycle achieved maximum dose
	Shell 3 cm		80% iCycle achieved maximum dose
	Shell 4 cm		80% iCycle achieved maximum dose
	Conformality		0.80

Table 3.2 - End

3.2.6 Validation procedure and statistical testing

The automated procedure was validated on a set of 41 patients consecutively treated between January and August 2015 (cf. 3.2.1). The list of patients and fractionation

schedules are shown in Table 3.3 and Fig. 3.3. Plan quality was assessed by the radiation oncologists and automated plans were compared to clinical plans by the use of a list of dosimetric indicators selected by the physicians. Statistical significance of the differences was evaluated with a two tailed Wilcoxon signed rank test. A $p < 0.05$ was considered as statistically significant.

Table 3.3: Prescribed doses and fractionation regimens. Latin enumeration indicates the patients employed as training set.

n	Patient ID	Prescribed dose (Gy)	Number of planned fractions	Dose per fraction (Gy)
I	GDGNSCLC3	66	33	2
II	GDGNSCLC4	66	33	2
III	GDGNSCLC6	66	33	2
IV	GDGNSCLC8	66	33	2
V	GDGNSCLC9	66	33	2
VI	GDGNSCLC10	66	33	2
VII	GDGNSCLC13	66	33	2
1	GDGCPerspIM1	39	13	3
2	GDGCPerspIM2	60	30	2
3	GDGCPerspIM3	66	33	2
4	GDGCPerspIM4	66	33	2
5	GDGCPerspIM5	60.5	22	2.75
6	GDGCPerspIM6	45	15	3
7	GDGCPerspIM7	60	30	2
8	GDGCPerspIM8	66	33	2
9	GDGCPerspIM9	66	33	2
10	GDGCPerspIM10	66	33	2
11	GDGCPerspIM11	45	15	3
12	GDGCPerspIM13	66	33	2
13	GDGCPerspIM18	66	24	2.75
14	GDGCPerspIM19	60.5	22	2.75

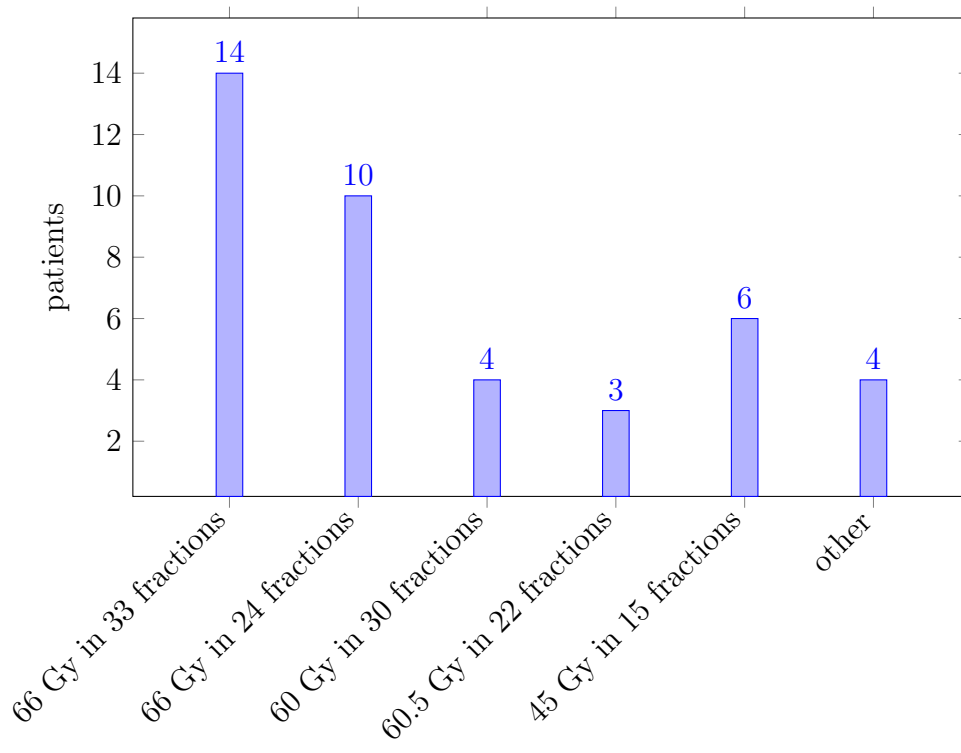
Continued on next page

Table 3.3 – *Continued from previous page*

n	Patient ID	Prescribed dose (Gy)	Number of planned fractions	Dose per fraction (Gy)
15	GDGCPerspIM20	66	33	2
16	GDGCPerspIM21	45	15	3
17	GDGCPerspIM22	66	33	2
18	GDGCPerspIM24	66	24	2.75
19	GDGCPerspIM25	66	33	2
20	GDGCPerspIM26	60.5	22	2.75
21	GDGCPerspIM27	66	24	2.75
22	GDGCPerspIM28	55	20	2.75
23	GDGCPerspIM29	66	24	2.75
24	GDGCPerspIM30	45	15	3
25	GDGCPerspIM31	66	33	2
26	GDGCPerspIM32	57.75	21	2.75
27	GDGCPerspIM33	66	24	2.75
28	GDGCPerspIM34	66	24	2.75
29	GDGCPerspIM35	30	10	3
30	GDGCPerspIM36	66	24	2.75
31	GDGCPerspIM37	66	24	2.75
32	GDGCPerspIM38	66	24	2.75
33	GDGCPerspIM39	66	33	2
34	GDGCPerspIM40	66	33	2
35	GDGCPerspIM41	60	30	2
36	GDGCPerspIM42	45	15	3
37	GDGCPerspIM43	66	33	2
38	GDGCPerspIM44	60	30	2
39	GDGCPerspIM45	66	33	2
40	GDGCPerspIM46	45	15	3
41	GDGCPerspIM47	66	24	2.75

Table 3.3 - End

Figure 3.3: Validation set of patients



3.2.7 Comparison with manually generated VMAT plans

Since VMAT was not introduced in clinical routine at the time of the study, all the 41 comparisons were made with respect to clinically delivered IMRT plans. To perform a comparison with manually generated plans with the same delivery modality, it was asked an experienced dosimetrist to generate VMAT plans from scratch without any previous knowledge about the iCycle output or the IMRT clinical plans. Plans were made for a subset of ten randomly selected patients. The required time for each plan was at about 3-4 hours.

3.2.8 Dose escalation

When during the manual planning procedure it was not possible to achieve the full dose of 66 Gy without violating at least one of the clinical constraints, the number of planned fractions, and consequently the prescribed dose, was reduced following a clinical schedule. Dose was reduced from 66 Gy to 60 Gy or 60.5 Gy depending on the fractionation schedule. When even a dose of 55 Gy was not feasible, the applied schedule was a prescription dose of 45 Gy delivered in 15. In few cases lower doses were prescribed (cf. 3.2.6). Intermediate reductions of the number of planned fractions were not clinically investigated due to working time limitation. Nevertheless, the automated procedure would easily allow to generate plans for fraction-by-fraction dose reduction without increase of the operator workload, at least at the iCycle pre-optimization stage.

3.2.9 Delivery machines

The treatment plan will be delivered on an Elekta Sinergy system (Fig. 3.4). The machine offers a total field size of $40 \times 40 \text{ cm}^2$ equipped with an MLCi2 (2×40 leaves of 1 cm) with active leakage reduction. For positioning verification, the machine is equipped with MV and kV imaging.



Figure 3.4: Elekta Sinergy system

3.3 Considerations about the iCycle wish list

3.3.1 Random sampling in iCycle optimization

During the iCycle optimization, the goals of the maximum dose constraints were set at about 5% lower than what requested by the clinical requirements (Fig. 3.2 and Table 3.1). This precaution was adopted because, during the optimization process, iCycle randomly sampled only a certain percentage of the voxels in a structure; especially when dealing with maximum dose constraints, this meant that it was not strictly excluded to have a negligible number of voxels which exceeded the requirement. For the same reason, the maximum dose constraint at 107% of the prescribed dose was repeated on several structures (i.e., patient, CTV, PTV). With this precaution it was easily increased the number of sampled voxels into the target structures (i.e., where high dose was expected).

3.3.2 Scattering length

iCycle dose distributions could not be identically reproduced by the treatment planning system, mainly because iCycle was not equipped with a leaves sequencing algorithm and because it employed a pencil beam dose simulation algorithm, due to a reduced com-

putation time requirement, while Monaco was based on a Monte Carlo dose simulation algorithm, which was as a whole judged as more accurate and reliable. Discrepancies between the two dose simulation algorithms could be revealed when dealing with tissue inhomogeneities, i.e. very high density tissues (like bones) or very low density tissues (such as the lungs). Especially in lung cancer dose distributions, it was found an underestimation of the lateral scattering of the photons in the pencil beam calculation; this meant that the low dose region was smaller than what estimated by the Monte Carlo algorithm and this was mirrored, for instance, in a higher V_{5Gy} in the healthy lungs structure. The problem was tackled by doubling the scattering length, i.e. the radius into which the scattering phenomena were simulated, from the standard iCycle setting of 30 mm to 60 mm, and by relaxing the requirements in the translation from the output of iCycle to the Monaco template (Table 3.2).

3.3.3 Conformality and mean lung dose reduction

In the developed wish list (Fig. 3.2) the third objective focused on conformality in terms of reducing the maximum dose 4 cm far from the PTV to 60% of the prescribed dose. Fourth objective operated on a further mean lung dose reduction to 15 Gy. This disposition was selected because, as tested, just switching the priorities of these two objectives resulted in iCycle plans with little hot spots far from the PTV.

3.3.4 PTV minus expanded spinal cord (5 mm)

As shown in section 3.2.4, the second objective in the final wish list was applied to the PTV structure to which the spinal cord, expanded by 5 mm, was subtracted. Since the maximum dose constraint on the spinal cord was significantly far from the prescribed dose (between 46.3 Gy and 50 Gy, depending on the fractionation regimen), it was not feasible to achieve the PTV LTCP goal when the spinal cord was close or overlapping the PTV. In fact, LTCP arose tremendously in presence of wide underdosed areas. The conflict between the spinal cord constraint and the goal of the first objective led the optimizer to waste the entire optimization room in trying to lower as much as possible the LTCP (with goal set to 1), obtaining inhomogeneous dose distribution in the PTV. The subtraction of the expanded spinal cord did not affect plans in which the spinal cord was far from the PTV but allowed to steer the unavoidable, acceptable, underdosage

closer to the spinal cord (Fig. 3.5). The margin of 5 mm was selected by testing several values.

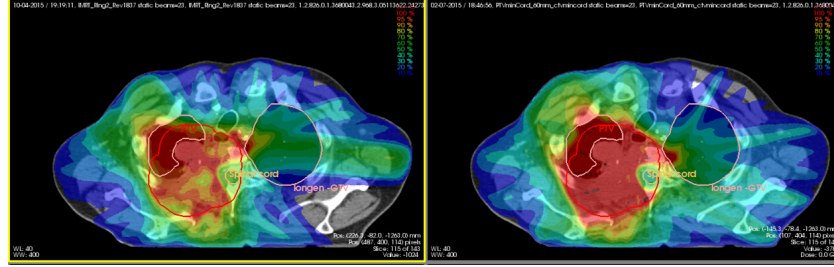


Figure 3.5: Comparison between a plan in which the LTCP cost function is applied to the entire PTV (left) and a plan in which LTCP cost function is applied to PTV minus spinal cord expanded by 5 mm (right). Both plans are iCycle dose simulations. In the second plan the underdosed region is steered toward the spinal cord. Dose distribution on the PTV (red contour) is more conformal and homogeneous.

3.4 Evaluation tools: DVHs and scatterplots

A cumulative dose volume histogram (DVH) was a histogram in which the total volume receiving a dose greater than, or equal to, a given dose was plotted against dose (cf. 1.4.6). DVHs were used to compare different treatment plans to the same patient. Nevertheless, since they did not bring any spatial information about the dose, their analysis should always be supported by a careful observation of the dose distributions on the patient slice by slice.

The strength of DVHs was their ability in giving clear messages about the dose distribution at the first sight. An example is shown in Fig. 3.6. The interpretation of these diagrams strongly depended on the organs they aimed to describe.

- Target structures (GTV, CTV, PTV, cf. 1.4.4): since the aim of the plan was to ensure the highest target coverage, the DVH should take place as much as possible on the upper right side of the plot. Furthermore, an important desired feature of the target dose distribution was homogeneity: this meant that, although underdose was harmful in terms of fighting the tumor, also overdosage was considered dangerous and should be rejected. In terms of DVHs, both properties were expressed by the steepness of the curve. Summarizing, the DVH for a target structure should be

as similar as possible to a step function placed on the prescription dose or slightly beyond it.

- Parallel complication mechanism structures (healthy lungs, esophagus, heart): for these structures the organ function could be maintained by a sufficiently large critical volume while the remaining volume could be sacrificed when needed. This was often mirrored by objectives on keeping the irradiated volume under certain thresholds at some reference doses, such as 20 Gy and 5 Gy for the healthy lungs (Table 3.1). The DVH curve should be as low as possible, but it was generically not possible to avoid either low dose to a wide region and/or high dose to a small area.
- Serial complication mechanism structures (spinal cord, plexus): for these organs (cf. 3.1.5) the only critical parameter was the maximum dose; DVH shape was substantially irrelevant.

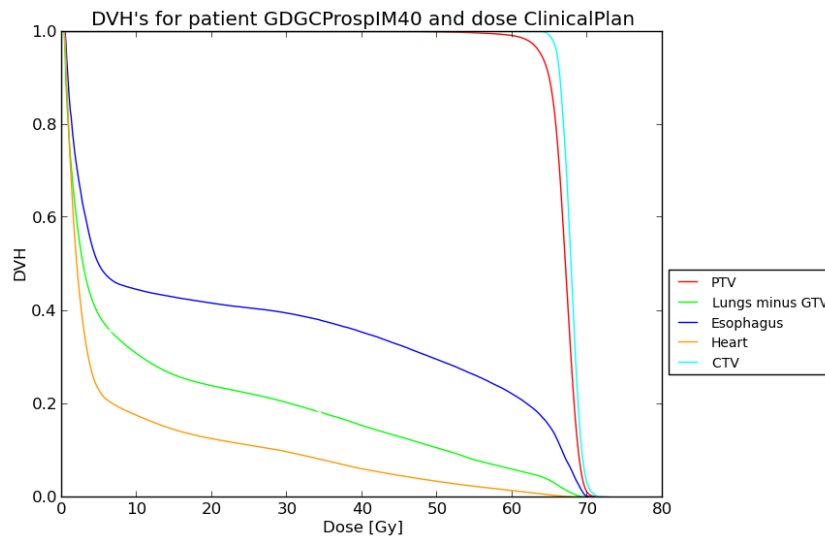


Figure 3.6: Example of DVH. Target DVHs (PTV, CTV) follow the shape of a step function, while OARs DVHs should be kept as low as possible.

From a DVH it was possible to extract dose volume reference points, expressed as volume receiving at least a reference dose (V_{refGy}) or a percentage of the prescribed dose (V_{ref}), or as dose delivered to at least a reference volume (D_{ref}) (cf. 1.4.6). Scatter-plots were considered an useful tool to compare a large set of coupled plans (such as

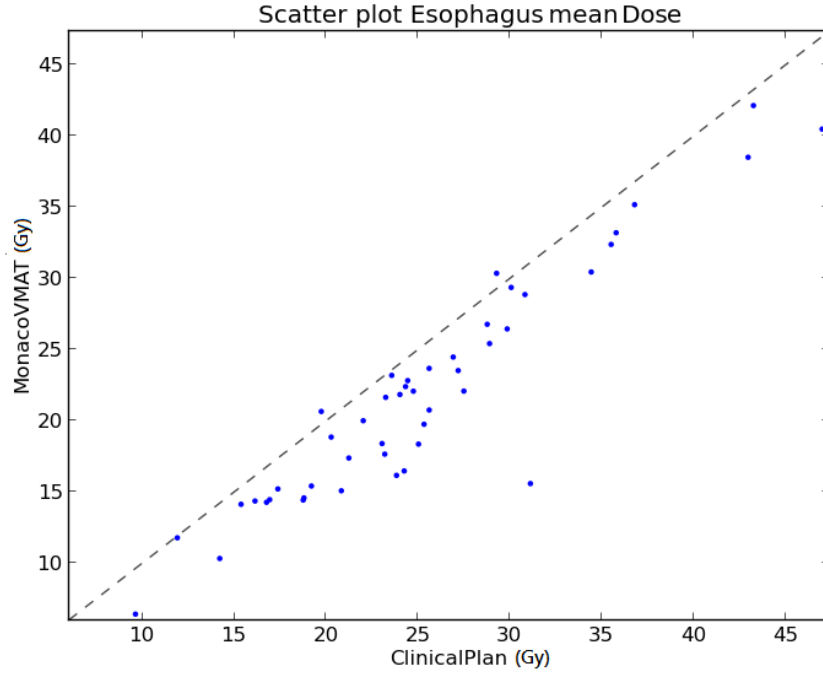


Figure 3.7: Example of scatterplot for esophagus mean dose. Points lie almost always in the lower right corner, that is where the value achieved in the clinical plan is higher than for the MonacoVMAT plan. This behaviour show an improvement in esophagus sparing by the automated plan.

the comparison between clinically delivered plans and automated plans for this study). Scatterplots showed one, or more than one, dose volume reference point for a certain structure, assigning the two axes to the two groups of plans to compare and plotting the bisector line, representing the equivalence line. A point was therefore plotted with coordinates $(x, y) = (plan\ 1, plan\ 2)$. In our notation, the x -axis was assigned to the clinical plan and y -axis to the automated plans. For scatterplots representing dose volume reference points describing the target coverage, the aim was then to obtain points characterized by $y > x$, that is lying in the upper left corner of the plot. On the other hand, plotting organs at risk reference points yearned for placing the points in the lower right corner of the figure, that is $x > y$. An example is shown in Fig. 3.7.

3.5 Uncertainties

In radiotherapy treatment planning a proper uncertainties assessment is often a hard task. Uncertainties could be mainly divided in dosimetric and anatomical uncertainties.

A dosimetric validation of the employed treatment planning system was previously performed, proving that the dose distributions measured in either water or in anthropomorphic phantoms were well within acceptance limits of 2% or 2 *mm* distance-to-agreement[31].

Anatomical uncertainties evaluation should consider several factors, including tumor shrinkage within the treatment cycle and intra-fraction motion due to free breathing condition of the patient during the dose delivery. This analysis was inapplicable to our patients, since the availability of the single 50% expiration images set only. Nevertheless, in clinical practice only the dose calculated on this image acquisition is evaluated. Previous studies[32] based on IMRT plans for locally advanced NSCLC proved that the observed dosimetric variations in PTV V_{95} , MLD and lungs V_{20Gy} were small on average (2.5%, 3.1%, 2.2% respectively); nevertheless, the interfractional changes in tumor volume, mobility, and patient setup was sometimes associated with dramatic dosimetric consequences. A consequence was the recommendation of the introduction of adaptive radiotherapy in NSCLC treatment. Adaptive radiotherapy (ART) aims at adjusting the treatment plan during the treatment cycle to ensure proper target coverage and to reduce normal tissue complications. In the adaptive process, the changes are monitored systematically for the individual patients and when predetermined criteria are violated, an adaptive treatment plan is made [33].

Chapter 4

Results

4.1 Overview

With the applied wish list and automated conversion to Monaco plans, 85% (35/41) of the automatically generated Monaco VMAT (autoVMAT) plans were clinically acceptable as judged by two physicians. All the acceptable autoVMAT plans were evaluated as better than the corresponding manually generated, clinically delivered IMRT plans, due to a combination of a better PTV coverage, dose conformality and sparing of the lungs, heart and esophagus. The remaining 6 plans violated at least one of the clinical constraints (Table 3.1), i.e., the PTV coverage (V_{95}) and/or lungs minus GTV mean dose (MLD) and V_{20Gy} (cf. 4.6). All plans fulfilled the planning constraints for the spinal cord, the heart and the plexus. The comparison between the autoVMAT and clinical IMRT plans for all relevant dose statistics is shown in Figg. 4.1 and 4.2. Differences between the clinical plans and the autoVMAT plans are plotted such that positive values are in favor of the autoVMAT plans, that is the opposite value is plotted for the target coverage ($-PTV D_{99}$, $-PTV V_{95}$) and the actual value of the difference is plotted for the organs at risk. The displayed Wilcoxon test p-values were calculated over the entire validation cohort of 41 patients. The pronounced predominance of positive bars confirms the overall improvement in plan quality for autoVMAT plans compared to the clinically delivered IMRT plans.

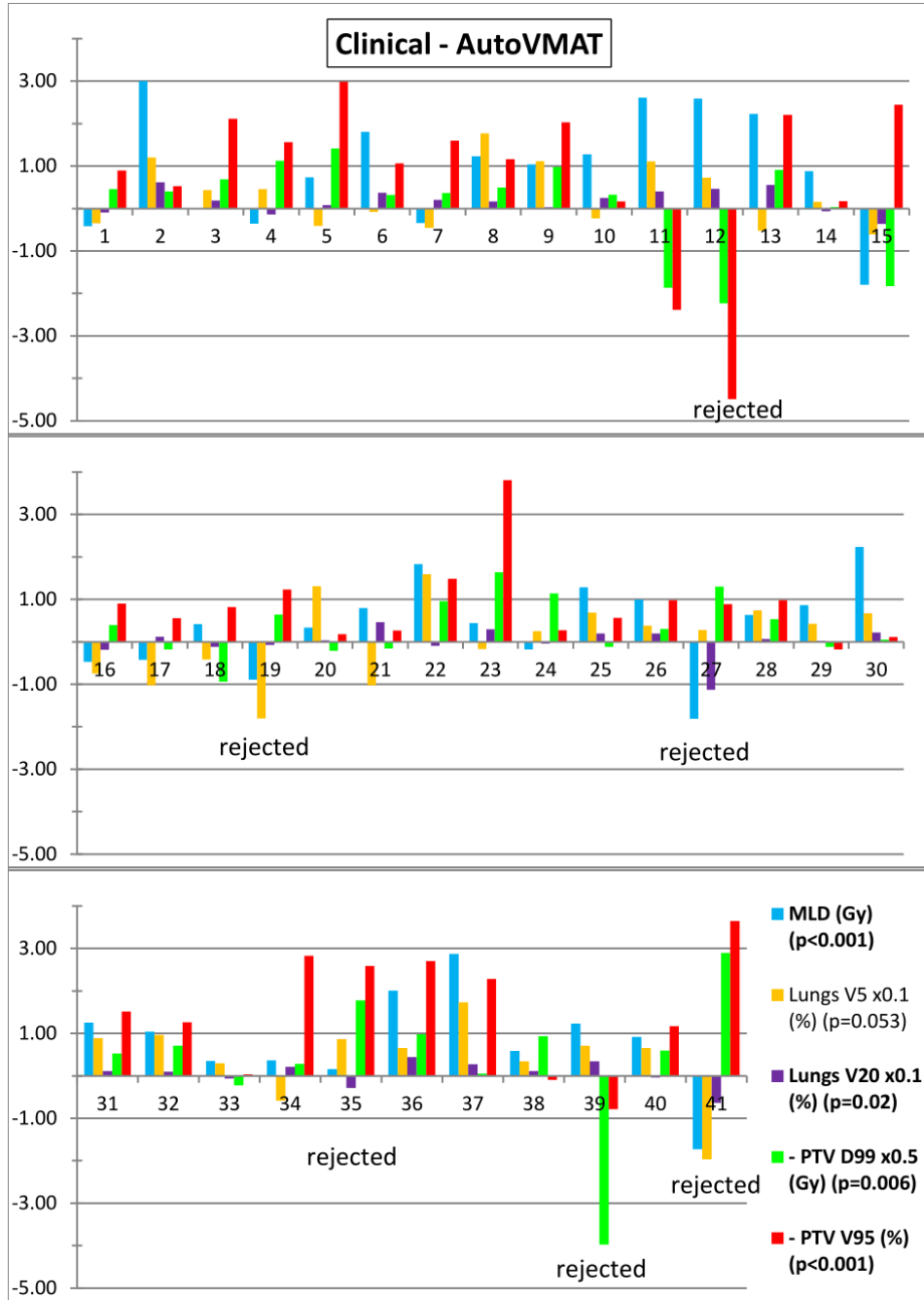


Figure 4.1: Differences between clinical plans and autoVMAT plans for mean lung dose (MLD), lungs V_{5Gy} , lungs V_{20Gy} , PTV $D_{99\%}$ and PTV $V_{95\%}$. Positive values are in favor for the autoVMAT plans. For visualization purposes the differences of the V_{5Gy} and V_{20Gy} of the lungs and PTV D_{99} were multiplied by 0.1, 0.1 and 0.5 respectively.

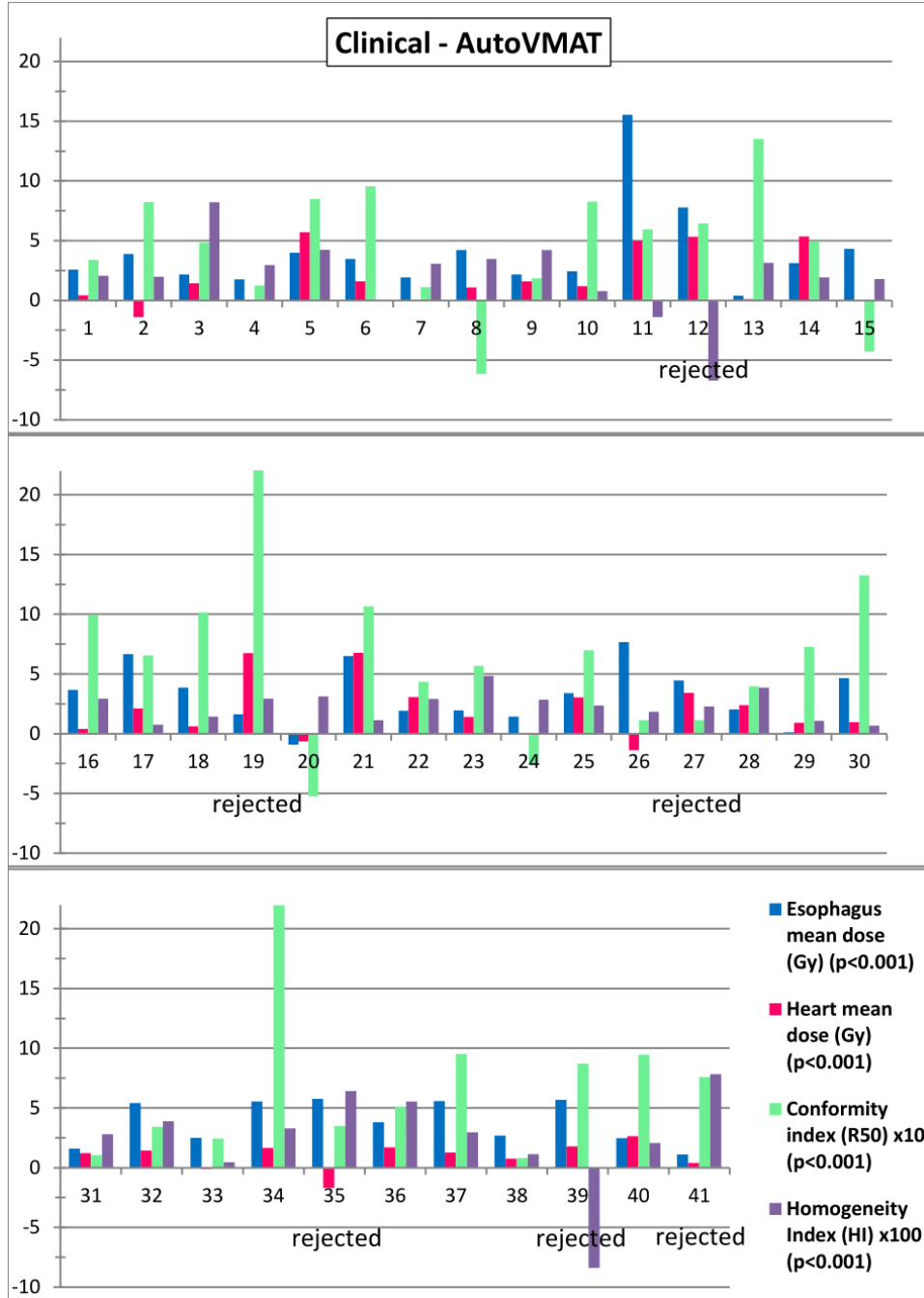


Figure 4.2: Differences between clinical plans and autoVMAT plans for esophagus mean dose, heart mean dose, conformity index R_{50} and homogeneity index (HI). Positive values are in favor for the autoVMAT plans. For visualization purposes the differences of the R_{50} and HI were multiplied by 10 and 100 respectively.

4.2 PTV coverage

PTV coverage was assessed by the use of two dosimetrical parameters:

- PTV V_{95} : the volume receiving at least 95% of the prescribed dose was the main indicator of the target coverage. V_{95} was clinically constrained to be higher than 95% of the planning target volume.
- PTV D_{99} : this parameter expresses the so called “near minimum dose”, i.e., the dose delivered to at least 99% of the PTV.

PTV mean dose was not selected as quality index because the difference between two plans could be strongly affected by different, unwanted, overdose. Evaluating the 35 acceptable autoVMAT plans with respect to the clinical IMRT plans, the average improvement in PTV V_{95} was 1.1% (SD=1.1%), while PTV D_{99} increased by 0.6 Gy (1.2%, SD=1.5 Gy). Differences were statistically relevant ($p < 0.001$) for a Wilcoxon test. For both PTV parameters, autoVMAT plans aimed to obtain higher results, that is a better target coverage. In a scatterplot as Fig. 4.3, points should lie above the equality line, i.e., in the sector where $y > x$. This behaviour was especially showed in the V_{95} plot, in which in only three cases (two of which were labelled as unacceptable plans) the coverage achieved with the automated procedure was lower than what previously achieved by manual planning in the IMRT clinical plan. The D_{99} range of values was wide due to the several prescription doses in the validation set (from 30 Gy to 66 Gy).

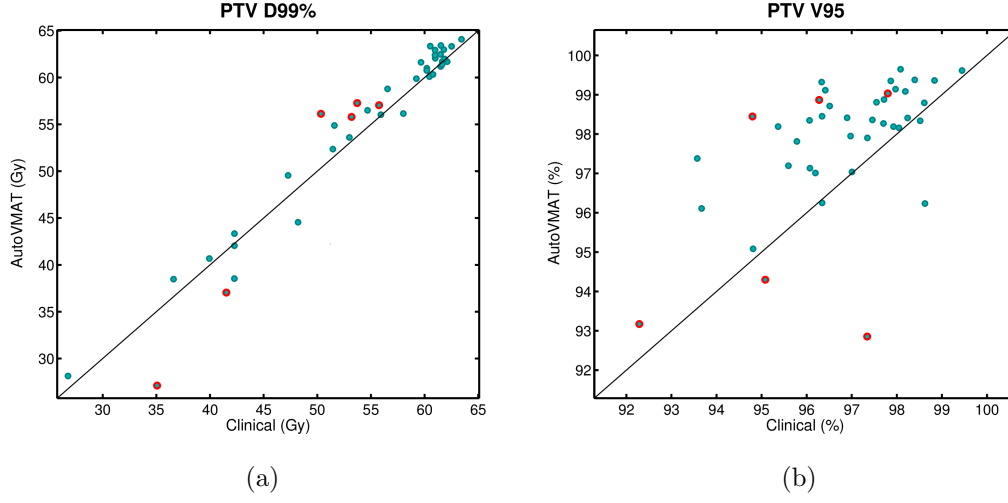


Figure 4.3: Scatterplots of PTV D_{99} (a) and PTV V_{95} (b). Red circles indicate the plans that were not clinically acceptable. Points lying above the equality line show improvement for autoVMAT plans.

4.3 Lungs minus GTV

The healthy lung tissue was often the most dose limiting organ at risk. The dose to this organ was measured by:

- Mean lungs minus GTV dose (MLD): the clinical constraint at Erasmus MC was set to 20 Gy for NSCLC treatment.
- Lungs V_{20Gy} : 20 Gy was considered an important threshold for lung tissue functionality. Lungs V_{20Gy} had to be lower than 35% of the volume.
- Lungs V_{5Gy} : the clinical requirements list stated as maximum volume 60% of the total healthy lung volume, but in practice this threshold was often raised to 70%. It was also experienced during the meetings with the physicians that, since the V_{5Gy} was lower than 60%, it was better to focus on other organs sparing or on achieving a higher level of conformality.

Mean lung dose in the 35 acceptable autoVMAT plans was reduced on average by 0.9 Gy (4.6%, SD=1.0 Gy, $p < 0.001$); the average difference in lungs V_{20Gy} was 1.3% (SD=2.1%, $p < 0.001$) in favor of the automated plans. For lungs V_{5Gy} an average

reduction of 3.2% was observed ($SD=7.6\%$, $p = 0.029$). As well as for the other organs at risk, points lying below the equality line showed a better sparing for autoVMAT plans with respect to clinical IMRT ones (Fig. 4.4). In consideration of the above, lungs V_{5Gy} distribution was more scattered than others (Fig. 4.4(c)).

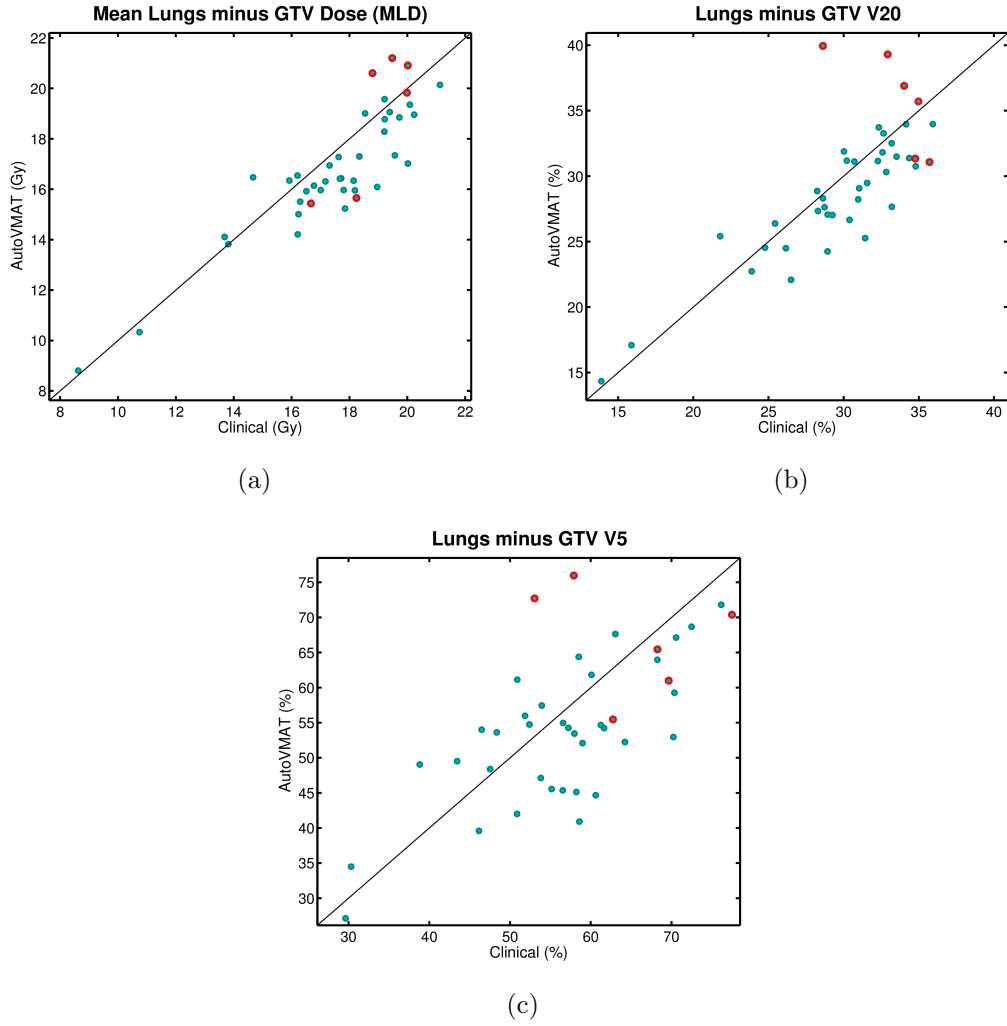


Figure 4.4: Scatterplots of lungs minus GTV mean dose (a), V_{20Gy} (b) and V_{5Gy} (c). Red circles indicate the plans that were not clinically acceptable. Points lying below the equality line show improvement for autoVMAT plans.

4.4 Esophagus and heart

Esophagus and heart were organs at risk that were not characterized by clinical constraints, i.e., a plan was not rejected due to exceeding a clinical goal for these organs. Evaluation was made taking into account the following parameters:

- Mean esophagus dose
- Esophagus V_{45Gy} : the esophagus was sensitive to high dose, so it was necessary to monitor the volume receiving at least 45 Gy, that should be kept below 25% of the total volume.
- Mean heart dose: the heart was considered a low priority organ at risk, mainly because the toxicity effects showed after several years.

Considering the 35 acceptable autoVMAT plans, esophagus mean dose was reduced on average by 3.6 Gy (15%, SD=2.8 Gy, $p < 0.001$) and V_{45Gy} decreased by 4.6% (SD=4.9%, $p < 0.001$) with respect to the clinical IMRT plans. Heart mean dose showed a reduction of 1.5 Gy (13%, SD=1.8 Gy, $p < 0.001$). Scatterplots for these dose statistics are shown in Fig. 4.5.

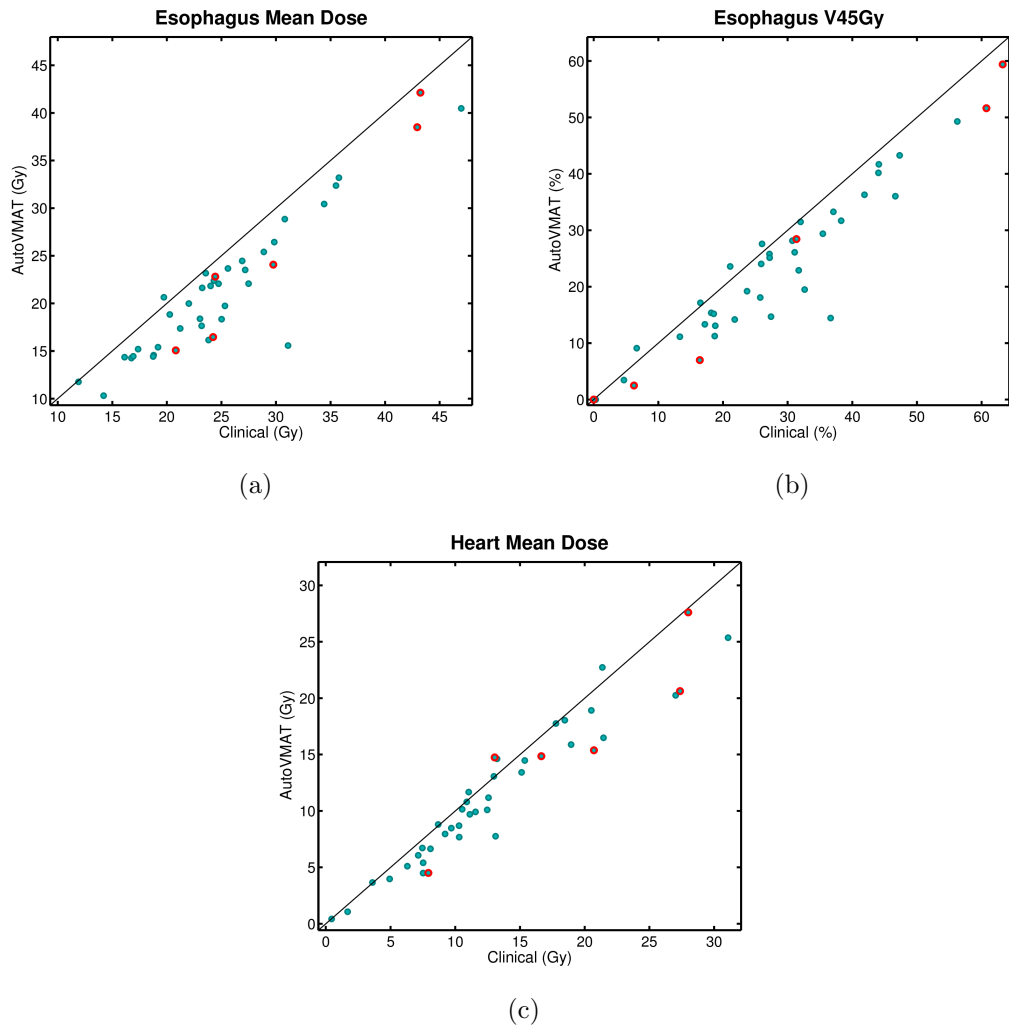


Figure 4.5: Scatterplots of esophagus mean dose (a), esophagus V_{45Gy} (b) and heart mean dose (c). Red circles indicate the plans that were not clinically acceptable. Points lying below the equality line show improvement for autoVMAT plans.

4.5 Dose conformality and target dose homogeneity

Dose conformality and target dose homogeneity were assessed by the following indexes:

- R_{50} : the ratio between the total volume receiving at least 50% of the prescribed dose (patient V_{50}) and the planning target volume.
- Homogeneity index (HI): the HI was an objective parameter to assess the homogeneity in the distribution of the dose to the PTV and the steepness of the PTV DVH, defined as:

$$HI = \frac{D_2 - D_{98}}{D_{50}}$$

For both indexes a reduction showed an improvement in plan quality (Fig. 4.6). An average reduction of 10.5% (SD=10.7%, $p < 0.001$) and 0.025 (22%, SD=0.017, $p < 0.001$) in the 35 acceptable autoVMAT plans with respect to the corresponding clinical IMRT plans was observed respectively for R_{50} and HI.

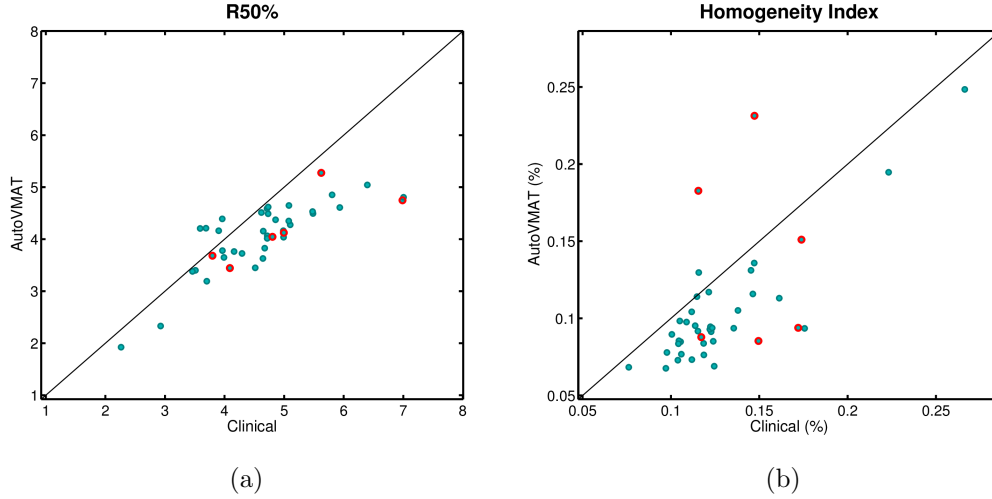


Figure 4.6: Scatterplots of R_{50} (a) and homogeneity index (b). Red circles indicate the plans that were not clinically acceptable. Points lying above the equality line show improvement for autoVMAT plans.

4.6 Unacceptable plans

In six cases (15% of the validation patients set), autoVMAT plans were not deemed clinically acceptable, due to a violation of at least one clinical constraint. In two cases PTV coverage was not acceptable ($V_{95} < 95\%$, $V_{90} < 99\%$); in three cases MLD and lungs V_{20Gy} exceeded the clinical constraint of 20 Gy and 35% respectively; in one case only V_{20Gy} violated the clinical goal. For all six plans that were initially not acceptable plans, it took a dosimetrist less than 10 minutes hands-on time to manually fine-tune the VMAT plan in Monaco to make it acceptable by applying slight changes to the Monaco cost functions list. In contrast, to generate a VMAT plan from scratch 3-4 hours were required. Dose statistics that violated the clinical constraints are shown in Table 4.1. The existence of unacceptable plans could be mainly ascribed to an inappropriate translation of the iCycle plan into a Monaco template; an example is reported in section 4.9.2.

Table 4.1: Dose statistics that violated the clinical constraints for the six unacceptable plans

Patient ID	Structure	Dose statistics
GDGCPerspIM1	PTV	$V_{90} = 96.5\%$ $V_{95} = 94.3\%$
GDGCPerspIM2	Lungs minus GTV	$MLD = 21.2 Gy$ $V_{20Gy} = 39.3\%$
GDGCPerspIM5	Lungs minus GTV	$V_{20Gy} = 36.9\%$
GDGCPerspIM31	Lungs minus GTV	$MLD = 20.6 Gy$
GDGCPerspIM41	Lungs minus GTV	$MLD = 20.9 Gy$
GDGCPerspIM42	PTV	$V_{90} = 96.6\%$ $V_{95} = 92.3\%$

4.7 AutoVMAT vs manual VMAT planning

For a subset of ten patients an experienced dosimetrist prospectively planned VMAT plans in Monaco without prior knowledge of the corresponding Erasmus-iCycle output or the clinically used IMRT plan. AutoVMAT plans were judged by a radiation oncologist as equivalent or better in quality with respect to manually generated VMAT plans for all the patients in the subset. Average differences were not statistically significant, except for lungs V_{5Gy} ($p < 0.02$), esophagus mean dose ($p < 0.02$) and esophagus V_{45Gy} ($p < 0.02$), all in favor of the autoVMAT procedure, and conformity index R_{50} ($p = 0.029$), in favor of the manually generated plans, although the sample was limited to 10 elements.

Differences between manually generated VMAT plans and autoVMAT plans are reported in Table 4.2. In figure 4.7 and 4.8 scatterplots are shown for the main dose statistics. Points in the scatterplots were on average equally distributed on both sides of the equivalence line. Furthermore, a reduction in PTV coverage was often coupled with a better sparing of the lungs and vice versa; this meant that both plans took place in proximity of the Pareto-optimality boundary, i.e., an objective could be improved only at the cost of a loss in the achieved value of another objective.

Table 4.2: Dose statistics comparisons between autoVMAT and manually generated VMAT plans

Structure	Dose metric	ManualVMAT-AutoVMAT	St. Dev.
PTV	V_{95}	-0.3%	1.4%
PTV	D_{99}	0.0 Gy	1.8 Gy
Lungs minus GTV	Mean dose	0.2 Gy	1.0 Gy
Lungs minus GTV	V_{20Gy}	0.5%	2.2%
Lungs minus GTV	V_{5Gy}	6.3%	3.2%
Esophagus	Mean dose	2.2 Gy	1.8 Gy
Esophagus	V_{45Gy}	3.2%	2.2%
Heart	Mean dose	0.2 Gy	1.1 Gy
	R_{50}	-0.33	0.37
	HI	0.010	0.019

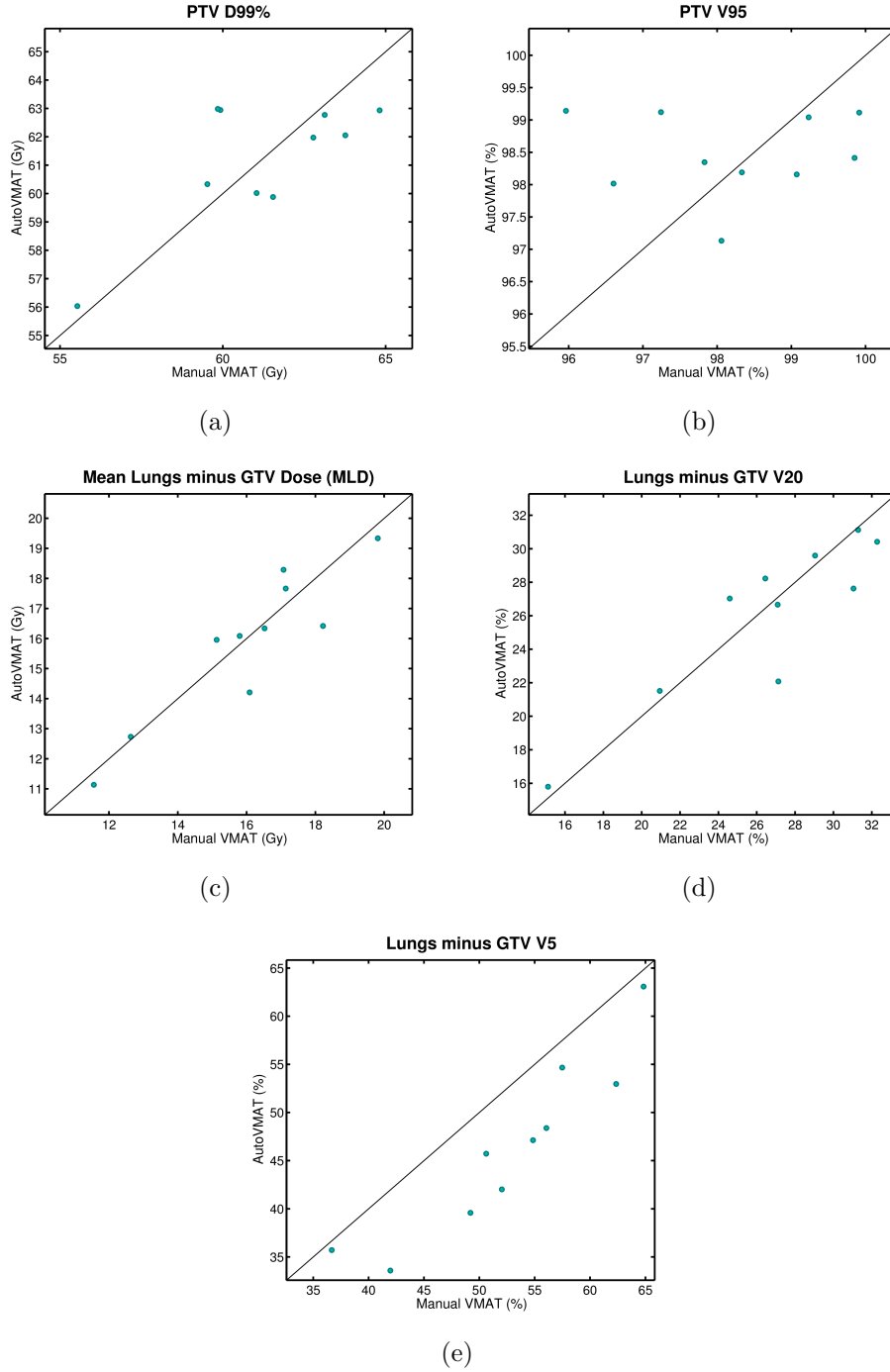
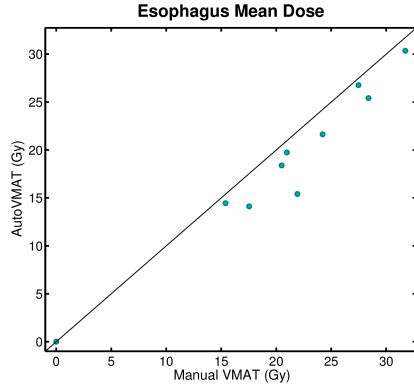
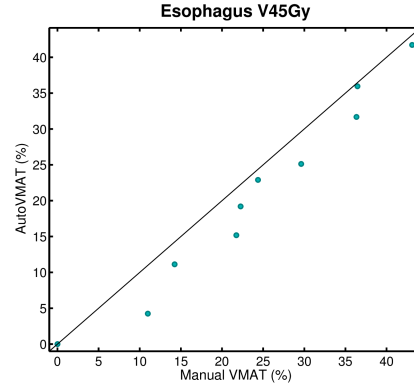


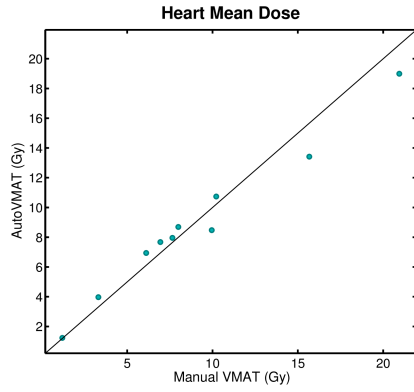
Figure 4.7: Scatterplots of PTV D_{99} (a), PTV V_{95} (b), lungs minus GTV mean dose (c), V_{20Gy} (d) and V_{5Gy} (e).



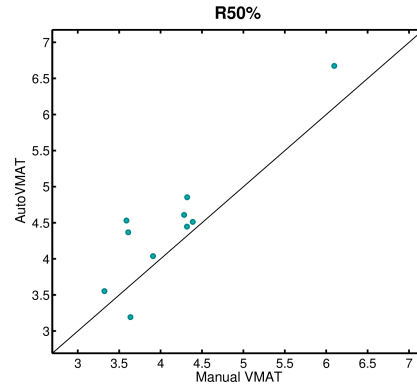
(a)



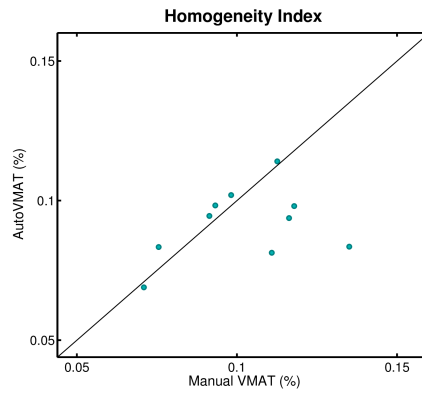
(b)



(c)



(d)



(e)

Figure 4.8: Scatterplots of esophagus mean dose (a) and V_{45Gy} (b), heart mean dose (c), R_{50} (d) and homogeneity index (e).

4.8 Dose escalation

For 6 out of 11 patients with a prescription dose of less than 66 Gy in the clinical plan, it was possible to escalate the tumor dose and obtain acceptable plans as judged by a physician with the use of the automated plan generation procedure without exceeding any of the clinical constraints. For two patients dose escalation from 45 Gy to 55 Gy was possible, for other patients from 55 Gy to 60 Gy, 60 Gy to 66 Gy (two patients), and 60.5 Gy to 66 Gy, respectively. When achieved within the clinical requirements, a higher dose was always evaluated by a physician as an improvement in terms of tumor fight.

4.9 Examples

4.9.1 Clinical plans, iCycle plans, AutoVMAT plans

The automated planning procedure required an image set, selected at 50% of the expiration phase, on which the organs at risk and the target volumes were delineated. Views were available in axial, sagittal and coronal mode (Fig. 4.9), although the axial view (Fig. 4.9(a)) was the most employed by the radiation oncologist during the evaluation. The image set for patient GDGCPerspIM7 was composed by 148 slices in the axial view. The PTV spreaded from slice 67 to 116. The clinically prescribed dose was 60 Gy in 30 fractions due to impossibility in the manual planning procedure to achieve the prescription dose of 66 Gy without violating any of the clinical constraints.

For each patient, three plans were available: the clinical IMRT plan, the iCycle plan, that simulated the VMAT delivery mode with an IMRT setting of 23 equiangular beams (cf. 3.1.6), and the actually deliverable VMAT plan in Monaco (autoVMAT). A comparison between the three dose distribution is shown in the following Table 4.3.

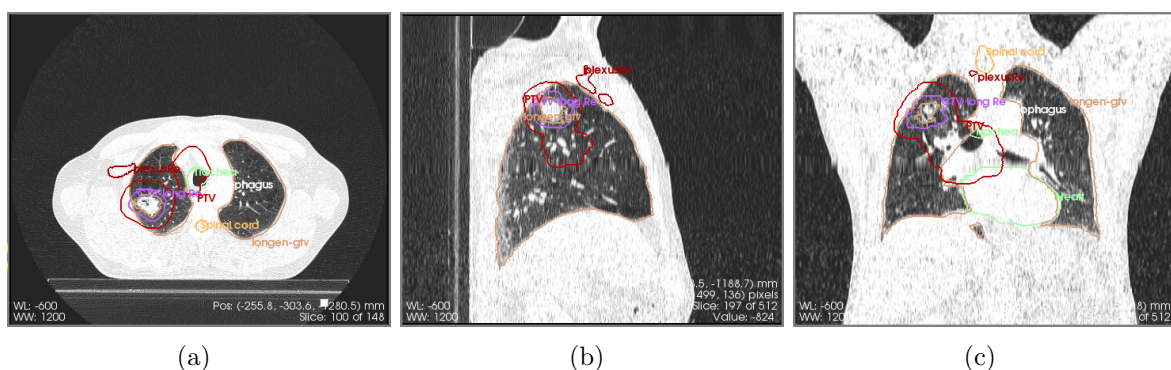
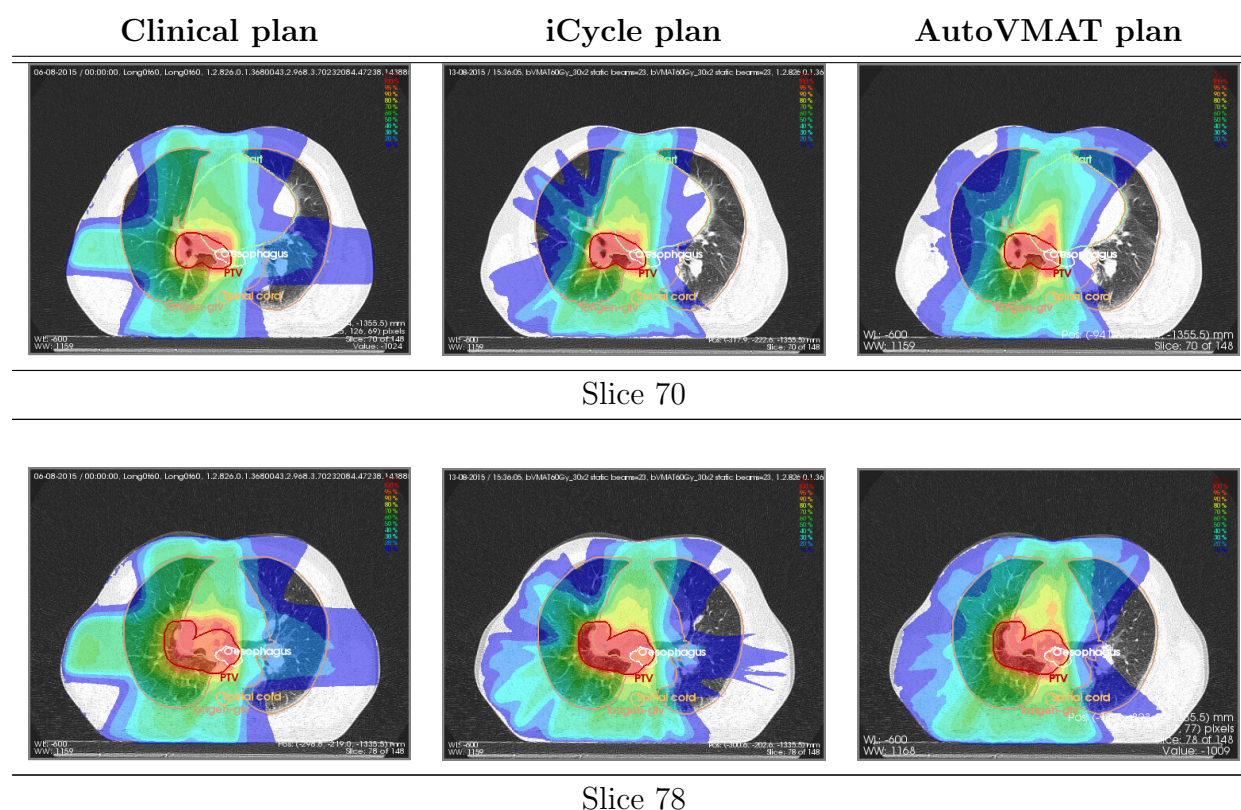


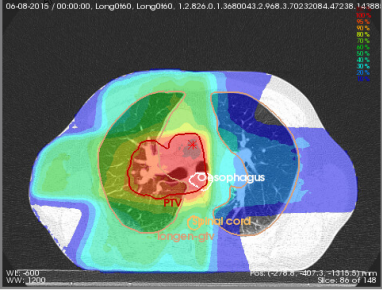
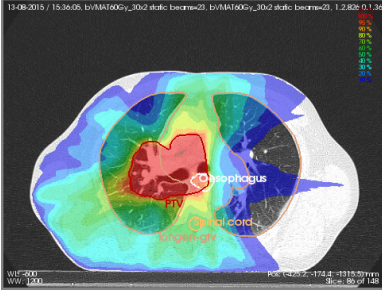
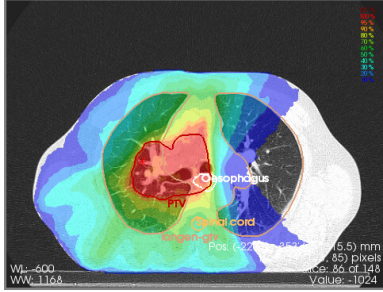
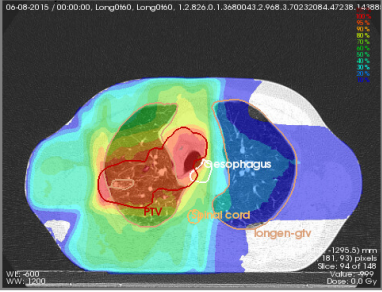
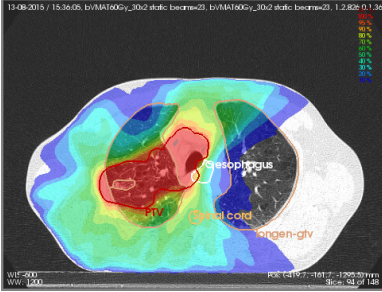
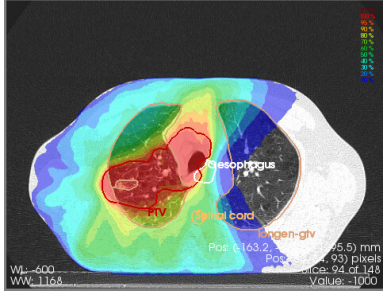
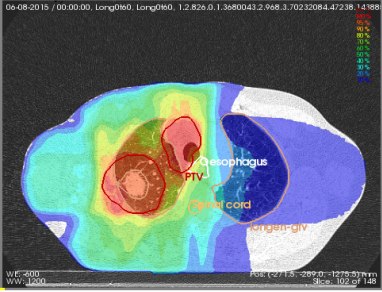
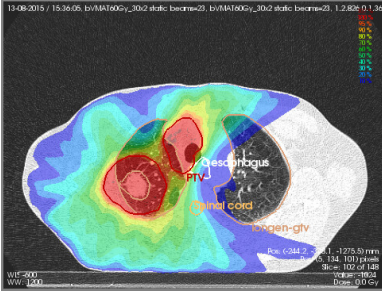
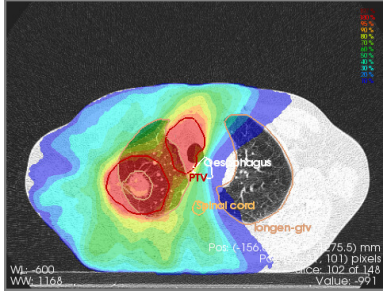
Figure 4.9: Image set and volumes delineation for patient GDGCPerspIM7 in axial (a), sagittal (b) and coronal view (c)

Table 4.3: Comparison between dose distributions of clinical plan, iCycle plan and autoVMAT plan for patient GDGCPerspIM7. The percentage in the dose distribution intensity scale is expressed in terms of the prescribed dose of 60 Gy.



Continued on next page

Table 4.3 – *Continued from previous page*

Clinical plan	iCycle plan	AutoVMAT plan
		
Slice 86		
		
Slice 94		
		
Slice 102		

Continued on next page

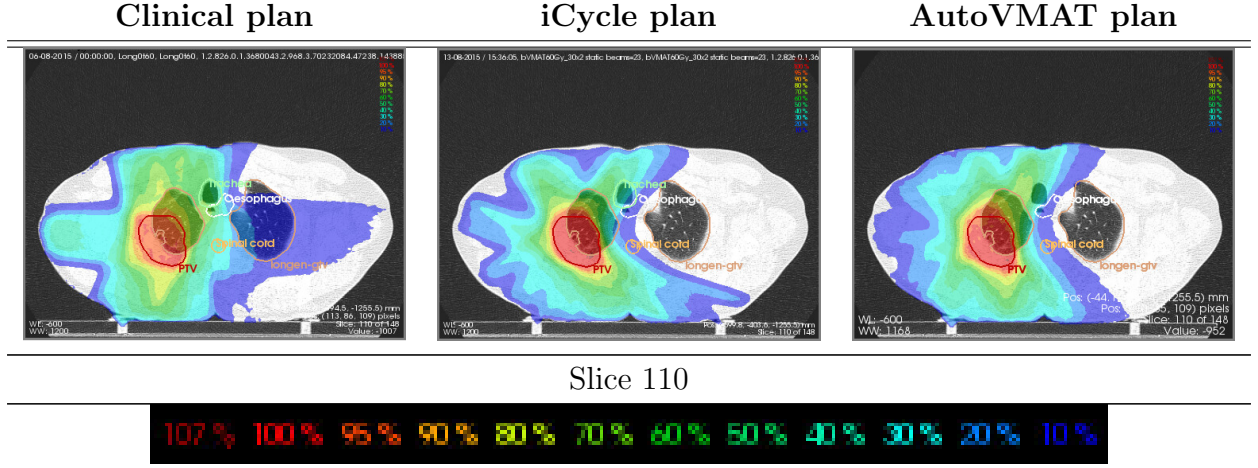
Table 4.3 – *Continued from previous page*

Table 4.3 - End

The clinical IMRT plan employed 6 beams with angles 0° , 15° , 180° , 210° , 270° and 340° . The angle selection was based on the dosimetrist's experience and could be sub-optimal. For this patient, the employment of the 270° angle was a cause of the irradiation of the contralateral lung (i.e., the opposite lung, with respect to the tumor site) with a wide low-dose region. The dark blue region specified the area receiving at least 10% of the prescribed dose of 60 Gy, i.e., 6 Gy.

The main information about the dose distribution were encompassed in the dose volume histograms (DVHs), the most useful tool for radiotherapy treatment plan evaluation due to the ability to summarize a lot of information about the dose distribution in one plot. DVHs for the clinical, the iCycle and the autoVMAT plans are shown in Figure 4.10.

The DVHs showed a better sparing of all the OARs (lungs-GTV, heart, esophagus) in the iCycle and autoVMAT plans with respect to the clinical plan because the DVHs for these organs were mainly lower than the solid line (clinical plan). On the other hand, for those plans the DVHs referring to the target volumes (PTV, CTV) were shifted towards the upper right corner and closer to the shape of a step function, meaning a better target coverage and a more homogeneous dose to the target. The positive effects were enhanced in the iCycle dose distribution with respect to the actually deliverable autoVMAT plan due to dose simulation algorithm and the absence of the sequencing algorithm (cf. 3.2.5).

The strongest gain for automated planning was in lungs sparing, in particular in the

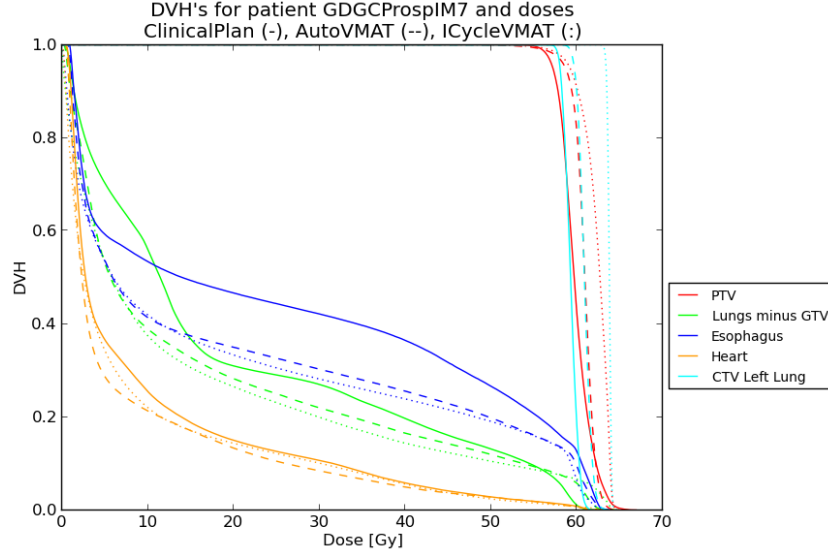


Figure 4.10: Comparison between dose volume histograms of clinical plan (solid line), autoVMAT plan (dashed line) and iCycle plan (dotted line) for patient GDGCPerspIM7

low dose region, where V_{5Gy} dropped from 70.2% (clinical plan) to 53.5% and 53.0% for the iCycle plan and the autoVMAT plan respectively. This could be noticed directly from the dose distribution by looking at the dark blue region (volume receiving at least 6 Gy) that covered the contralateral lung in the clinical plan, while this organ was almost completely spared in the two automated plans. Also the healthy lungs mean dose was remarkably spared from 19.0 Gy to 15.1 Gy and 16.1 Gy respectively in the iCycle and autoVMAT plans. The difference of 1 Gy between the two automated plans was partially ascribed to the translation from iCycle to Monaco, in which the value obtained after the preoptimization was relaxed by 5%, i.e., 0.8 Gy. The most significant dose statistics are reported in table 4.4.

Table 4.4: Main dose statistics of the three plans for patient GDGCPerspIM7

Structure	Dose metric	Clinical plan	iCycle plan	AutoVMAT plan
PTV	V_{95}	96.1%	98.8%	98.3%
PTV	D_{99}	55.9 Gy	56.7 Gy	56.0 Gy
Lungs - GTV	Mean dose	19.0 Gy	15.1 Gy	16.1 Gy
Lungs - GTV	V_{20Gy}	31.0%	26.5%	28.2%
Lungs - GTV	V_{5Gy}	70.2%	53.5%	53.0%
Esophagus	Mean dose	25.3 Gy	18.9 Gy	19.7 Gy
Esophagus	V_{45Gy}	31.7%	21.6%	22.9%
Heart	Mean dose	9.2 Gy	8.4 Gy	8.1 Gy

4.9.2 Fixing unacceptable plans

Patient GDGCPerspIM42 had a prescription dose of 45 Gy in 15 fractions. DVHs of the main organs at risk and target volumes for the clinical plan and the iCycle plan are shown in Fig. 4.11. The DVHs for the iCycle dose distribution showed a very remarkable improvement in terms of healthy lung tissue, esophagus and heart sparing, while the PTV coverage was comparable to the clinical plan (Table 4.5).

After the standard translation into a Monaco template, the plan obtained in Monaco was judged as not acceptable by the physicians. In fact, while the lungs minus GTV DVH was able to follow the shape of the one in the iCycle dose distribution, the target coverage did not fulfill the clinical constraints (Fig. 4.12 and Table 4.5).

In this case, the level of agreement between the iCycle and Monaco dose simulation algorithms was significantly lower than usual, so that, to achieve the goals for the lungs minus GTV structure, the goals of the cost functions related to the target coverage in the Monaco template were sacrificed and turned to infeasible (cf. 3.1.7) after short time.

In order to give Monaco more optimization room to properly achieve the goals about the target coverage, the relaxation of the lungs minus GTV goal from iCycle to Monaco was increased from 5% to 10% (cf. 3.2.5). The new obtained plan (labelled as autoV-MATmod) fulfilled all the clinical constraints and was judged by the physician as better than the clinical plan. DVHs and dose statistics are shown in Fig. 4.13 and Table 4.5. A further investigation on the reason of the lower level of agreement between the two dose

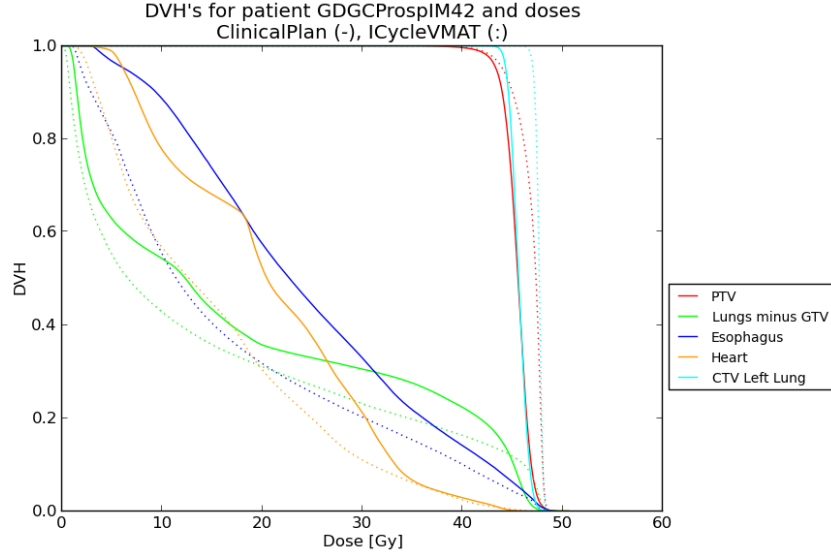


Figure 4.11: DVHs of the main organs at risk for the clinical plan (solid line) and the iCycle dose distribution (dotted line) for patient GDGCPerspIM42

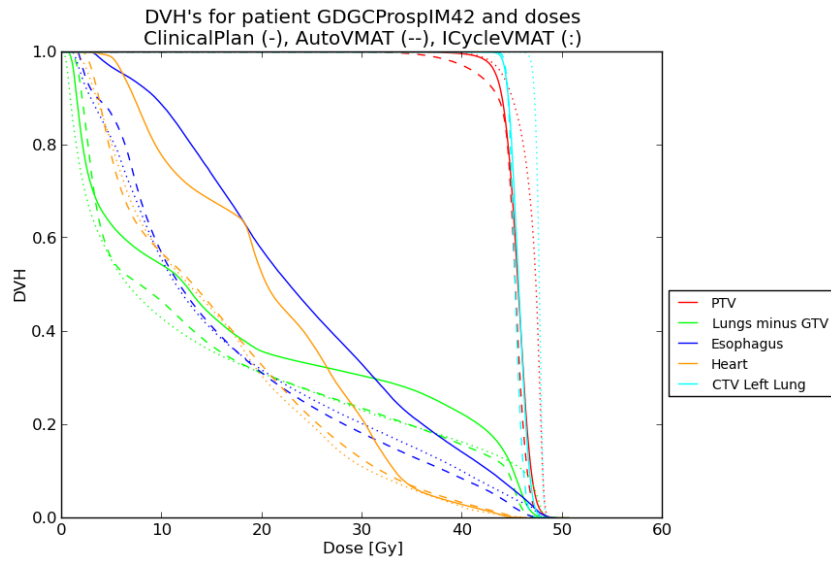


Figure 4.12: DVHs of the main organs at risk for the clinical plan (solid line), the iCycle dose distribution (dotted line) and the autoVMAT plan (dashed line) for patient GDGCPerspIM42

distribution algorithms might lead to improvement in the percentage of the acceptable plans in the automated procedure.

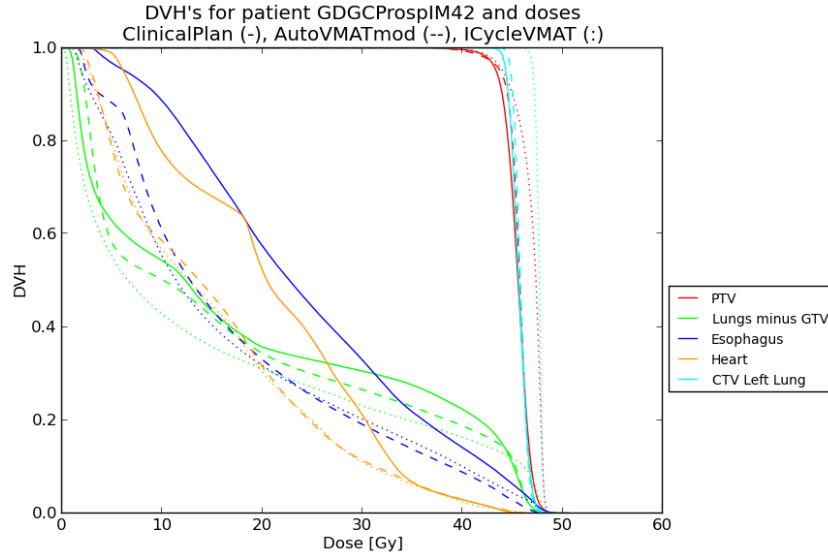


Figure 4.13: DVHs of the main organs at risk for the clinical plan (solid line), the iCycle dose distribution (dotted line) and the autoVMAT plan after the relaxation in the translation of the MLD (dashed line) for patient GDGCProsplM42

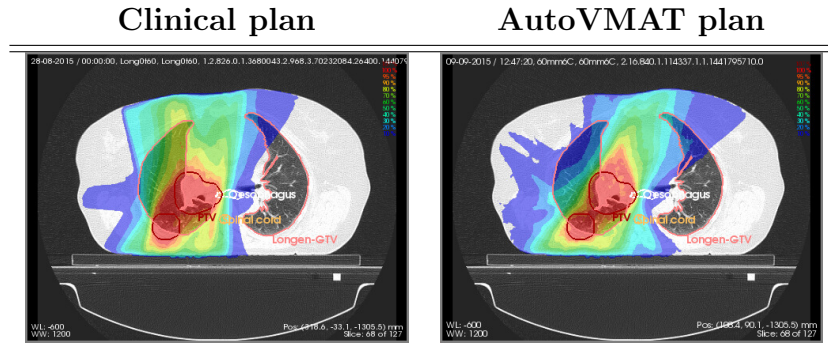
Table 4.5: Main dose statistics for the clinical plan, the iCycle plan, the autoVMAT with the standard translation and the autoVMAT plan with the modified translation

Structure	Dose metric	Clinical	iCycle	AutoVMAT	AutoVMATmod
PTV	V_{95}	97.3%	98.1%	92.9%	97.3%
PTV	D_{99}	41.5 Gy	41.8 Gy	37.0 Gy	40.8 Gy
Lungs - GTV	Mean dose	18.2 Gy	15.2 Gy	15.6 Gy	17.2 Gy
Lungs - GTV	V_{20Gy}	35.7%	31.0%	31.1%	34.3%
Lungs - GTV	V_{5Gy}	62.7%	55.1%	55.5%	58.0%
Esophagus	Mean dose	24.2 Gy	16.6 Gy	16.5 Gy	17.2 Gy
Esophagus	V_{45Gy}	6.2%	4.3%	2.5%	2.8%
Heart	Mean dose	20.7 Gy	15.0 Gy	15.4 Gy	15.3 Gy

4.9.3 Dose escalation

Patient GDGCPerspIM44 had a prescription dose of 60 Gy in 22 fractions (2.75 Gy per fraction) because the dosimetrist could not achieve the prescription dose of 66 Gy without violating the clinical constraints related to the healthy lung tissue. The autoVMAT plan obtained following the automated plan generation procedure was judged by the physicians as remarkably better than the corresponding clinical plan, due to the better PTV coverage and lungs sparing. It was interesting to notice that, while the mean dose and the V_{20Gy} decreased by 2.3 Gy and 5.5% respectively, the V_{5Gy} increased from 48.4% to 53.6%. Nevertheless, since this value was below the threshold of 60%, the physicians accepted this loss. The reason of the different shapes of the DVHs of the clinical plan and the autoVMAT plan could be found in the strongly different selection of the beam directions. While the clinical plan employed six beam angles (0° , 10° , 180° , 195° , 220° , 270° , 340°) mainly in the anterior-posterior direction (i.e., close to 0° and 180°), the VMAT plan employed the full arc. This was mirrored in a wider low dose region and, consequently, in a higher V_{5Gy} for the lungs and a strongly lower shape of the DVH at higher doses (Fig. 4.14), but also in a remarkably higher level of conformality of the dose distribution (especially in slices 84 and 92).

Table 4.6: Dose distributions for the clinical IMRT plan (left) and the autoVMAT plan (right) for patient GDGCPerspIM44. The percentage in the dose distribution intensity scale is expressed in terms of the prescribed dose of 60 Gy. The dose distribution in the clinical plan is mainly placed along the anterior-posterior direction, while the autoVMAT plan employs the full arc. This is mirrored in the automated plan by a higher level of conformality and a better sparing of the lungs at medium and high dose, while the low dose region increases.

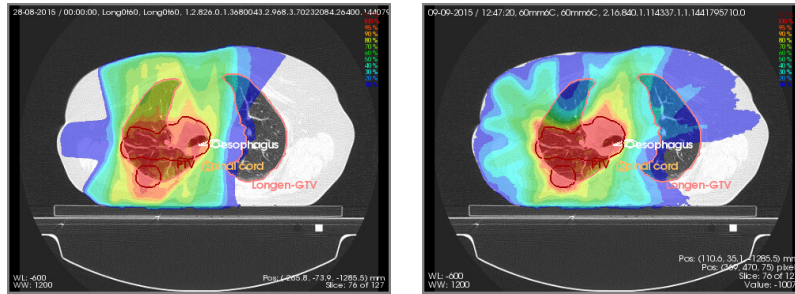


Continued on next page

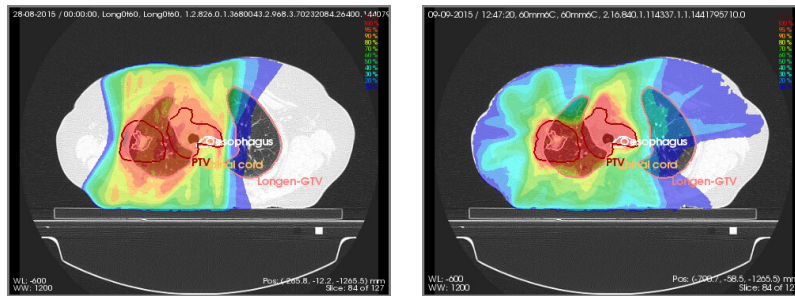
Table 4.6 – *Continued from previous page*

Clinical plan	AutoVMAT plan
---------------	---------------

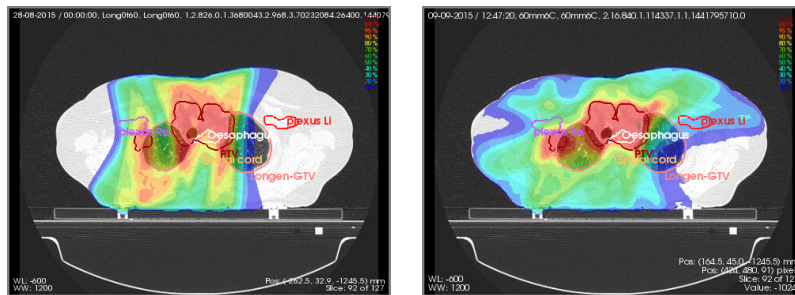
Slice 68



Slice 76



Slice 84



Slice 92

Continued on next page

Table 4.6 – Continued from previous page

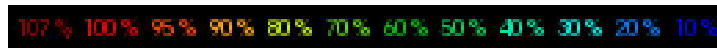
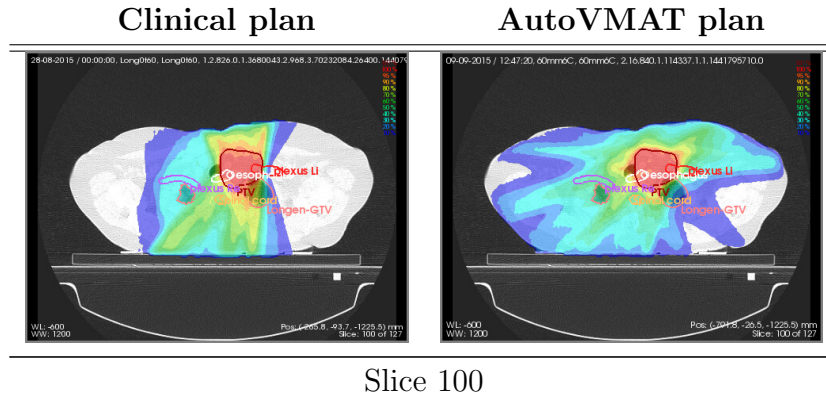


Table 4.6 - End

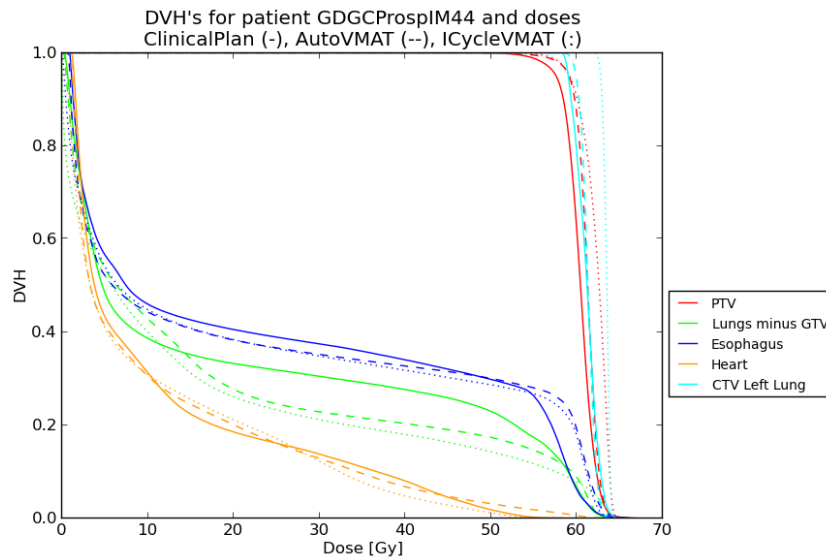


Figure 4.14: DVHs for the clinical plan (solid line), the iCycle VMAT plan (dotted line) and the autoVMAT plan (dashed line) for patient GDGCPerspIM44 with a prescribed dose of 60 Gy

For patient GDGCPerspIM44 an attempt of dose escalation was made. The prescription dose was increased to the full dose of 66 Gy. The automated procedure generated a plan able to achieve a good target coverage with the increased prescribed dose without

violating any of the clinical constraints. The DVH is shown in Fig. 4.15, while the main dose statistics for the three plans are shown in Table 4.7.

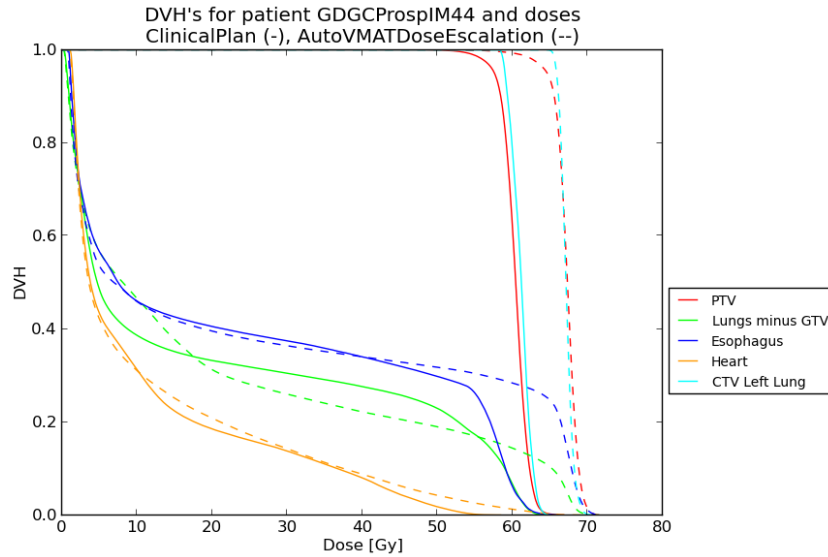


Figure 4.15: DVHs of the clinical plan with a prescription dose of 60 Gy (solid line) and autoVMAT plan with prescription dose increased to 66 Gy (dashed line) for patient GDGCPerspIM44

Table 4.7: Main dose statistics for clinical and autoVMAT plan with prescribed dose of 60 Gy and for autoVMAT plan with prescribed dose of 66 Gy. V_{95} refers to 57 Gy for the first two plans and to 62.7 Gy for the last one.

Structure	Dose metric	Clinical	AutoVMAT 60 Gy	AutoVMAT 66 Gy
PTV	V_{95}	96.5%	99.1%	97.9%
PTV	D_{99}	54.7 Gy	56.5 Gy	61.0 Gy
Lungs - GTV	Mean dose	19.6 Gy	17.3 Gy	19.8 Gy
Lungs - GTV	V_{20Gy}	33.2%	27.7%	31.2%
Lungs - GTV	V_{5Gy}	48.4%	53.6%	56.6%
Esophagus	Mean dose	23.6 Gy	23.2 Gy	25.6 Gy
Esophagus	V_{45Gy}	32.0%	31.5%	32.9%
Heart	Mean dose	10.9 Gy	10.8 Gy	11.6 Gy

4.10 Further implications

4.10.1 Hands-on working time reduction

The employment of the automated procedure entailed a remarkable reduction in hands-on working time for the dosimetrists. The working time requested to start the process was at about 5 minutes and when manual fine tuning of the results was needed, this was on average brief. As a whole, the overall hands-on working time decreased from 3-4 hours to 10 minutes. Furthermore, plan quality was totally independent on operator's skills and experience.

4.10.2 VMAT employment

The automated procedure proved that using VMAT as delivery modality allowed to achieve higher overall plan quality. The employment of VMAT technique reduced the delivery time with respect to IMRT (from 20 to 8 minutes on average), with positive effects in terms of less intra-fraction tumor and organs motion and more patient's comfort during the treatment.

Chapter 5

Conclusions and perspectives

5.1 Conclusions

In this study the in-house developed optimizer Erasmus-iCycle was used to develop a fully automated procedure for radiotherapy treatment planning of non-small cell lung cancer. VMAT plans were automatically generated in combination with the treatment planning system (TPS) Monaco and evaluated by two physicians. Comparisons were made with respect to previously delivered, manually generated IMRT plans.

Since VMAT was not introduced in clinical practice at the time of the study, a dosimetrist generated ten VMAT plans manually, without any prior knowledge about the clinical IMRT plans or the autoVMAT plans. Plans were evaluated by a physician and compared to the corresponding autoVMAT ones.

On a subset of patients for whom the prescribed dose was reduced in clinic to avoid violations of the clinical constraints a dose escalation following the clinical schedules was performed.

The main conclusions of the study are summarized below.

- The automated treatment planning procedure produced autoVMAT plans that fulfilled all the clinical constraints in 85% of the cases (35 out of 41 patients).
- All the acceptable autoVMAT plans were judged by two radiation oncologists as better than the corresponding clinically delivered IMRT plans, due to a combination of better PTV coverage, dose conformality and sparing of lungs, heart and

esophagus. All average differences were statistically significant in a Wilcoxon signed rank test.

- For the six automated VMAT plans that were initially not acceptable, it took a dosimetrist less than 10 minutes hands-on time to manually fine-tune the VMAT plan in our TPS to make it acceptable. In contrast, to generate a VMAT plan from scratch 3-4 hours were required.
- An oncologist physician evaluated and compared autoVMAT plans with respect to VMAT plans manually generated by an experienced dosimetrist. Overall plan quality was equal or superior in autoVMAT plans. Average differences were mainly in favor of the autoVMAT plans although mostly not statistically significant.
- The use of the automated procedure allowed to escalate the dose in 6 out of 11 plans of patients for whom the full tumor dose of 66 Gy was not clinically achievable without violating the dose constraints. The increment was substantial (at least 5 Gy).
- The employment of the automated planning procedure allowed to reduce the hands-on working time from 3-4 hours to at about 10 minutes per plan. The VMAT delivery modality decreased the treatment delivery time from about 20 to about 8 minutes, with benefit for the patient.

5.2 Perspectives

5.2.1 VMAT and IMRT delivery modality

Since VMAT was not introduced in clinic at the time of the study, the comparisons were mainly made with respect to clinically delivered IMRT plans. Consequently, it was difficult to assess whether the overall improvement in plan quality was to be mainly ascribed to the automation or to the different delivery technique. Nevertheless, the test performed on the ten randomly selected patients reasonably proved that the overall plan quality of autoVMAT plans was at least equal to the quality of plans manually generated by an experienced dosimetrist. A comparison between clinically delivered and automatically generated IMRT plans, without any clinical purpose and only for scientific

interest, was outside the scope of the study and would have required the generation of a different wish list.

5.2.2 Two-step approach and unacceptable autoVMAT plans

The automated planning procedure was based on a pre-optimization with Erasmus-iCycle, followed by a conversion to a Monaco deliverable plan. After the conversion into a Monaco plan, Pareto-optimality, the strong point of iCycle, was not proved anymore. In fact, the Pareto-optimal solution was achieved in conditions of ideal fluence (i.e., in absence of a leaves sequencing algorithm that simulated a real MLC) and with a simplified pencil beam dose simulation algorithm. Nevertheless, plans took place very close to the Pareto-optimality boundary, so that the autoVMAT plans could be interpreted as, at least, a very good starting point in a treatment planning procedure. This meant that only secondary or negligible improvements in plan quality could be achieved by an expert dosimetrist starting from the autoVMAT plan results.

In the few cases of unacceptable plans, the reason could be ascribed to an inappropriate conversion into Monaco deliverable plans. In these plans, the level of agreement between the iCycle output and Monaco was lower than the average and the conversion needed stronger relaxation in some cost functions goals. Further investigation on a site-specific conversion could lead to secondary improvements.

Improvements in the overall score could be achieved by equipping iCycle of a more sophisticated dose simulation algorithm, in order to achieve pre-optimized dose distribution with a higher level of agreement with actually deliverable dose distributions. Even better, an intriguing way would be to develop a higher level of integration between Erasmus-iCycle and Monaco.

5.3 Clinical introduction

The clinical introduction of the automated VMAT planning procedure for NSCLC treatment at Erasmus MC Cancer Institute has been started in October 2015. A full speed employment has been scheduled at the beginning of 2016.

Bibliography

- [1] Alberts B., Johnson A., Lewis J., Morgan D., Raff M., Roberts K., Walter P., *Molecular Biology of the Cell - 6th edition*, Garland Science, 2014
- [2] PulmCCM.org, <http://pulmccm.org/main/2015/interventional-pulmonology/who-needs-mediastinoscopy-after-negative-ebus-staging-for-lung-cancer/>
- [3] American Cancer Society, *Global Cancer Facts & Figures - 3rd Edition*, Atlanta, American Cancer Society, 2015
- [4] Podgorsak E. B., *Radiation Oncology Physics: a handbook for teachers and students*, International Atomic Energy Agency, Vienna, 2005
- [5] Khan F. M., *The Physics of Radiation Therapy*, Lippincott Williams & Wilkins, Philadelphia, 2009
- [6] Mayles P., Nahum A., Rosenwald I. C., *Handbook of Radiotherapy Physics - Theory and Practice*, Taylor&Francis, 2007
- [7] Cancer Research UK, <http://www.cancerresearchuk.org/about-cancer/cancers-in-general/treatment/radiotherapy/follow-up/long-term-side-effects-of-radiotherapy>, 2014
- [8] National Cancer Institute (USA), <http://www.cancer.gov/about-cancer/coping/survivorship/follow-up-care/follow-up-fact-sheet>, 2010
- [9] A. Barrett, J. Dobbs, S. Morris, T. Roques, *Practical radiotherapy planning - fourth edition*, Hodder Arnold, London, 2009

- [10] V. Ekambaram, R. Velayudham, *Analysis of low dose level volumes in intensity modulated radiotherapy and 3-D conformal radiotherapy*, Int J of Cancer Therapy and Oncology, Vol. 2, 2014
- [11] WebMD, <http://www.webmd.com/lung/>
- [12] American Cancer Society, <http://www.cancer.org/cancer/lungcancer-non-smallcell/detailedguide/non-small-cell-lung-cancer-what-is-non-small-cell-lung-cancer>
- [13] American Cancer Society, <http://www.cancer.org/cancer/lungcancer-non-smallcell/detailedguide/non-small-cell-lung-cancer-treating-surgery>
- [14] American Cancer Society, <http://www.cancer.org/cancer/lungcancer-non-smallcell/detailedguide/non-small-cell-lung-cancer-treating-chemotherapy>
- [15] American Association of Physicists in Medicine, <http://www.aapm.org/meetings/amos2/pdf/29-7928-56081-919.pdf>
- [16] A. Bezjak, R.B. Rumble, G. Rodrigues, A. Hope, P. Wardex and Members of the IMRT Indications Expert Panel, *Intensity-modulated Radiotherapy in the Treatment of Lung Cancer*, Clinical Oncology 24, Pag. 508–520, 2012
- [17] I. de Bree, M.G.E. van Hinsberg and L.R. van Veelen, *High-dose radiotherapy in inoperable non-small cell lung cancer: Comparison of volumetric modulated arc therapy, dynamic IMRT and 3D conformal radiotherapy*, Medical Dosimetry 37, Pag. 353–357, 2012
- [18] E.M. Quan et al, *Automated VMAT treatment planning for stage III lung cancer: how does it compare with IMRT?*, Int J Radiat Oncol Biol Phys, Vol. 84, Pag. e69–e76, 2012
- [19] P.W.J. Voet, S. Breedveld, M.L.P. Dirkx, P.C. Levendag, B.J.M. Heijmen, *Integrated multicriterial optimization of beam angles and intensity profiles for coplanar and noncoplanar head-and-neck IMRT and implications for VMAT*, Medical Physics, Vol. 39, No. 8, Pag. 4858–65, 2012

- [20] X. Zhang, X. Li, E.M. Quan, X. Pan and Y. Li, *A methodology for automatic intensity-modulated radiation treatment planning for lung cancer*, Phys. Med. Biol. 56, Pag. 3873-93, 2011
- [21] P.W.J. Voet, M.L.P. Dirkx, S. Breedveld, A. Al-Mamgani, L. Incrocci, and B.J.M. Heijmen, *Fully Automated Volumetric Modulated Arc Therapy Plan Generation for Prostate Cancer Patients*, Int J Radiat Oncol Biol Phys, Vol. 88, No. 5, Pag. 1175–79, 2014
- [22] J.P. Tol, M. Dahele, J. Peltola, J. Nord, B.J. Slotman and W. FAR Verbakel, *Automatic interactive optimization for volumetric modulated arc therapy planning*, Radiation Oncology, 2015
- [23] C. Cheng, I.J. Das, *Treatment plan evaluation using dose–volume histogram (DVH) and spatial dose–volume histogram (Zdvh)*, Int J Radiat Oncol Biol Phys, Vol. 43, Pag. 1143–50, 1999
- [24] P.W.J. Voet, M.L.P. Dirkx, S. Breedveld, D. Fransen, P.C. Levendag, and B.J.M. Heijmen, *Toward Fully Automated Multicriterial Plan Generation: A Prospective Clinical Study*, Int J Radiation Oncol Biol Phys, Vol. 85, Pag. 866-872, 2012
- [25] S. Breedveld, P. Storchi, P.W.J. Voet, B.J.M. Heijmen, *iCycle: integrated, multi-criterial beam angle and profile optimization for generation of coplanar and non-coplanar IMRT plans*, Medical Physics, Vol. 39, Pag. 951-963, 2012
- [26] S. Breedveld, P. Storchi, M. Keijzer, A. Heemink, and B.J.M. Heijmen, *A novel approach to multi-criteria inverse planning for IMRT*, Physics in Medicine and Biology, Vol. 52, Pag. 6339-53, 2007
- [27] Y.Y. Haimes, L.S. Lasdon, and D.A. Wismer, *On a bicriterion formulation of the problems of integrated system identification and system optimization*, IEEE Trans. Syst. Man Cybern., 1971
- [28] Elekta, *Monaco Biological Optimization Technical Reference*, Vers. 2.00, 2012
- [29] Elekta, *Monaco User Guide*, Vers. 5.00.00, 2014
- [30] Elekta, <https://www.elekta.com/radiotherapy/>

- [31] D. Grofsmid, M.L.P. Dirkx, H. Marijnissen, E. Woudstra, and B.J.M. Heijmen, *Dosimetric validation of a commercial Monte Carlo based IMRT planning system*, Medical Physics, Vol. 37, Pag. 540-549, 2010
- [32] K.R. Britton, G. Starkschall, H. Liu, J.Y. Chang, S. Bilton, M. Ezhil, S. John-Baptiste, M. Kantor, J.D. Cox, R. Komaki, R. Mohan, *Consequences of anatomic changes and respiratory motion on radiation dose distributions in conformal radiotherapy for locally advanced non-small-cell lung cancer*, Int. J. Radiation Oncology Biol. Phys., Vol. 73, 2009
- [33] D.S. Møller, A.A. Khalil, M.M. Knap, L. Hoffmann, *Adaptive radiotherapy of lung cancer patients with pleural effusion or atelectasis*, Radiotherapy and Oncology, Vol. 110, 2014